HYDROCHEMICAL INVESTIGATON OF THE SOUTH-WEST MICROBIALITE COMMUNITIES, WESTERN AUSTRALIA (2022-23).

Interim Report to the Wester Australian Department of Biodiversity, Conservation and Attractions (DBCA).

Report Issued February 2025, by the EpstromNet Research Group.

Lead Author: Dr Matt Forbes (hydro-geochemist).

Honorary Research Fellow.
School of Earth, Atmospheric and Life Sciences
University of Wollongong, Wollongong, Australia. 2522.
Contact +61 416278693
Matthewsforbes71@gmail.com

EPSTROMNET RESEARCH TEAM

EPStromNet partners are leading international researchers from three continents aiming to address key scientific questions underpinning the fundamental nature of rocky coast microbial-geological systems. The aim is to provide contemporary baseline information regarding the environmental and hydrological functioning of these communities, and associated threats. The investigative program is a multi-disciplined approach to the coastal microbialite communities, with aspects including geology and geomorphology, water quality, invertebrate communities, diatom assemblages, photosynthetic properties, oxygen and carbon cycles, and microbial DNA-RNA composition. Below is a list of the EPStromNet researchers, and their key affiliation.

EPSTROMNET SOUTH-WEST CAPES FIELD RESEARCH TEAM

Dr Matthew Forbes, University of Wollongong, NSW, Australia

Dr Gavin Rishworth, Nelson Mandela University, South Africa

Professor Graham Underwood, University of Essex, UK.

Professor Andrew Cooper, Ulster University, Northern Ireland, UK.

Mr Tom Garner, Ulster University, Northern Island, UK.

Dr Natalie Hicks, University of Essex, UK.

Dr Carla Dodd, Nelson Mandela University, South Africa.

OTHER EPSTROMNET RESEARCH MEMBERS

Professor Terry McGenity, University of Essex, UK.

Dr Alan Smith, University of KwaZulu-Natal, South Africa.

Dr Hayley Cawthra, Council for Geoscience, South Africa.

Professor Janine Adams, Nelson Mandela University, South Africa.

Dr David Clark, University of Essex, UK.

This work was completed by the above team during December 2022 under the DBCA permits CE006749 and FT61001164. It was funded by the National Environmental Research Council (NERC) NE/V00834X/1 EPStromNet (Extant Peritidal Stromatolite Network).

EXECUTIVE SUMMARY

This report summarises hydrochemical investigations undertaken on the microbialite community pools of the Western Australian South-west Capes region during the 2022-23 summer. This work was undertaken by the Extant Peritidal Stromatolite Network (EPStromNet), a National Environmental Research Council (NERC UK – NE/V00834X/1) funded research group, as part of a global investigation into coastal microbialite systems. The EPStromNet team completed this work under DBCA research permits CE006749 and FT61001164, with the field visit to the Augusta microbialite communities (AMC) occurring in December 2022. As part of the field visit, microbialite materials and associated community waters were sampled and analysed as part of the greater global research program.

The three key microbialite systems targeted were Quarry Bay (site code W7), Contos Springs (site code W8) and Canal Rocks (site code W9). The research aims were to firstly understand the environmental (including hydrological) functioning of the AMC, and secondly to compare to these functioning parameters of similar systems identified in South Africa and Ireland. The environmental functioning evaluation is an on-going process being completed via the analysis of a combination of geology and geomorphology, water quality, invertebrate communities, diatom assemblages, photosynthetic properties, oxygen and carbon cycles, and microbial DNA-RNA composition.

This report focusses on the hydrochemical (water quality) aspect of the greater research project, providing an updated assessment for three sites. Parameters evaluated in the hydrochemical assessment included the field measurements of pH, electrical conductivity (EC), temperature, dissolved oxygen, total alkalinity, redox potential and dissolved CO_2. These measurements were completed for four individual microbialite pools (A-D) at each of the three sites (W7, W8 and W9), thus providing 12 sample locations, with in flow and out flow points bringing the total sample locations to 24. Laboratory hydrochemistry included major cations and anions, nutrients and stable water isotopes ($\delta^{18}O$ and $\delta^{2}H$).

The 2022 field results identified mild pool water temperatures (20 - 30°C), pH in the circum-neutral to slightly alkaline (7-9) range and moderate salinity (5,000 - 10,000 µS/cm). Positive oxidation-reduction potentials indicate general oxidating conditions, with moderate alkalinity (200 – 400 mg/L) and dissolved carbon dioxide (30 - 80 mg/L) also measured for the pool waters.

The pool waters are a sodium-chloride-carbonate (Na-Cl-HCO_3) dominated system, with minimal sulphate. Nutrients in the form of nitrogen and phosphate are low, with total nitrogen, primarily in the form of nitrate, at 1 mg/L or lower, and total phosphate, below limits of detection. This suggests that anthropogenic inputs into the microbial pool systems are negligible. Stable water isotope ($\delta^{18}O$ and $\delta^{2}H$) results for the pools are consistent and similar to other values determined for cave waters in the proximal karst system. This implies a short seepage pathway to the microbialite pools, that the pool water is not significantly modified, and as such there is a strong connection between pool waters and the regional

karst groundwater system. This suggests that these coastal outflows might be useful as monitoring locations for inland aquifers.

Saturation Index (SI) calculations and comparisons with regional water quality suggest that microbial driven precipitation of carbonate (calcite) occurring within the pools modifies the pool hydrochemistry by decreasing concentrations of alkalinity and calcium between inflows and outflow points.

Comparisons of the 2022-23 hydrochemistry data presented here with previous hydrochemical investigations completed between 2008-10 by the Western Australian Department of Biodiversity, Conservation and Attractions (DBCA) indicates very little temporal changes in water quality across that time period. This includes consistent alkaline conditions, a similar salinity range, Na-Cl-HCO_3 dominance and continued low sulphate and nutrients levels.

Less quantifiable are the changes in water quantity over time. Current flow rates of 1 - 4 L/min were measured at several locations; however, at many points flow into the pools was not able to be quantified due to the nature of the flow or the visual absence of it. Some anecdotal evidence around the Contos Springs site suggests that the current flow rates of 1 – 4 L/min may be lower than that for previous decades. Furthermore, recent investigations of the regional groundwater system indicates that the region has experienced centuries of reducing recharge. This is thus likely affecting water availability to the microbialite pool systems, which have potentially been in place for several thousand years. It is possible the overall microbialite communities currently exist in an overall drying environment, which is a significant threat.

Recommendations for further investigations include the establishment of a routine monitoring program of the spring's health in terms of both water quality and quantity. This includes ongoing measurements of spring flow rates, periodic seasonal (winter and summer) water chemistry monitoring, sampling and analysis. The installation of shallow piezometers above gradient of the microbial pools sites is also recommended. These piezometers would prove to be invaluable for obtaining information regarding water quality and spring water availability, via routine sampling and the installation of water level loggers that measure seepage levels as a proxy for seepage flow.

Contents

LIST OF FIGURES

LIST OF TABLES

INTRODUCTION AND BACKGROUND

Introduction

Microbially mediated tufa deposits (or microbialite pool systems) are defined as organic deposits that have accreted because of the associated benthic microbial community trapping and binding detrital sediment, and or forming the locus of mineral precipitation (e.g. Burne and Moore 1987, Reid et. al., 2000, Suarez-Gonzalez et al., 2019). Microbialite formations have been documented on a variety of rocky coasts under many geomorphic and climatic settings (e.g. Smith and Uken, 2003; Forbes et al., 2010; Perissinotto et. al., 2014; Rishworth et. al., 2020; Cooper et al. 2022; Garner et al. 2024, 2025). These formations occur in the high intertidal and supratidal zones with the discharge of mineralised freshwater a key ingredient to their development. Depending on the nature of this discharge and coastal geomorphology, microbialite development can occur on cliff faces, shore platforms, or within boulder zones.

One such microbial pool community exists at several locations in the South-west Capes region of Western Australia (Figure 1). The microbial communities are referred to as the Augusta Microbial Threatened Ecological Community (TEC), with the TEC ranked as endangered in 2001 (Onton et al. 2009). The Augusta Microbial Communities (AMC) have been periodically evaluated and described in terms of their biological, geomorphological and hydrological characteristics and functioning (e.g. Onton and Forbes 2009; Forbes et. al. 2010; Cooper et al. 2022, Garner et al. 2025). These works have identified that carbonate rich groundwaters that seep out onto the coastal bedrocks are vital for the bio-mediated processes and subsequently the formation of the carbonate deposits.

Water quality data was first characterised between 2008-09 for many of the main AMC locations between Cape Naturaliste and Leeuwin. As part of the current international EPStromNet research program several of the sites that were first investigated in 2008-09 (Forbes et al. 2010) were re-visited, with water quality field and laboratory analysis repeated. This report details those results, provides a comparative evaluation to the historical 2008-09 data and assesses water quality in relation to other regional water quality data sets.

Geology, Hydrogeology and Climate

The AMC sites are located in the south-west cape region, on the western coastal fringe of the distinctive anvil-shaped promontory, known as the Leeuwin–Naturaliste geographic region, Western Australia (Figure 1). Much of the area is incorporated into the Leeuwin-Naturalise National Park. Key townships of the south-west capes region are, from north to south, Busselton-Dunsborough, Margaret River and Augusta.

The south-west cape region is Mediterranean climate, with dry summers and mild, wet winters. Annual precipitation (Cape Leeuwin meteorological station) is approximately 1100 mm, with most rainfall occurring between April and October. Evaporation rates are in the order of 1000 mm/yr^{-1} (BoM, 2024).

The coastal Leeuwin–Naturaliste Ridge is a strip of Pleistocene aged, karstified, variably cemented, sandy coastal dune limestone/calcarenite named the Tamala Limestone (Playford et. al., 1976, Lipar and Webb 2014). The Tamala limestone extends from Cape Naturaliste to Cape Leeuwin, and outcrops in many locations. Underlying much of the Tamala Limestone unit is the Proterozoic Leeuwin Complex (540–780 Ma), impermeable, strongly metamorphosed, primarily impermeable granitic gneiss (Myers, 1994). The Leeuwin Complex and the basement beneath the Perth Basin to the east form part of the Pinjarra Orogen. The Dunsborough Fault forms a structural boundary between the eastern margin of the Leeuwin Complex and the Perth Basin (Lasky 1993).

Groundwater flow paths in the coastal zone are controlled by the topography of the bedrock of the Leeuwin Complex and the presence of solution chambers and voids (karstic features) that form conduits which channel groundwater in preferred directions. The transmissivity of the Tamala Limestone is large due to the presence of karstic features, high porosity and low specific retention, which restricts the development of an extensive water table for this catchment. Groundwater moves towards to the coast in a west to south-west direction discharging at the limestone -bedrock contact across an area occupied by the spring and a shallow swampy seepage basin of reeds and rushes.

Spring expressions are evident in many locations along the South-west Capes coastal zone. These spring expressions occur primarily at the contact between the Leeuwin Complex and the overlying Tamala Limestone. In the Augusta area, this spring expression is known as the Leeuwin Spring (e.g. DoW 2007). The presence of the Leeuwin Spring is likely related to karstic features, such as solution voids and doline structures within the Tamala Limestone ridge east of the spring (Appleyard, 1989). This has resulted in a concentration of groundwater discharge to a very small area of catchment.

Groundwater is recharged by the infiltration of rainfall within the catchment situated up slope to the ridge crest of the Tamala Limestone; however, most rainfall in this area is lost to evaporation, with only a small fraction reaching groundwater. Furthermore, previous studies have identified that significant decreases in rainfall decline (Smith et al. 2000) and in turn groundwater recharge (Preistley et al. 2020) have been occurring on both decadal and century time scales. There has also been a major expansion in the viticulture industry in the Marget River region in the last few decades that has significantly increased the demand for water resources (e.g. Johnson 2000; DoW 2011) and likely affected the groundwater balance in many locations proximal to the coastal fringe.

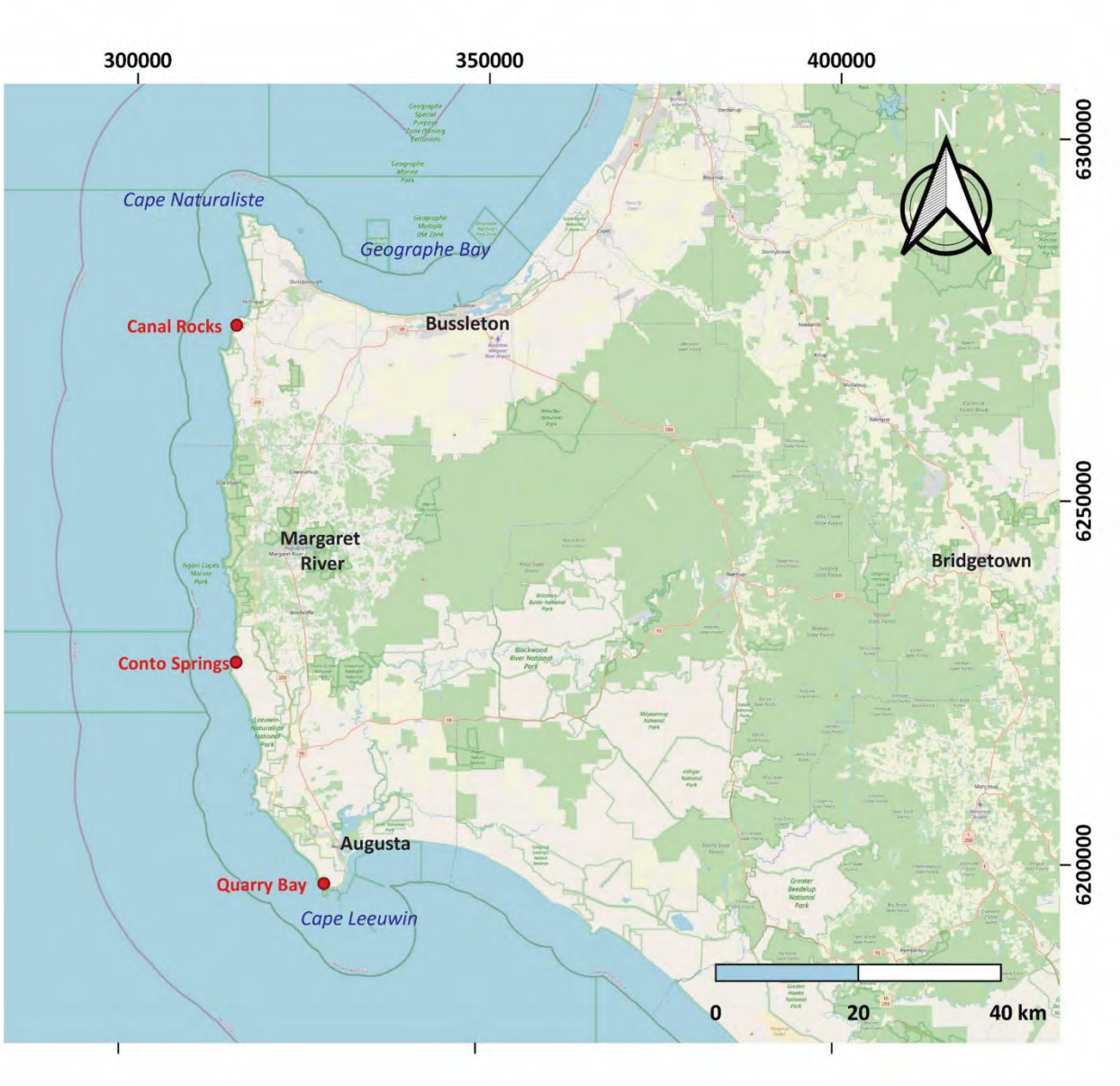

Figure 1 **South-west Capes Region with location key microbialite investigation sites**

FIELD INVESTIGATIONS

Site Visit and Descriptions

During November-December 2022, the EPStromNet research team undertook a five-day field visit to the AMC locations. Three key locations were chosen for the research program, the structure of which replicate similar programs undertaken in both the Eastern Cape of South Africa and the north coast of Ireland at sites of similar appearance. The locations chosen were Quarry Bay (W7), Contos Springs (W8) and Canal Rocks (W9). At each of these three locations, four sub-sites pools (A-D) were chosen for the suite of investigations to be undertaken. Each pool location is detailed in Table 1.

Table 1 Site Locations

Site	Code	Northing (m CRD94)	Easting (m CRD94)
Quarry Bay A	W7A	6196177	328398.8
Quarry Bay B	W7B	6196085	328420.9
Quarry Bay C	W7C	6195912	328577.5
Quarry Bay D	W7D	6195926	328656.4
Contos Springs A	W8A	6226310	315508.6
Contos Springs B	W8B	6226616	315597.5
Contos Springs C	W8C	6226589	315595.5
Contos Springs D	W8D	6226626	315605.0
Canal Rocks A	W9A	6272742	314713.1
Canal Rocks B	W9B	6272905	314831.1
Canal Rocks C	W9C	6272933	314858.9
Canal Rocks D	W9D	6272793	314755.9

This section provides a description of the geomorphological and hydrogeological composition of the AMC sites. The terminology used here to describe facets of the study sites in the following site descriptions follows work published by Forbes et al. (2010), Cooper et al. (2022); and Garner et al. (2024, 2025).

Quarry Bay (W7 A to D)

The Quarry Bay site (Figure 2) is the largest and most diverse of the AMC site located in the South-west Capes region. Quarry Bay encompasses an area of more than 2 km of coast-line length and comprising a variety of different microbialite communities including waterfall and spring seepage deposits. Photos of the four pool sites investigated are provided in Figure 3.

Approximately 300 metres (m) north of the Quarry Bay car park is a distinct limestone cliff area, where an extensive microbialite community has developed on and below it (W7D). Two main types are identified, firstly a speleothem-tufa like form, existing on the upper and middle overhang areas of the limestone cliff. Below the limestone cliff itself a thin sheet and some bubble-shaped microbial laminates have developed in the waterfall splash zone.

An extensive area representing a network of spring seepages, discharge aprons and barrage pools commence north of the main waterfall area at Quarry Bay and continues intermittently for another 700 m to the north (W7A, B and C). These pools and discharge aprons are located on granite bedrock in the supratidal zone and cover an area of approximately 100 m^2. The barrage-pool walls consist of lithified rimstone tufa (10 cm in height). Bubble microbial laminates of variable thickness (2–8 cm) dominate within the pools themselves. Lithified tufa facies are evident on flat bedrock areas representing inactive discharge apron fans, whereas thin (4 cm) sheet-like laminate tufa represent the active spring discharge aprons and are closely related to the location of current spring seeps.

To the south of W7D and the Quarry Bay carpark is the Augusta Water Wheel, a unique site in that the microbial community here has colonized a structure built in 1895 (Cresswell 2003). This AMC is generally comprised of thin (5 cm) laminates of bubble form that have developed within the flow duct to the wheel, and in the pools on the ground below the wheel. Thin (5 cm) sheet varieties have developed on vertical walls below the wheel. Some pools exist as shallow (10 cm) depressions in the exposed granitic bedrock and have no barrage wall features. While this site is described here, it was not incorporated into the greater project as there were no similar sites in South Africa or Ireland to which it could be compared to.

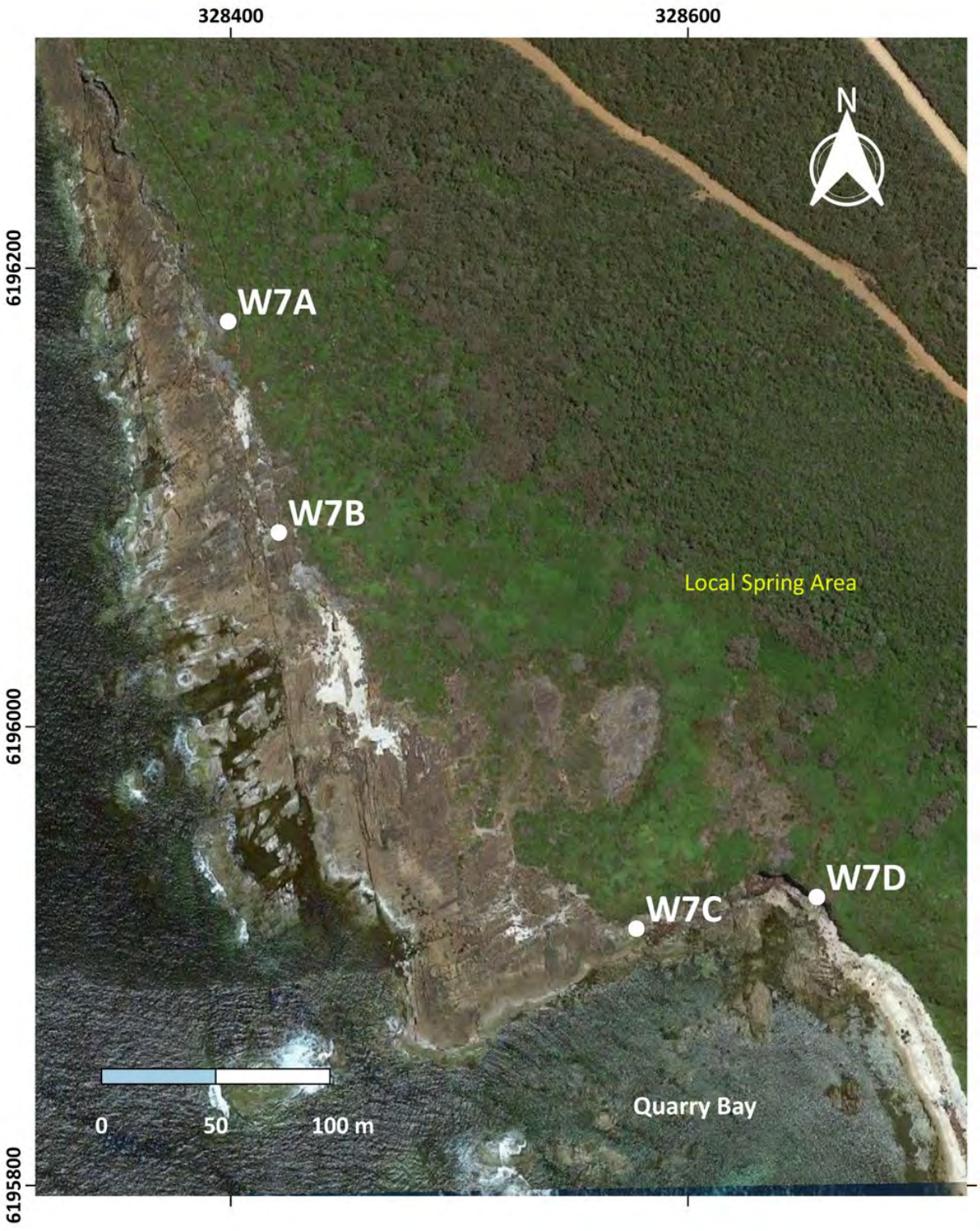

Figure 2 **Sample Location Sites for Quarry Bay**

Figure 3 Photos of Quarry Bay Sampling Sites

Contos Springs (W8 A to D)

The Contos Springs AMC is located in two distinct coastal areas (Figure 4). The system consists of a number of large (1–5 cm) diameter barrage-type pool deposits, spanning an area of over 100 m^2. The pools have developed within large granite bedrock depressions in the supratidal zone (Figure 5), where spring-water slowly flows into the pools from seeps located at the base of the adjacent steep limestone escarpment. Due to proximity of this site to the ocean, mixing of spring and ocean waters occurs in the pools, especially during periods of high swell and large tides. Various tufa facies are identified at the Contos site; the lithified rimstone tufa associated with the barrage pool walls (up to 20 cm high) and lithified sheet tufa on bedrock as part of extinct discharge aprons. Bubble form microbial laminates are evident within the pools, whereas thin sheet laminates are associated with flat bedrock areas. This latter variety is in close association with the active groundwater seeps.

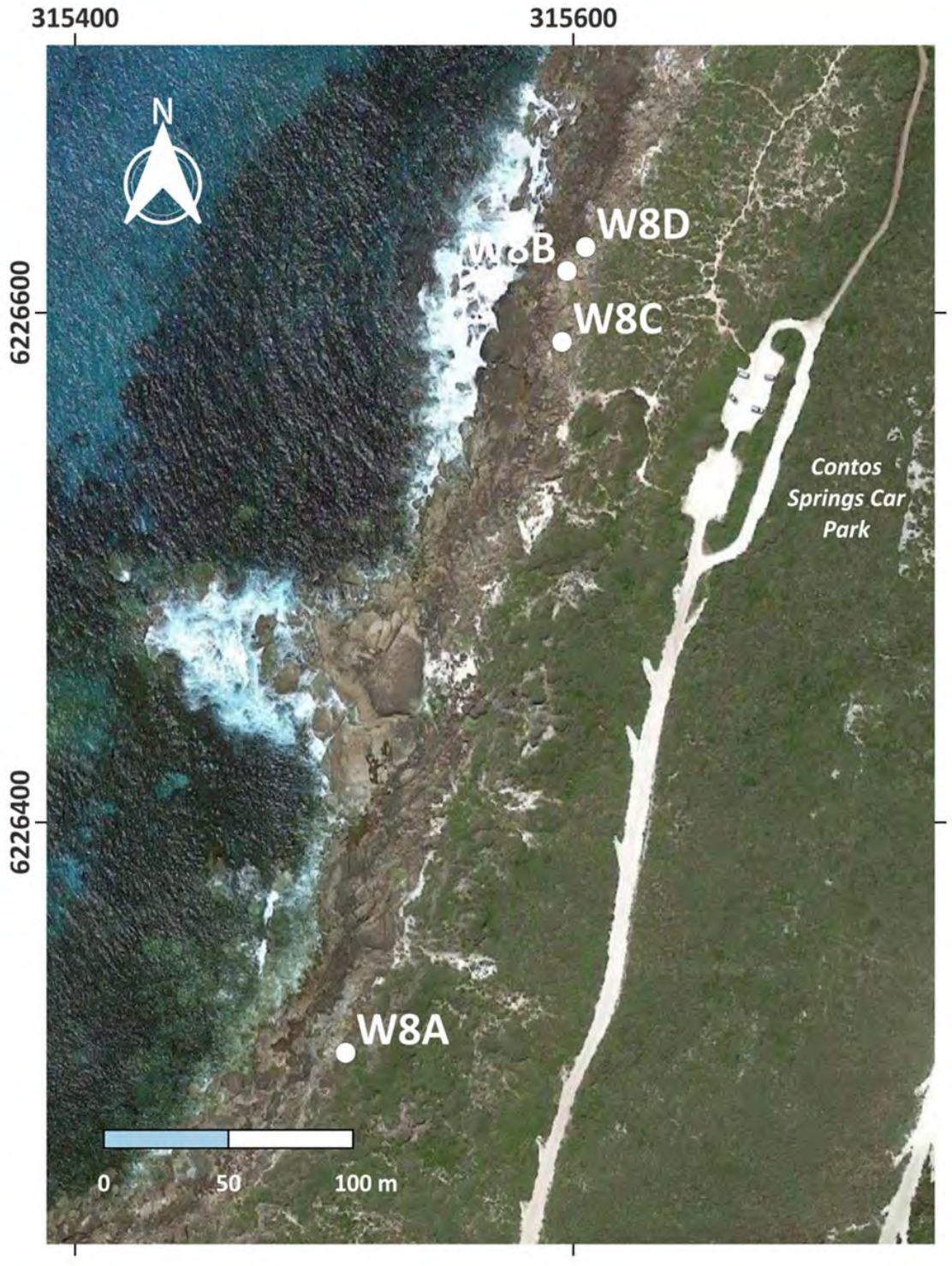

Figure 4 **Sample location Sites for Contos Springs**

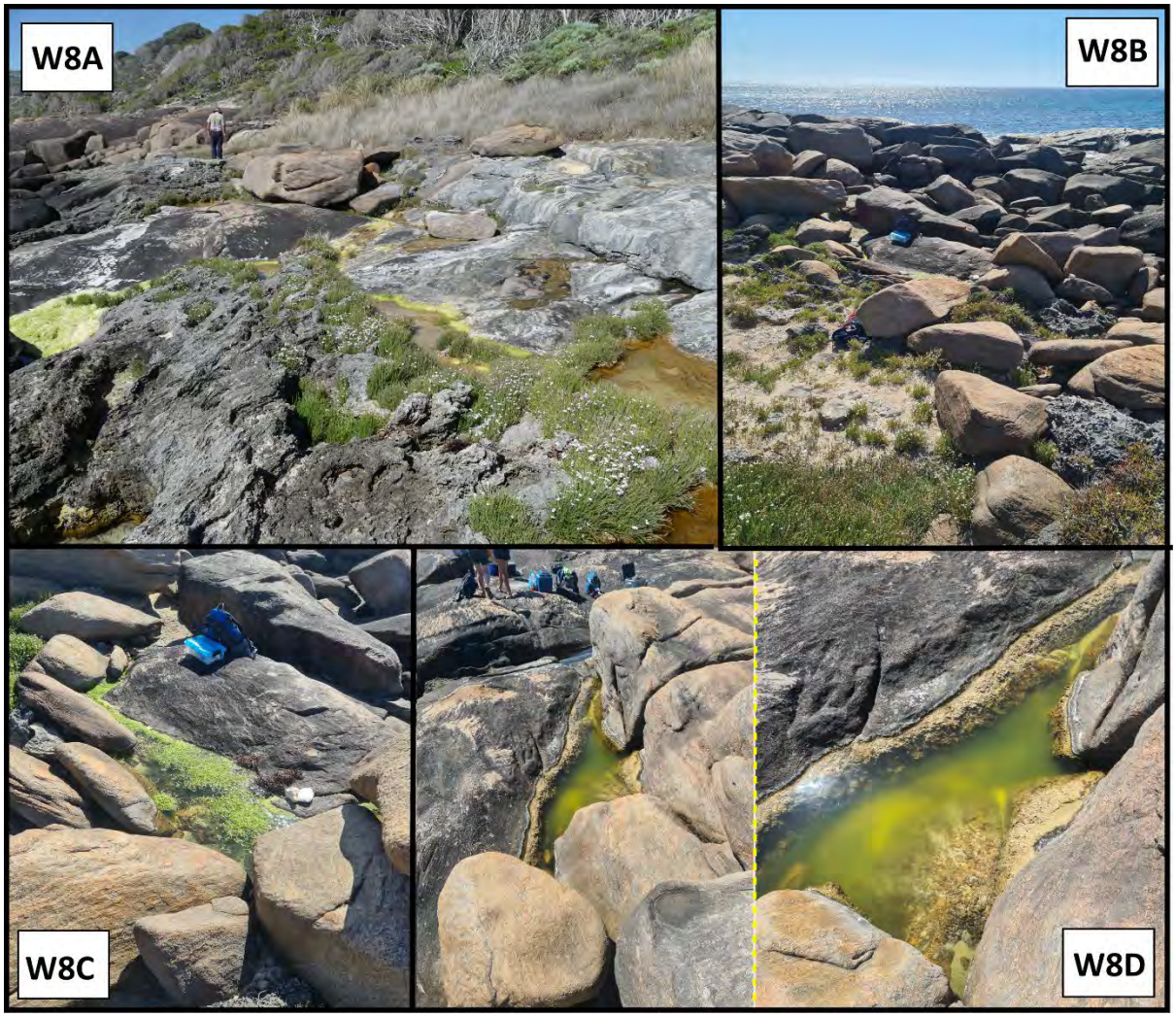

Figure 5 Photos of Contos Springs Sites

Canal Rocks (W9 A to D)

The Canal Rocks AMC (Figure 6 and 7) were first described by Forbes et al. (2010) as consisting of less than half a dozen small (1 m diameter) barrage pools over granite and limestone, which are fed through thin (10 cm) flow channels by very low flow freshwater seepages (W9A). Barrage pools are restricted to preferential flow paths of the spring seeps, determined by bedrock geomorphology. Autochthonous microbialite features occur in the form of phytotherm bubble.

Further inspection of the area in 2022 identified a number of larger more complex systems to the north of W9A, at locations W9B, W9C and W9D. Pools here are up to 10 m diameter (at W9B) and fed by more prevalent (measurable) flow of 1 – 4 L/min. The flow is noticeably discharging from the calcarenite ridge at which the pools sit at the base of. These pools also contain thicker (10 cm) microbialite sheets on the floor and sides of the pool systems.

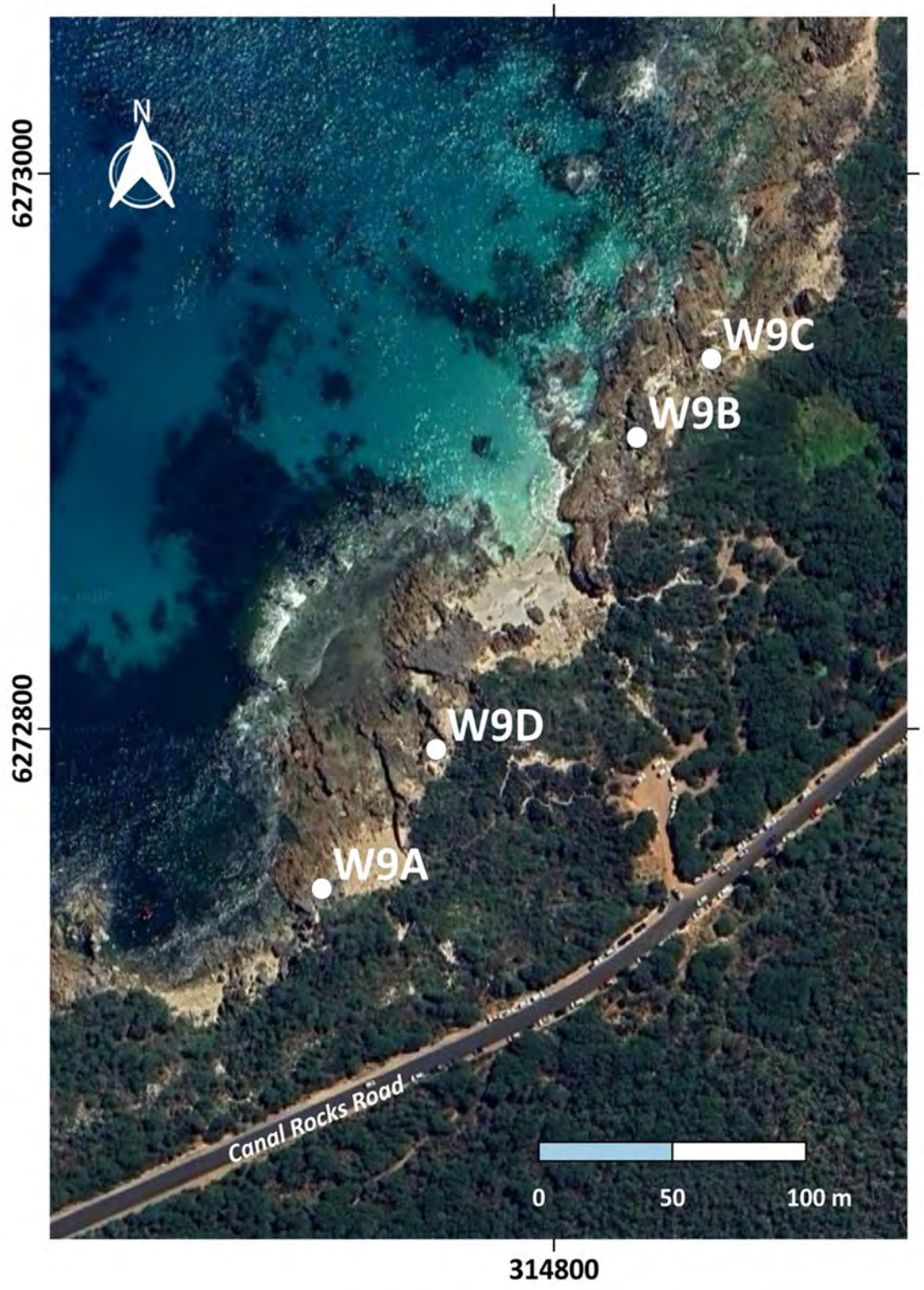

Figure 6 **Sample Location Sites for Canal Rocks**

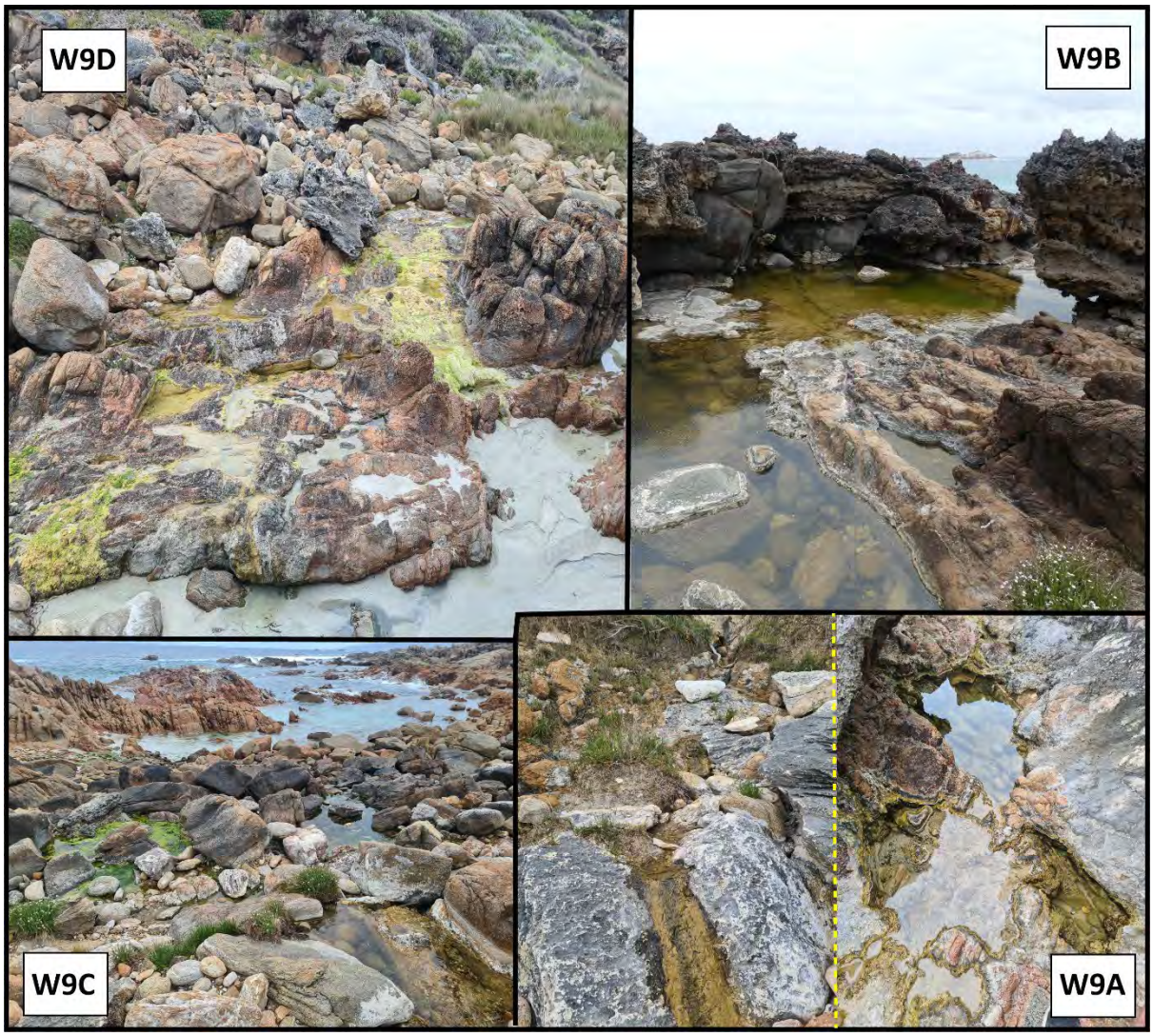

Figure 7 Photos of Canal Rocks Sites

METHODOLOGY

Field Parameters

Electrical conductivity (EC), salinity, pH, dissolved oxygen (DO), oxidation-reduction potential (ORP) and temperature were measured in the field using a calibrated YSI water quality field probe.

Both total alkalinity and dissolved carbon dioxide (CO_2) were measured, where possible, using HACH field titration kits, with results presented in mg/L.

Spring Flow Rates

At the entry and exit point of each pool locations, where visible seepage flow was identified, a flow rate was measured. To determine the flow rate a container of known volume was placed below the active flow and the time it took to fill that container was measured to provide the flow rate. Measurements were provided in litres per minute (L/min).

Major Ions and Nutrients

Samples for major ionic and nutrient analysis were collected from designated inflow and out flow points at each of the 12 locations, thus providing an overall batch of 24 water quality samples.

Laboratory analysis consisted of EC and pH, major cations (Na, Ca, Mg, K) and anions (Cl, SO_4, HCO_3, F). Nutrient analysis was also completed, this included reactive phosphorous (TRP), ammonia (NH_3), nitrate (NO_3), nitrite (NO_2), and total nitrogen (TN), which is NH_3, NO_3 and NO_2 combined. This analysis was undertaken at the ALS laboratories Perth Western Australia. All results and methods for ALS, including analyte detection limits are detailed in Appendix I.

Stable Water Isotopes

Stable water isotope analysis was completed on a sub-set of pool water samples from the three sites. The analysis was completed at the Biogeochemistry Research Infrastructure Platform (BIOGRIP) Node for Water and Soil Biogeochemistry at the Stellenbosch University, South Africa. Samples were analysed using a Los Gatos Triple Liquid Water Isotope Analyser (LGR T-LWIA-45_EP, Canada). Sample aliquots (1.9 ml) were filtered through 0.22 μm cellulose acetate syringe filters into 2 ml glass vials with PTFE septum caps. Each sample array was started with two calibration standards and a control standard, followed by 10 unknowns, and concluded with another sets of standards. The standard errors for three calibration standards for $\delta^{18}O$ and $\delta^{2}H$ were ± 0.2 – 0.7 ‰ and ± 0.2 – 0.9 ‰ respectively. Each sample run was composed of a maximum of four arrays. Each standard/sample was measured with nine injections, of which the first four were discarded and the results of the last five were averaged for absolute isotope ratios. The absolute isotope ratios are converted to δ-values through linear regression by using the known δ-values (with respect to Vienna Standard Mean Oceanic Water - VSMOW) of calibration standards before each array of 10 unknowns. Two sample runs per sample were performed and the mean δ-values were reported.

RESULTS

Spring Flow Rates

Only a sub-set of locations were identified to have measurable seepage flows into and/or out of the pools. These included three inflows at two Quarry Bay sites (W7C and W7D) and an additional measurement at Canal Rocks W9D. The four inflow rates determined were relatively consistent at 1 - 2 L/min. Out flows at these locations were measured as being an order of magnitude lower than the inflows at 0.1 L/min or less. All other inflows are deemed to be 0.1 L/min or lower.

Field Water Chemistry

Field water chemistry is presented in Figure 8. EC was generally below 10,000 µS/cm and in many cases below 5,000 µS/cm, meaning pools waters are classified as medium to highly saline. Several sites including W7B, W7C, W8C and W9A, displayed high variability in salinity. At these sites EC could be up to 25,000 µS/cm, with these high readings attributed to a strong influx of seawater directly into the pool mixing with the seepage groundwaters.

Pool water temperatures varied between 20 and 30°C with these differences reflecting sampling day and time. For example, the sampling at Contos Springs (occurred on 30th November 2022 when temperatures at Cape Leeuwin (BoM # 9518) were 3°C higher (24°C) that the day prior and the day after. Thus, microbial pool waters can be thought to be in intrinsically linked to the daily ambient temperatures with minimal buffering by the temperature of the inflowing spring water. The range of pH of the microbial AMC pool waters were consistently slightly alkaline (8 – 9). Oxidation Reduction Potential (ORP) were generally positive (50 -100 mV) indicating primarily oxidising environments for all sites.

Field total alkalinity ranged between 200 and 400 mg/L. For Quarry Bay, values were between 240 and 390 mg/L and an average of 313 mg/L. Alkalinity values are slightly lower at both Contos Springs and Canal Rocks averaging 275 mg/L. Dissolved CO_2 values ranged from 20 to 80 mg/L. Both Quarry Bay and Contos Springs had average CO_2 concentrations at 50 mg/L, while Canal Rocks were a little lower at 38 mg/L.

Laboratory General Chemistry

EC, pH, and total alkalinity were also determined at the Perth ALS laboratory. Laboratory EC was in the same range as field EC, between 2,000 to 9,000 µS/cm with the majority below 5,000 µS/cm. Laboratory pH also replicate those in the field being alkaline (~8 to 9) for all sites. Total Dissolved Solids (TDS) calculated from lab EC are between 700 and 6,000 mg/L. Total alkalinity values ranged between 150 and 350 mg/L, with bicarbonate (HCO_3) being the dominating form.

Comparisons of pH and total alkalinity values between inlet and outlets for all 12 pools identified distinct and consistent trends with pH increasing from inlet to outlet and total alkalinity decreasing from inlet to outlet. At several pool outflow points (W7B, W7C, W8A, W8C, W9B) carbonate (CO_3) alkalinity represents up to 10% of the total alkalinity. This reflects slight increases in pool water pHs to above 8.3 generating alkalinity in the carbonate form, while pHs of below 8.3 see bicarbonate ions tend to be the more dominant species of total alkalinity.

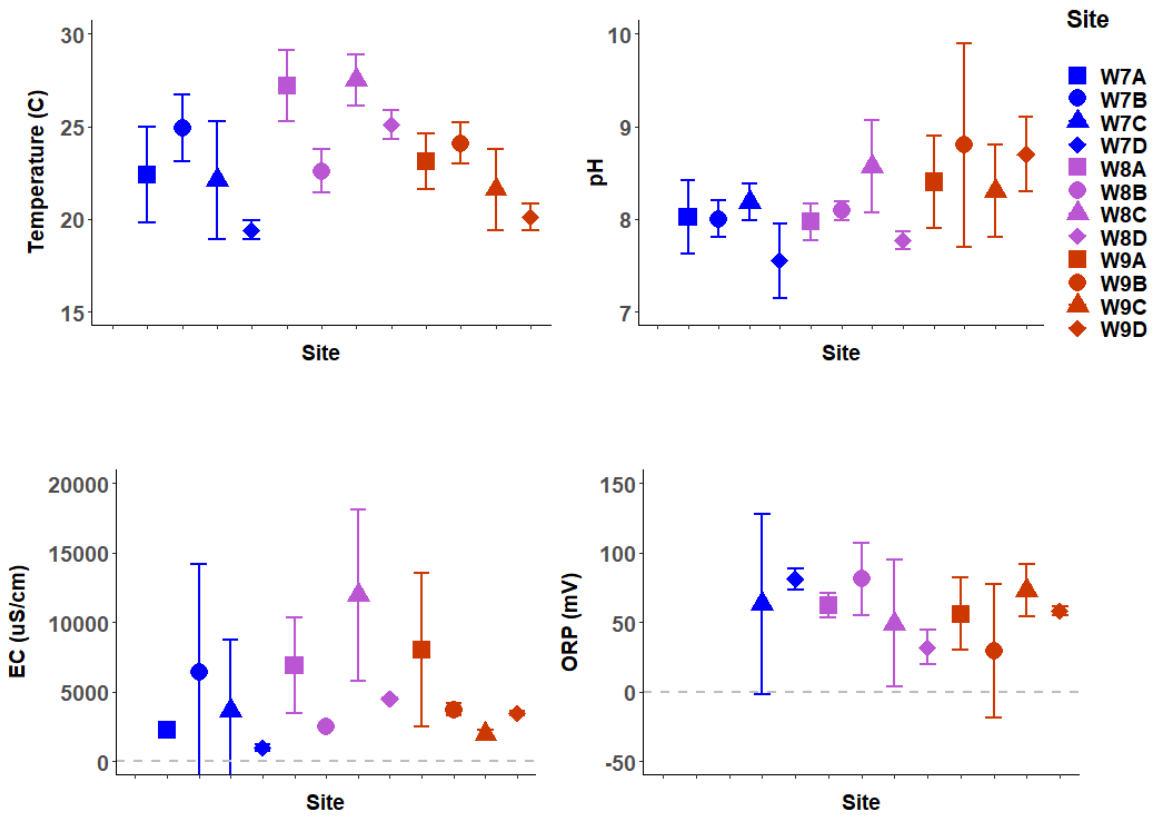

Figure 8 Average field measurements of temperature, pH, EC and ORP for the 12 field sample locations across the three field tufa sites.

Major Ionic Chemistry

Major ionic chemistry for the pool waters is presented as site specific piper plots (Figures 9,10, 11), with a Durov Plot in (Figure 12**)** used to present a combined comparative view of water chemistry for all sites. Microbialite pool water chemistry can be described as Na-Cl-HCO_3 dominated, with cations are Na>Ca>Mg>K and while anions area Cl>HCO_3>SO_4.

Minimal variation in ionic chemistry composition between sites is observed; however, Quarry Bay is slightly more Ca-CO_3 rich, compared to the strong Na-Cl signature seen for most microbialite pool waters. Despite a similar ionic composition at Contos Springs, higher overall concentrations reflect the site's higher TDS and EC profile.

Hydrochemical comparisons of the pool water ionic composition compared with that of rainfall, seawater and regional karst waters (Eberhard 2004) show that the karst waters are clearly more Ca-CO_3 rich, while rainfall and seawater ionic compositions are clearly more Na-Cl dominant (Figures 9,10, 11). This supports the concept of karst seeps and rainfall-seawater being two distinct hydrochemical end-members of the microbialite pools waters.

Similar to the slight difference in pH and alkalinity between pool inflow and outflow locations, there are also subtle differences in ionic chemistry. Generally, the outward flow locations have lower Ca concentrations than the corresponding inward flow locations. This is due to $CaCO_3$ precipitation occurring within the microbial pool systems as the water flows through the pool system. This precipitation process results in the general increase in pH and decrease in alkalinity in the outflow pool waters compared to the inflow locations.

Nutrients

Overall total reactive phosphorous (TRP) concentrations were below the lab detection limit of 0.01 mg/L, with one exception, an outflow location at Canal Rocks (W9DO), where TRP was 0.01 mg/L.

Total nitrogen (TN) at Quarry Bay ranged from 0 mg/L to 0.52 mg/L. Site D had the highest concentrations in the range of 0.52 mg/L for the inward flows and 0.33 mg /L for the outward flows. For this site all TN was in the form of NO_3. All three other sites had TN concentrations less than 0.15 mg/L with the outflow point generally being lower that in the inflow point. Especially at Site C where TN concentrations for inflow were 0.1 mg/L and below detection limits at the outflow point.

For Contos Springs, TN levels were generally higher, ranging from between 0.1 to 1.25 mg/L. Again, NO_3 was the dominant form, with minimal representation of the NH_3 form. In three out of the four pool locations the TN value of the inward flow point was higher than the outward flow point.

TN concentrations at Canal Rocks were intermediate, between Quarry Bay and Contos Springs values, ranging between 0.02 to 0.35 mg/L. Again, NO_3 was more dominant than NH_3 and, again the inward flow points to the pool had higher concentrations than most of the outward flow points.

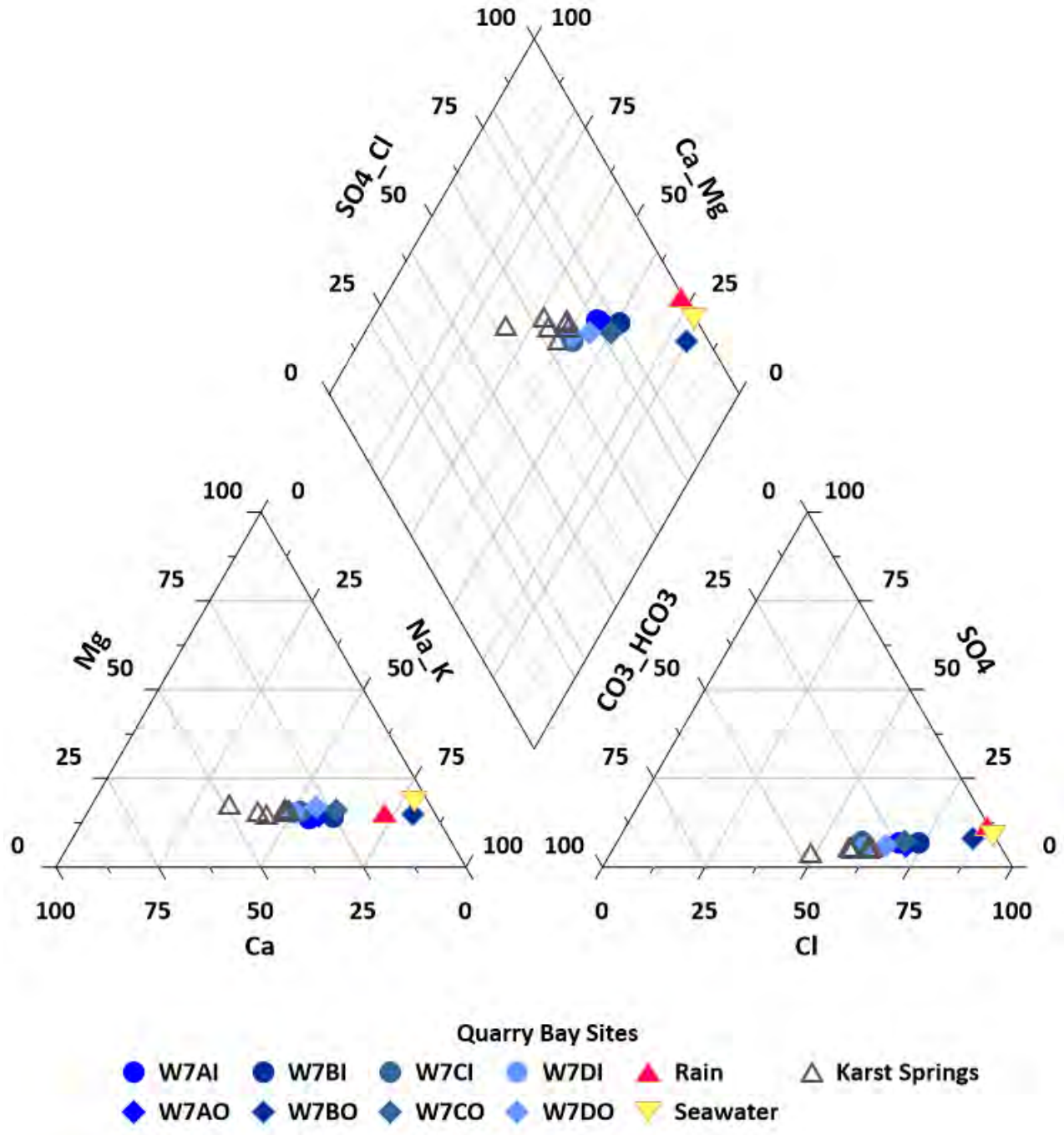

Figure 9 Quarry Bay 2022 Piper Plot

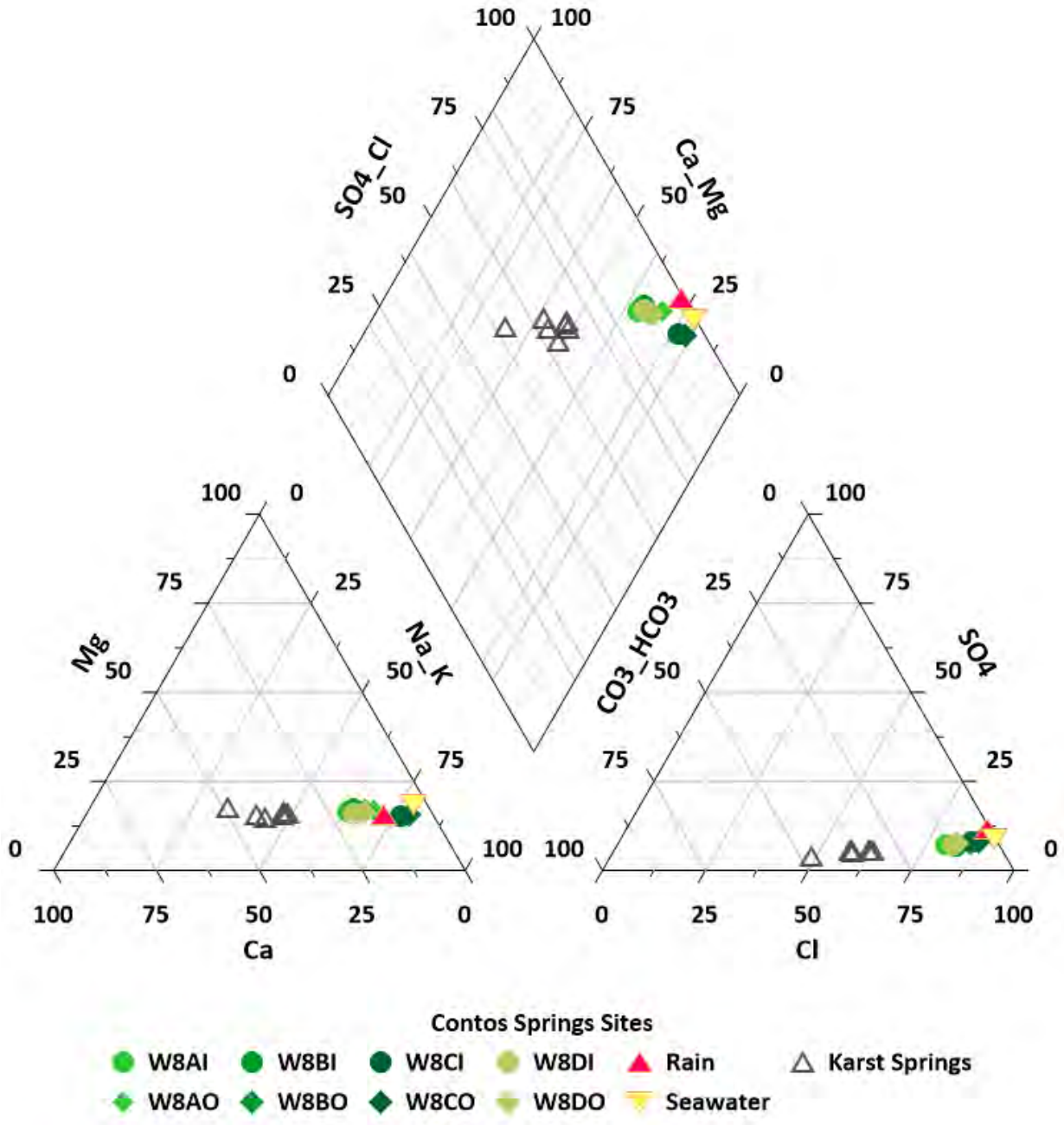

Figure 10 Contos Springs 2022 Piper Plot

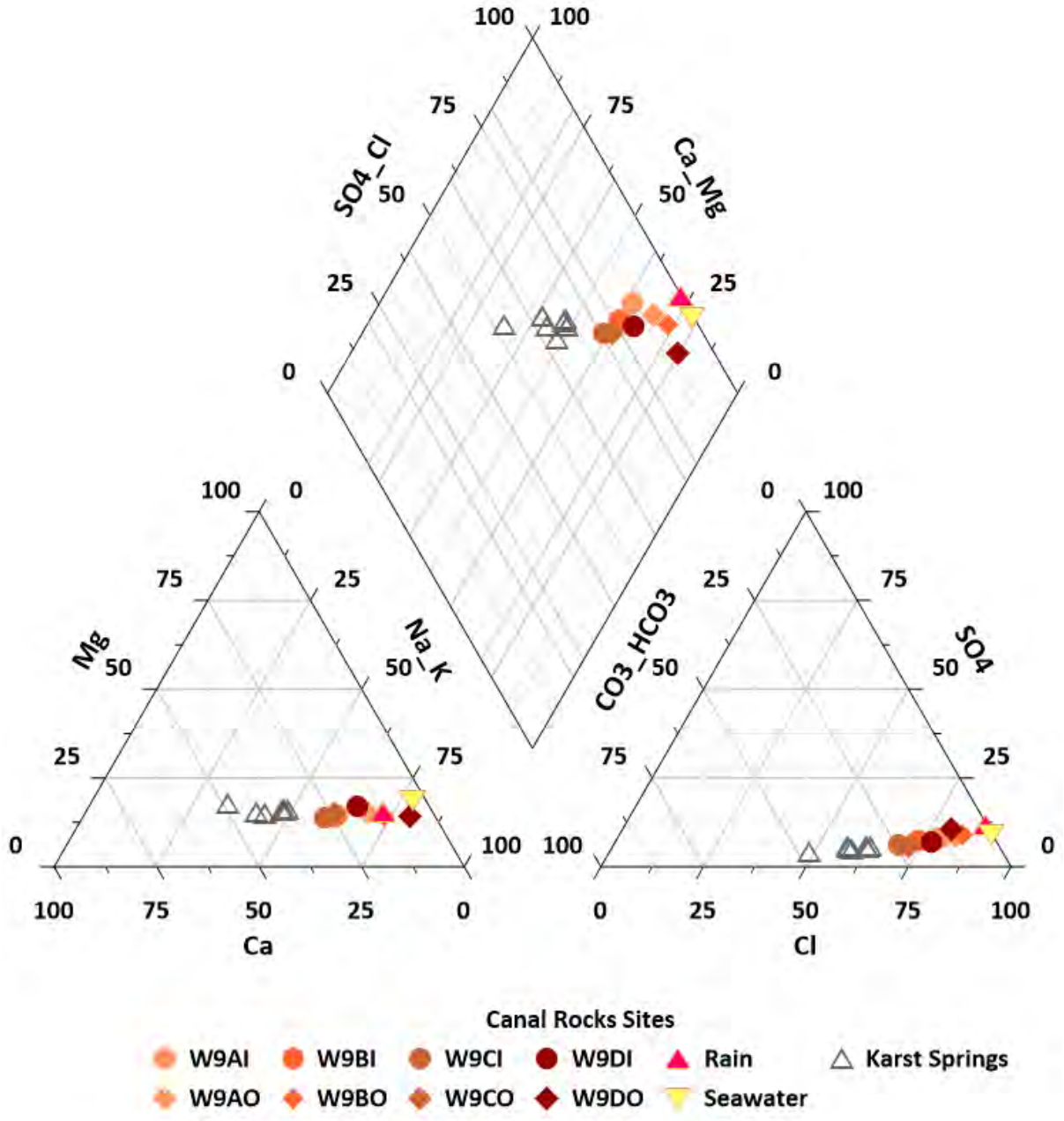

Figure 11 Canal Rocks Piper Plot

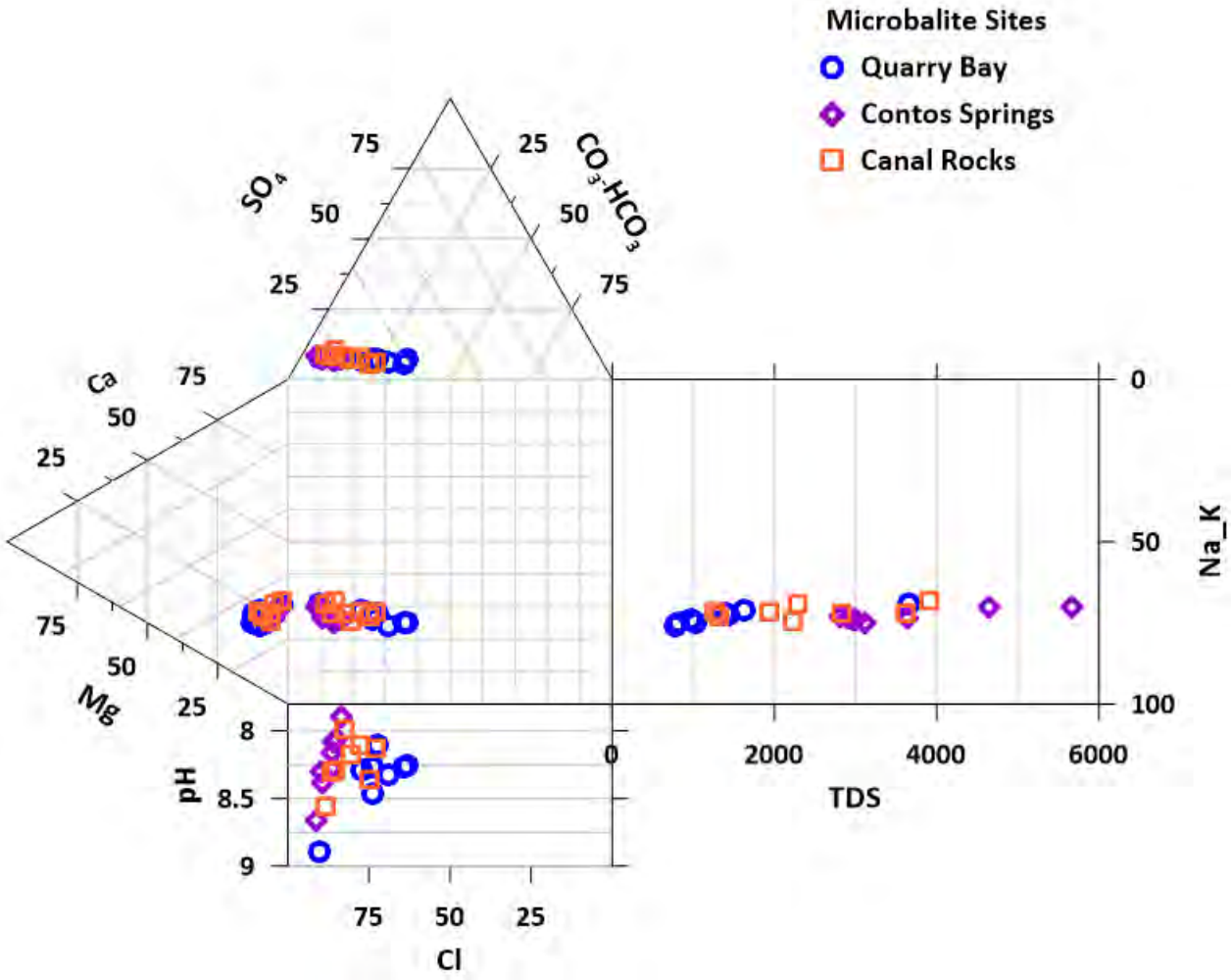

Figure 12 Combined 2022 Durov Plot for All Sites

Stable Water Isotopes

Stable water isotopes were analysed for a total of 13 samples from across the three locations, with a majority of samples collected from Quarry Bay. Consistent stable isotope values were determined for all samples with $\delta^{18}O$ values between -3 ‰ and -5.5 ‰ and $\delta^{2}H$ range between -13 ‰ and -23 ‰.

Deuterium excess (d-excess) is a second order stable isotope parameter measured in a meteoric water to understand both the source and the evolution of moisture during transport (Dansgaard 1964). Deuterium excess correlates with conditions at the oceanic source of precipitation and is expressed as a function of both oxygen and hydrogen isotopes in water. D-excess = $\delta^{2}H - 8 \times \delta^{18}O$. Consistent d-excess values are identified for all samples at between 11 ‰ and 23 ‰.

Calibrated $\delta^{18}O$ and $\delta^{2}H$, along with d-excess results are presented in Table 2.

Table 2 Stable Water Isotope Results

Site	Sample	$\delta^{2}H$ (‰) VSMOW	$\delta^{18}O$ (‰) VSMOW	D-excess (‰)	EC (µS/cm)
Quarry Bay	W7AI	-22.9	-5.32	19.66	2121
Quarry Bay	W7AI	-21.2	-5.06	19.28	2176
Quarry Bay	W7BI	-18.7	-4.59	18.02	2633
Quarry Bay	W7BI	-15.2	-3.89	15.92	2682
Quarry Bay	W7CI	-17.1	-4.45	18.5	1676
Quarry Bay	W7CI	-21.5	-5.37	21.46	2114
Quarry Bay	W7CO	-18.4	-4.85	20.4	1792
Quarry Bay	W7DI	-22.0	-5.52	22.16	816
Contos Springs	W8BI	-13.2	-3.23	12.64	4600
Contos Springs	W8A2	-19.3	-4.60	17.5	4753
Contos Springs	W8C2	-13.1	-3.11	11.78	8096
Canal Rocks	W9CI	-21.6	-5.07	18.96	7553
Canal Rocks	W9DI	-21.1	-5.05	19.3	4538

DISCUSSION

Hydro-geochemical Overview

Field and laboratory water quality data presented in this report allows for a comprehensive understanding on the hydro-chemical functioning of the AMC pools located at Quarry Bay, Contos Springs and Canal Rocks, south-west Western Australia. The water chemistry across the pools in all three sites identify Na-Cl-CO_3 dominated systems. The cation signature is Na>Ca>Mg>K and an anion signature of Cl>HCO_3>SO_4. All sites are slightly to moderately alkaline (pH 7.5 – 9.5); however, salinity (EC) is quite variable. This is attributed to inputs of variable mixes of fresh seep water and saline sea waters into the microbialite pool systems. Nutrients inputs, and concentrations, are very low, with phosphorous generally below limits of detection, and total nitrogen, dominated by the most stable form nitrate relative ammonia and nitrite, is below 1 mg/L.

Some minor changes in chemistry are identified between the inflow and outflow locations of the microbialite pool systems. These changes include an increase in pH and salinity, and conversely a decrease in alkalinity. These shifts are coupled with changes in ionic composition, particularly a decrease in calcium in the outflows, which is likely reflecting the bio-mediated precipitation of carbonate within the microbial pool systems. These processes will be evaluated further in the discussion.

2022 Water Quality Limits

The Western Australian Water Corporation has monitored the untreated water quality from the Leeuwin Spring Weir in accordance with the Australia Drinking Guidelines (DoW 2007). Water quality for the spring water is pH of 7.25 chloride of 225 mg/L and sodium of 120 mg/L. Salinity is 843 mg/L and NO_3+NO_2 is at 1 mg/L. Initial comparisons of microbialite pools water quality at Quarry Bay identifies similar characteristics, albeit with greater salinity in the microbialite pools, which is attributed to sea water inputs.

Comparisons with 2008-09 Water Quality Data.

During the 2008-09 assessment period water quality for all three sites were measured for both the summer and winter seasons, with this data being summarised by Forbes et al. (2010). In those investigations water temperatures ranged from 20°C - 24°C in the 2008-09 summer, like 2022. However, winter 2008 temperatures were much lower at below 16°C. The EC in pool waters were more variable in 2008-09 than the range measured in 2022, with a range of fresh (1000 µS.cm^{-1}) to saline (70,000 µs.cm^{-1}) conductivities observed historically. Extreme EC (>30,000 µs.cm^{-1}) concentrations identified in the 2008 summer months were due to evaporation and also following winter storm surges of seawater into the pool during winter months. As with 2022, slightly alkaline conditions were observed (pH 7 to 9) in 2008-09 and oxidation-reduction potential (ORP) of between 600 to 1000mV indicate oxidising conditions. Total nitrogen and phosphorous for all sites were the same as 2022 being generally below 1 mg/L.

Major hydrochemistry for the barrage pool sites in 2008-09 were considered as Na-Cl-HCO_3 dominated systems; during winter months barrage pools can exhibit Na-Cl concentrations equivalent to seawater. Cation order of dominance was Na Ca>Mg>K. Greater HCO_3

concentrations were observed during summer in comparison to winter. This summer peak is likely the result of reduced CO_2 degassing and in turn a decrease in carbonate precipitation resulting from reduced summer spring flows. Examination of HCO_3/Cl ratios in conjunction with Cl concentrations were used by Forbes et al. (2010) to examine the contributions of CO_2 degassing and seawater mixing to water composition. Increasing HCO_3/Cl ratios from winter to summer, combined with stable Cl concentrations suggests a reduction in CO_2 degassing during summer. In comparison, increase Cl relates to the effects of evaporation and or seawater mixing.

Comparisons of ionic water chemistry in piper plot format for the three sites between the 2008-09 and 2022 data sets is presented in Figure 13. This is to assess any significant changes in water composition. Evident is a slight shift in ionic water chemistry between the two time periods, primarily higher HCO_3 concentration relative to chloride, than compared to the samples recently measured in the 2022 summer. Whether this is due to permanent temporal changes is difficult to determine within the current dataset.

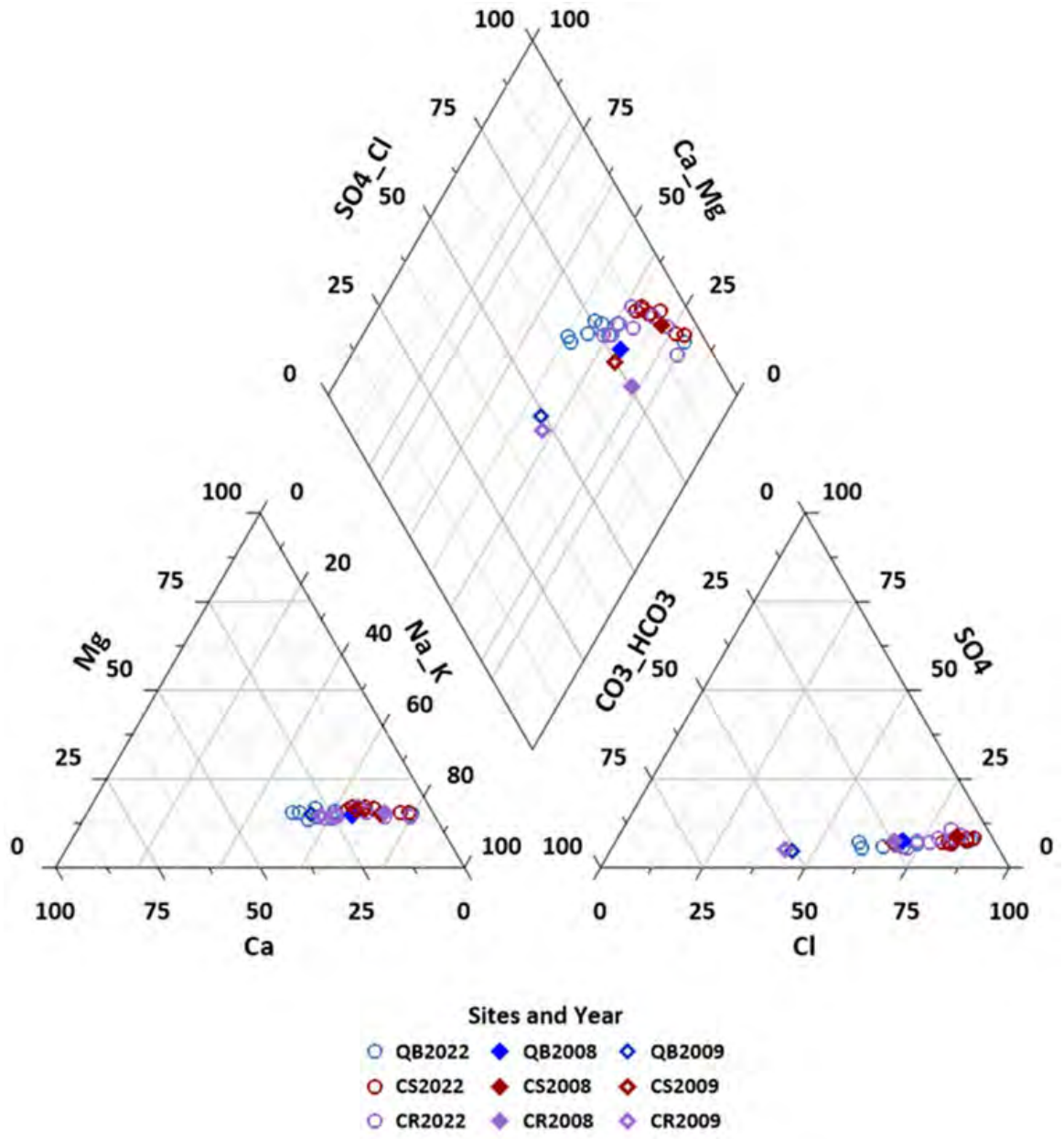

Figure 13 Piper Plot comparisons for pool water between 2008 (winter), 2009 (summer) and 2022 (this study, summer).

Hydrochemistry Ratios

Elemental ratios for microbial pool waters, when compared to similar ratios of potential end-members can provide insight into the generation of the water composition. Ratios chosen to analyse the tufa pool water composition include Na/Cl, Ca/Mg and HCO_3/Cl. End members include seawater, karst spring waters and rainfall, with data derived from Eberhard (2004) and Crosbie et al. (2012).

Ionic ratios are presented in Figure 14, evident are low Ca/Mg ratios for rainfall (0.3) and high Ca/Mg ratios for karst spring waters (2.2 – 3), with all pool waters falling between these values. Rainfall Ca/Mg ratios are generally like the pool waters. Comparisons of pool water inflows and outflows for each pool identify lower Ca/Mg ratios for the outflows compared to the inflows. While Na/Cl ratios are generally consistent between 0.6 and 0.9 Na/Cl, the ratios for the karst waters are overall slightly lower compared to pool waters and seawater.

Comparisons of Ca/Mg ratios with HCO_3/Cl ratios (Figure 14) identifies an even clearer end member mixing relationship for the pool waters. Again Ca/Mg ratios are greatest for karst waters, where seawater is the lowest, with rainfall like pool water. However, unlike Na/Cl, HCO_3/Cl vary in a similar fashion to Ca/Mg with karst waters having the highest values >0.3 and seawaters having the lowest <0.1, rainfall is also quite low (0.2). These ratios allow for some inferences about source waters and their contribution to the pools.

Essentially the carbonate rich karst rich waters contribute HCO_3 and Mg, while seawater contributes both Cl and Na. This end-member designation allows for a mixing model to be developed for the pool waters. A key observation is that the pool inflow chemistry is more akin in ionic ratios to that of the karst waters compared to pool outflow ionic chemistry, which has relatively lower HCO_3/Cl and Ca/Mg ratios. It is also observed that the Quarry Bay pools are more chemically linked to karst water composition than the Canal Rocks and the Contos Springs, with the latter being most similar to the ionic chemistry of seawater and rainwater.

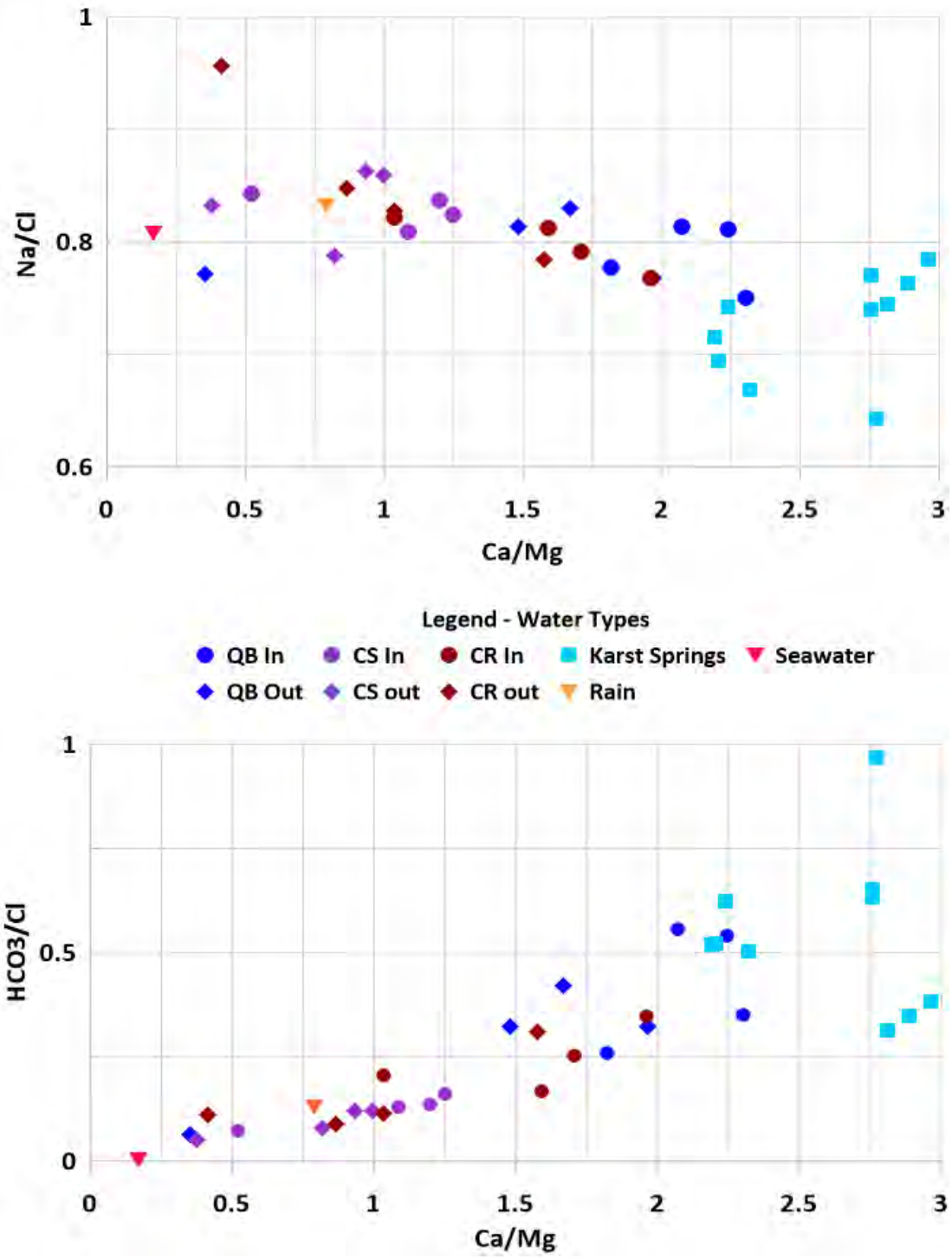

Figure 14 Hydrochemistry ratios for pool waters

Mineral Precipitation

To further understand the processes that drive changes in the microbialite pool water chemistry, Saturation Index (SI) calculations for calcite were evaluated. The calcite SI (SI_{cal}) is a useful means of describing, quantitatively the deviation of carbonate waters from equilibrium with respect to solid calcite-calcium carbonate (White 1988).

It is defined as:

$SI_{cal} = \log (K_{iap}/K_{eq})$

Where K_{iap} is the ion activity product of Ca_2+ and CO_3^{2-} and K_{eq} is a coefficient termed the thermodynamic equilibrium (or solubility product) constant (Ford and Williams 1989). The value of SI_{cal} indicates whether the solution is undersaturated (negative SI_{cal}), supersaturated (positive SI_{cal}), or at equilibrium (SI_{cal} = 0) with respect to calcite. Supersaturated waters will be capable of depositing calcium carbonate as materials such as tufa, whilst undersaturated waters will be chemically aggressive and capable of further dissolution of carbonates. Similar relationships can be derived for dolomite with the calculation of the saturation index for dolomite referred to as SI_{dol}.

The atomic ratio of calcium to magnesium (Ca/Mg) provides information on the type of rock-material that a water sample has been in contact with (White 1988). The parameter is derived from the measured concentrations

Ca/Mg = [Ca2+]/[Mg2+]

Mg dominated waters are derived through contact with ultrabasic rocks containing ferromagnesium minerals, whilst Ca dominated rocks are derived from limestones (White 1988). Ca/Mg = 1 for waters in contact with dolomite $CaMg(CO_3)_2$.

The determined SI_{cal} values are compared to Ca/Mg ratios to understand the processes that drive calcite precipitation. Comparisons SI_{cal} and SI_{dol} with Ca/Mg ratios for the microbial pool water sites are presented in Figure 15. The Ca/Mg ratio depends almost entirely on the limestone/dolomite ratio in the aquifer. Springs issuing from dolomite have a Ca/Mg ratio of 1, whereas limestone springs have Ca/Mg ratios of 3 to 10. Evident is the identification of three different water types; the first being Mg dominated, the second Ca dominated calcite saturated, and the third Ca-dominated calcite undersaturated. Contos Springs and Canal Rocks microbial pool waters are mostly Mg-dominated non-karst saturated, while Quarry Bay pool waters are Ca dominated saturated karst waters. Outflow pool water locations generally have lower Ca/Mg ratios than the relevant pool inflow locations water chemistry. This can be interpreted as the biomediation of the Ca and CO_3 in the pools by microbial processes.

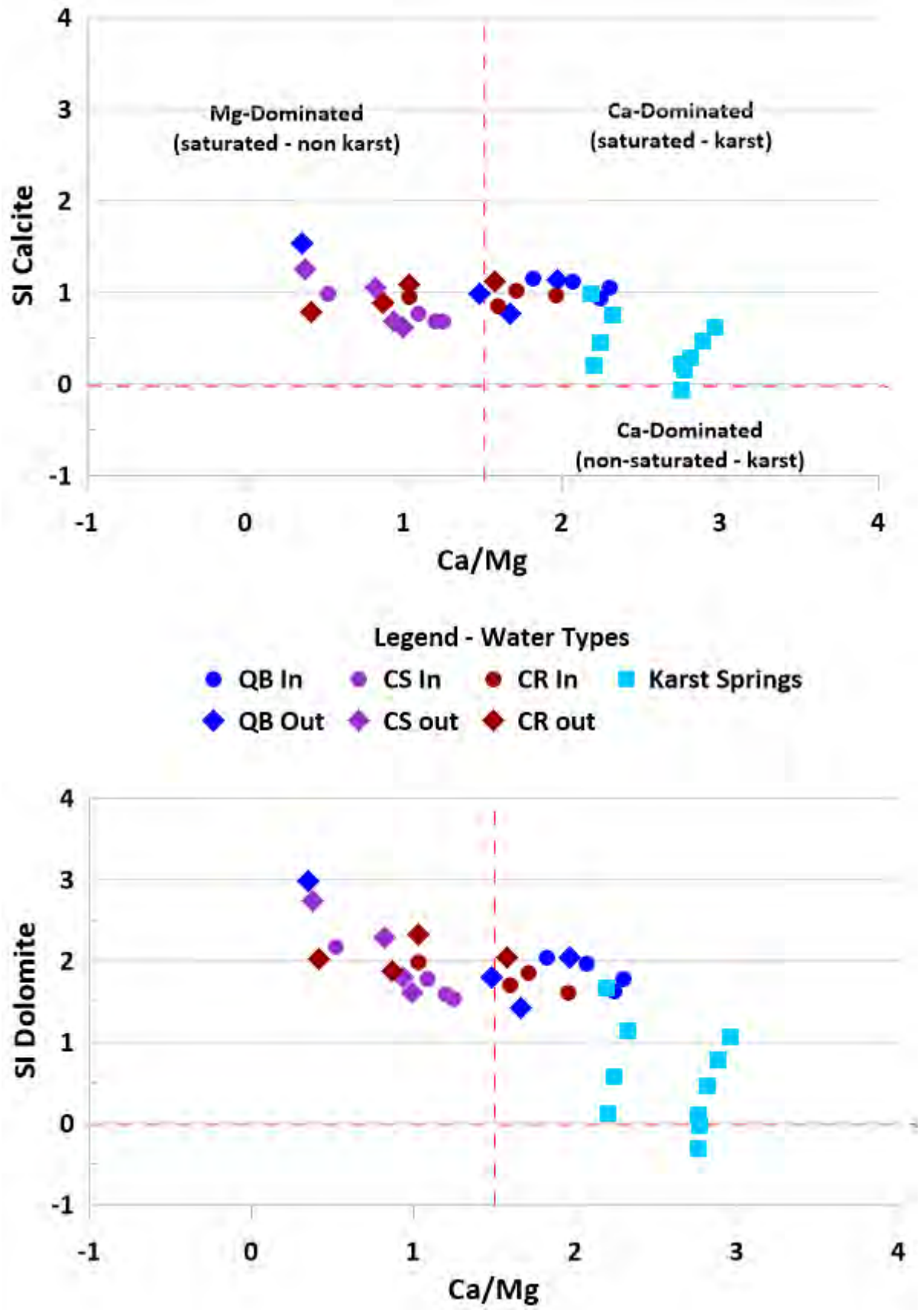

Figure 15 Saturation Indexes for calcite and dolomite

Water Isotope Signature

Stable water isotope data (Figure 16) for the three sites are combined to generate a local evaporation water line (LEWL), which is determined to be $\delta^2H = 4.16*\delta^{18}O+0.4$. This line can be compared to the local meteoric water line (LMWL) which is for Perth (Crosbie et al. 2012) Comparisons of stable water isotope data for the sites with other data collected for the region can shed insight to the hydrological functioning of the pool systems. Close correlation is observed between the microbialite pool waters stable isotope signature and those determined for cave drip waters in local cave in the Tamala Limestone (Griffiths et al. 2021; Priestley et al. 2020; 2023). This suggests little difference in the composition of these two waters and that their source is similar, which is hypothesised to be rainfall recharge through the Tamala Limestone.

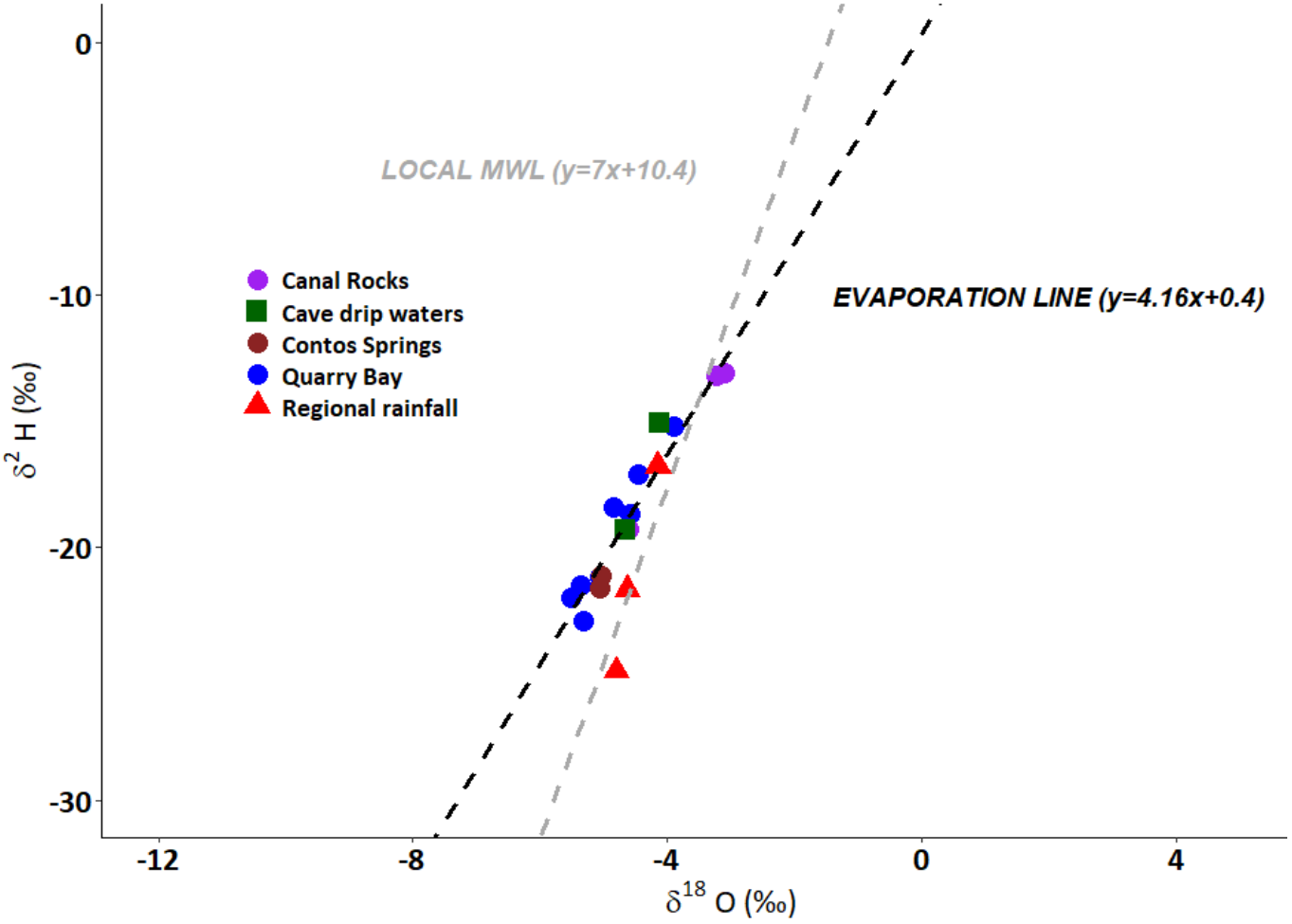

Figure 16 Stable Water Isotope Plot for Microbialite Site Pool Waters

SUMMARY

Microbialite pool water chemical composition

This report has used a combination of field chemistry parameters, major cation and anion analysis, nutrients and stable isotope results to characterise the hydrochemical functioning of the microbialite pools located at Quarry Bay, Contos Springs and Canal Rocks.

Pool water chemistry shows a consistent Na-Cl-CO_3 dominated systems across all three sites. The cation signature is Na>Ca>Mg>K and anion signature of Cl>HCO_3>SO_4. The slightly to moderately alkaline (pH 7.5 – 9.5) pH is also uniform; however, salinity (EC) is quite variable, which is attributed to the variable inputs into the system from fresh seep waters and saline sea waters. As a result, salinity varies with the microbialite pool proximal to the ocean, and also with weather cycles. In other words, salinities increase in pools adjacent to the ocean immediately after large swell events and storm surges. Despite this, salinity is still higher in the functioning microbialite pools compared to the fresh nature of the alkaline seepage inflows, with this contribution likely originating from sea spray inputs. Ionic chemistry and stable water isotope data supports the hypothesis that the pool waters originate from the regional karst aquifers and are modified by variable inputs of seawater both as storm surges and sea spray. In South Africa the coastal spring-fed microbialite pools are being investigated as potential monitoring locations for inland aquifer resources (Rishworth et al. 2024) and the link between karstic waters suggest that the AMCs might be useful in this regard too.

Beyond the overall consistent hydrochemical nature of the microbial pools, there are subtle differences in the inlet and outlet waters of the pools, which reflects the microbial fixation of carbonate that occurs within the pool systems, as well as some indications of nutrient uptake since outflow concentrations were mostly lower than inflow. Both HCO_3/Cl and Ca/Mg ratios increase when waters migrate through the pool systems, reflecting the precipitation of carbonates (primarily calcite) within the microbial pools. Nutrient inputs for the whole are very low, with phosphorous generally below detection and total nitrogen, in the form of nitrate and lesser ammonium below 1 mg/L.

These data have been formulated into an ecohydrological and hydrochemical conceptual model presented in Figure 17.

Ecological Water Requirements

Microbialite pool functioning and development is reliant on the presence and distribution of biotic elements, such as plants, algae, fungi and prokaryotes, throughout a spring system (Ford and Pedley 1996; Pentecost 2005, Jones and Renault 2010; Rishworth et al. 2017, 2020). Environmental parameters which can affect these biotic elements, and hence limit tufa development include temperature, pH, CO_2 degassing, nutrients, metals and other toxins and water composition.

Ecological water requirements for carbonate precipitation include suitable concentrations of HCO_3/CO_3, in 2008-09 concentrations were generally between 200 and 600 mg/L and can get as high as 1000 mg/L. In 2022 nutrient levels and carbonate concentrations are consistent with those determined during 2008-09 time period, which would suggest that no

major change has occurred to water quality has not changed in any major way over this time period.

The nutrient levels are seen to be below 1 mg/L, however, higher total nitrogen values (3 – 5 mg/l) observed at some inland water fall sites (Forbes et al. 2010) coincided with poor tufa development. Thus, such TN concentrations may be of a level that inhibits microbial growth via algae competition. Similar sites in South Africa have been identified with much higher TN concentrations (>10 mg/L) combined with strong microbialite functioning in the pools (Dodd 2024).

The spring water flow regime is another component than can affect the development of the microbialite pool systems and their persistence. Measured flow rates for 2022, where possible to quantify, identified flows into pools in the order of 1 to 4 L/min. Observations of former pools now dry, are likely result of seep flow diversions and would indicate that constant seep flow is an important driver of microbial pool growth and overall existence. These relict microbialite pool systems may also reflect a reduction in seep flows rather than a diversion.

Anecdotal evidence suggests that the creek-seep at Contos Spring (Contos Spring) is drier in 2022 than it historically was. Thus, long term quantification of seep flows and the water balance for the microbialite pools maybe more critical than the water quality, which appears to be relatively consistent. Recent research published by Preistley et al. (2023) investigated recharge rates in the karst systems via speleothem hydrochemistry indicated that groundwater recharge in the South-west Capes region has seen a significant decrease in the last 800 years compared to prior. Given that the microbial pool systems could be in the order of thousands of years in age, based on current sea level being stable for approximately 6000 years (Lambeck and Nakada 1990), then it is not unreasonable to argue that the current AMCs are experiencing an extended natural period of reduced flows across recent centuries. This pressure is being exasperated by groundwater extraction related to modern industries that the Margaret River region is famous for.

Recommendations

This report has provided a contemporary update of the hydrochemistry Augusta Microbial Communities first evaluated in 2008-09 by Forbes et al. (2010). The following recommendations are proposed based on the findings of this report. They are:

- Periodical monitoring of pool water quality (field and Lab), including ionic chemistry, nutrients and salinity;
- Pool water level measurements;
- Inflow and outflow measurements rates; and
- Groundwater level and quality monitoring.

This program should be instigated as bi-annual program. The author of this report can provide further information and guidance on the development of this program in consultation with DBCA staff members.

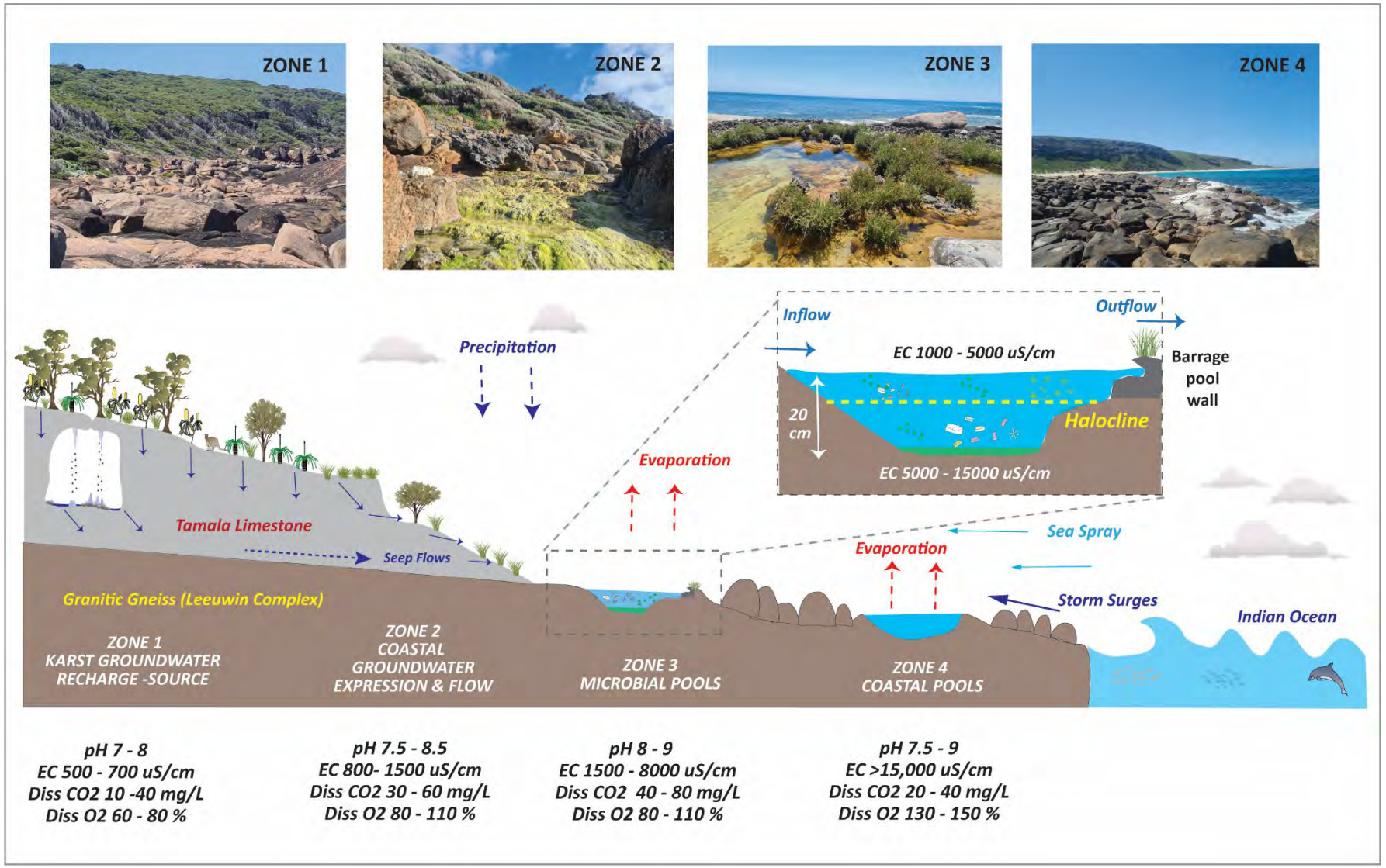

Figure 17 Ecohydrological and hydrochemical conceptual model for the Augusta Microbial Community (ACM) systems.

ADDITIONAL RESEARCH

In addition to the hydrochemistry work reported on here, a group of other components were sampled/measured during the November/December 2022 site visit. The focus of this additional work being the biological attributes and processes linked to the EPStromNet Project. These works are on-going requiring extensive lab and data analysis programs and will be reported at a later date once completed by the relevant international researchers.

Below is a summary of the list of the research component along with a brief summary of the program.

- **Microbial DNA-RNA:** a characterisation of the biofilm community using environmental metabarcoding;
- **Photosynthesis properties of microbialite pools:** quantification of photosynthetic efficiency linked to ambient temperatures (dark and light adaption);
- **Carbon Cycling:** a measure of primary productivity linked to respiration rates;
- **Geological and Geomorphological investigations:** multiple scale investigations of macrostructural processes and petrographic composition of microbialite facies; and
- **Invertebrate composition:** classification of the metazoan bioturbators that might disrupt microbialite growth and accretion.

In microbialite habitats the synergy between geological and biological processes is sometimes difficult to align. EPStromNet takes a unique “genes-to-geosphere” approach, bringing together expert researchers from diverse fields including cutting edge population and metagenomic approaches of biofilm communities and those who understand the formative geological and sedimentary drivers of coastal environments. This link is crucial in terms of understanding modern processes of supratidal spring-fed living microbialite ecosystem (SSLiME) formation and how this might inform the interpretation of past microbialite communities, as well as current connectivity hypotheses between local and global systems.

EPStromNet focusses on three elements: (1) global biodiversity assessment using metagenetics, (2) quantification of variability in biofilm processes, rates and gradients, and (3) global commonalities in geological and geochemical features. This comprises an integrated sampling campaign in all three global locations and will provide insights to SSLiME in a coordinated manner that thus far has not been possible without this multi-dimensional, global sampling strategy. It will also contribute to long-term sustainability of the global SSLiME network by facilitating collaboration between established and early-career academics across these disciplines and will coordinate knowledge-sharing workshops aligned with the project’s outcomes.

REFERENCES

Appleyard, S.J. 1989. Augusta Town Water Supply – decreasing yield of the Cape Leeuwin Spring, *Western Australia Geological Survey*, Hydrogeology Report No. 951.

Burne, R.V., Moore, L.S., 1987. Microbialites: Organosedimentray Deposits of Benthic Microbial Communities. Palaios, 2(3), 241-254. https://www.jstor.org/stable/3514674.

Cooper, A., Smith, A., Rishworth, G., Dodd, C., Forbes, M., Cawthra H., Anderson, C. 2022. Microbialites of Modern Siliclastic Rock Coasts. *Journal of Sedimentary Research*. 92, 619-634. DOI:10.2110/jsr.2021.071.

Cresswell G.J., 2003. The light of Leeuwin: The Augusta-Margaret River Shire History (new ed.) Margaret River, W.A: Augusta-Margaret River Shire History Group. ISBN 0731694449.

Crosbie, R., Morrow, D., Cresswell, R., Leaney, F., Lamontagne, S., Lefournour, M., 2012. New Insights to the chemical and isotopic composition of Rainfall across Australia. CSIRO Water for a Healthy Country Flagship Report ISSN: 1835-095X.

Dansgaard, W., 1964. Stable isotopes in precipitation. *Tellus* 16; 435-468.

Department of Water (DoW) 2007. Leeuwin Spring Catchment Area and Fisher Road Wellfield Water Reserve Drinking Water Source Protection Plan – Augusta Town. Water Resource Protection Series. Water Supply Report No. WRP 79.

Dodd, C., 2024. The Algoa Bay Region Groundwater Cycle – linking source to coast. Ph.D Thesis. Nelson Mandela University.

Eberhard, S.M., 2004. Ecology and hydrology of a threatened groundwater-dependent ecosystem: The Jewel cave karst system in Western Australia. PhD Thesis. Murdoch University.

Forbes M.S., Vogwill, R., Onton K. 2010. A characterisation of the coastal tufa deposits of south-west Western Australia. *Sedimentary Geology* 232, 52-65. https://doi.org/10.1016/j.sedgeo.2010.09.009.

Ford and Pedley 1996. A review of tufa and travertine deposits of the world. *Earth Science Reviews* 41, 117–175.

Ford and Williams 1989. Karst Geomorphology and Hydrology. Springer, Berlin.

Garner, T.W., Cooper, A.G., Smith, A.M., Rishworth, G.M., Forbes, M.S. 2024. Reviews and Synthesis: Tufa microbialites on rocky coastlines towards an integrated terminology. E*GUsphere*, 2024-243, 1-42. https://doi.org/10.5194/egusphere-2024-243.

Garner, T.W., Cooper, J.A.G., Smith, A. 2025. Marginal marine spring carbonates defining an emergent rocky shoreline at Cape Freycinet, Western Australia. Marine Geology. 481, 107496. https://doi.org/10.1016/j.margeo.2025.107496

Griffiths, A.D., Treble, P.C., Hope, P., Rudeva, I., 2021. Rainfall Stable Water Isotope Variability in Coastal South-western Western Australia and its relationship to climate on multiple timescales. *Journal of Geophysical Research: Atmospheres* 127. https://doi. org/10.1029/2021JD035433.

Johnson S.L., 2000. Assessment of groundwater resources in the Busselton-Capel Groundwater Area, Water and Rivers Commission, Hydrogeology Report 164.

Jones and Renault 2010. Calcareous spring deposits in continental settings. *Developments in Sedimentology* 61, 177–224.
Lambeck K., Nakada, M., 1990. Late Pleistocene and Holocene sea-level change along the Australian coast. Palaeogeography, Palaeoclimatology, Palaeoecology. Volume 89 (1-2), 143-176.

Lasky R.P., 1993. A structural study of the southern Perth Basin. Geological Survey of Western Australia. Report 31.

Lipar, M., Webb, J.A., 2014. Middle-late Pleistocene and Holocene chronostratigraphy and climate history of the Tamala Limestone, Cooloongup and Safety Bay Sands, Nambung National Park, south-western Western Australia. *Australian Journal of Earth Sciences*. 61, 1023-1039.

Myers 1994. Late Proterozoic high-grade gneiss complex between Cape Leeuwin and Cape Naturaliste. Geological Society of Australia (WA Division) Excursion Guidebook 6. 26pp.

Onton, K., Forbes, M.S., 2009. Augusta microbial threatened ecological community monitoring report. Technical report Department of Environment and Conservation, Bunbury, Australia.

Onton, K., Clarke, V. and Harding, C. 2009. Monitoring Protocol: Augusta Microbial Threatened Ecological Community. Version 1.0 (August 2009). Prepared for Significant Native Species and Ecological Communities – Resource Condition Monitoring Project, Department of Environment and Conservation, Western Australia.

Pentecost, 2005. Travertine. Springer Science and Business Media, Berlin.

Perrissinotto, R., Bornmna, T.G., Steyn, P., Miranda, N.A.F., Dorromgton, R.A., Matcher, G.F., Strydom, N, Peer, N., 2014. Tufa stromatolite ecosystems on the South African south coast. *South African Journal of Science*. 110. 10.1590/sajs.2014/20140011.

Playford, P.E., Cockbain, A.E., Low, G.H., 1976. Geology of the Perth Basin, Western Australia. *Western Australian Geological Survey Bulletin* 124.

Priestley S.C., Treble, P.C., Griffiths, A.D., Baker, A., NerilieJ. 2023. Caves demonstrate decrease in rainfall recharge of south-west Australian groundwater is unprecedented for the last 800 years. *Communications Earth and Environment* 4, 206.

Preistley S.C., Meredith, K.T., Treble, P.C., Cendon, D.I., Griffiths, A.D., Hollins, S.E., Baker, A., Pigois, J-H. 2020. A 35ka record of groundwater recharge in south-west Australia using stable water isotopes. *Science of the Total Environment*, 717. 135105. https://doi.org/10.1016/j.scitotenv.2019.135105.

Reid, R.P., Visscher, P.T., Decho, A.W., Stolz, J.F., DesMarais, D.J., 2000. The role of microbes in accretion, lamination and early lithification of modern marine stromatolites. *Nature* 406: 989-992. https://doi.org/10.1038/35023158.

Rishworth, G.M., Perissonotto, R., Bornman, T.G., Lemley, D.A. 2017. Peritidal stromatolites at the convergence of groundwater seepage and marine incursion: patterns of salinity, temperature and nutrient variability. *Journal of Marine Systems.* 167, 68-77.

Rishworth, G.M., Dodd, C., Perissinotto, R., Bornman, T.G., Adams, J.B., Anderson, C.R., Cawthra, H.C., Dorrington, R.A., du Toit, H., Edworthy, C., Gibb, R.-L.A., Human, L.R.D., Isemonger, E.W., Lemley, D.A., Miranda, N.A.F., Peer, N., Raw, J.L., Smith, A.M., Steyn, P.-P., Strydom, N.A., Teske, P.R., Welman, S., 2020. Modern supratidal microbialites fed by groundwater: functional drivers, value and trajectories. Earth-Science Reviews 210, 103364.

Rishworth, G.M., Dodd, C., O'Connell, T., Adams, J.B., Anderson, C., Bornman, T.G., Cawthra, H.C., Kock, L.D., Gama, P.T., Human, L.R.D., Lemley, D.A., Manziya, M., 2024. Coastal microbialite seeps as accessible monitoring locations of local aquifer resources. Report to the Water Research Commission, ISBN 978-0-6392-0645-5

Smith, I., McIntosh, P., Ansell, T.J., Reason C.J.C., McInnes, K., 2000. South-west Western Australia winter rainfall and its association with Indian Ocean climate variability. *International Journal of Climatology.* 20(15): 1913-1930.

Smith, A.M., Uken, R. 2003. Living marine stromatolites at Kei River mouth. South African Journal of Science, 99.

Suarez-Gonzalez, P., Benito, M.I., Quijada, I.E., Mas, R., Campos-Soto, S., 2019. 'Trapping and binding': a review of the factors controlling development of fossil agglutinated microbialites and their distribution in space and time. *Earth-Science Reviews* 194: 184-215. https://doi.org/10.1016/j.earscirev.2019.05.007.

White. W.B., 1988. Geomorphology and hydrology of karst terrains. Oxford University Press. New York.

APPENDIX I ALS Laboratory Results

ALS Environmental

CERTIFICATE OF ANALYSIS

Work Order	: **EP2216518**	Page	: 1 of 12
Client	: **EPStromnet Research Group; University of Essex**	Laboratory	: Environmental Division Perth
Contact	: DR MATTHEW FORBES	Contact	: Customer Services EP
Address	: 3SW.5.33A, Colchester Campus, Wivenhow Park COLCHESTER CO4 3SQ	Address	: 26 Rigali Way Wangara WA Australia 6065
Telephone	: ----	Telephone	: +61-8-9406 1301
Project	: Epstrom Research Group	Date Samples Received	: 05-Dec-2022 10:00
Order number	: ----	Date Analysis Commenced	: 07-Dec-2022
C-O-C number	: ----	Issue Date	: 08-Feb-2023 08:12
Sampler	: MATTHEW FORBES		
Site	: ----		
Quote number	: EP/929/22		
No. of samples received	: 24		
No. of samples analysed	: 24		

ilac-MRA NATA
Accreditation No. 825
Accredited for compliance with ISO/IEC 17025 - Testing

This report supersedes any previous report(s) with this reference. Results apply to the sample(s) as submitted, unless the sampling was conducted by ALS. This document shall not be reproduced, except in full.

This Certificate of Analysis contains the following information:

- General Comments
- Analytical Results

Additional information pertinent to this report will be found in the following separate attachments: Quality Control Report, QA/QC Compliance Assessment to assist with Quality Review and Sample Receipt Notification.

Signatories

This document has been electronically signed by the authorized signatories below. Electronic signing is carried out in compliance with procedures specified in 21 CFR Part 11.

Signatories	*Position*	*Accreditation Category*
Chris Lemaitre	Laboratory Manager (Perth)	Perth Inorganics, Wangara, WA

General Comments

The analytical procedures used by ALS have been developed from established internationally recognised procedures such as those published by the USEPA, APHA, AS and NEPM. In house developed procedures are fully validated and are often at the client request.

Where moisture determination has been performed, results are reported on a dry weight basis.

Where a reported less than (<) result is higher than the LOR, this may be due to primary sample extract/digestate dilution and/or insufficient sample for analysis.

Where the LOR of a reported result differs from standard LOR, this may be due to high moisture content, insufficient sample (reduced weight employed) or matrix interference.

When sampling time information is not provided by the client, sampling dates are shown without a time component. In these instances, the time component has been assumed by the laboratory for processing purposes.

Where a result is required to meet compliance limits the associated uncertainty must be considered. Refer to the ALS Contract for details.

Key : CAS Number = CAS registry number from database maintained by Chemical Abstracts Services. The Chemical Abstracts Service is a division of the American Chemical Society.
LOR = Limit of reporting
^ = This result is computed from individual analyte detections at or above the level of reporting
ø = ALS is not NATA accredited for these tests.
~ = Indicates an estimated value.

- As per QWI – EN55-3 Data Interpreting Procedures, Ionic balances are typically calculated using Major Anions - Chloride, Alkalinity and Sulfate; and Major Cations - Calcium, Magnesium, Potassium and Sodium. Where applicable and dependent upon sample matrix, the Ionic Balance may also include the additional contribution of Ammonia, Dissolved Metals by ICPMS and H+ to the Cations and Nitrate, SiO2 and Fluoride to the Anions.
- EA016: Calculated TDS is determined from Electrical conductivity using a conversion factor of 0.65.
- Sodium Adsorption Ratio (where reported): Where results for Na, Ca or Mg are <LOR, a concentration at half the reported LOR is incorporated into the SAR calculation. This represents a conservative approach for Na relative to the assumption that <LOR = zero concentration and a conservative approach for Ca & Mg relative to the assumption that <LOR is equivalent to the LOR concentration.

Analytical Results

Sub-Matrix: WATER (Matrix: WATER)			Sample ID	W7AI	W7AO	W7BI	W7BO	W7CI
			Sampling date / time	05-Dec-2022 00:00	05-Dec-2022 00:00	05-Dec-2022 00:00	05-Dec-2022 00:00	05-Dec-2022 00:00
Compound	CAS Number	LOR	Unit	EP2216518-001	EP2216518-002	EP2216518-003	EP2216518-004	EP2216518-005
				Result	Result	Result	Result	Result
EA005P: pH by PC Titrator								
pH Value	----	0.01	pH Unit	8.11	8.27	8.29	8.89	8.25
EA010P: Conductivity by PC Titrator								
Electrical Conductivity @ 25°C	----	1	µS/cm	2180	2230	2550	5710	1610
EA016: Calculated TDS (from Electrical Conductivity)								
Total Dissolved Solids (Calc.)	----	1	mg/L	1420	1450	1660	3710	1050
EA065: Total Hardness as CaCO3								
Total Hardness as CaCO3	----	1	mg/L	462	452	464	468	367
ED037P: Alkalinity by PC Titrator								
Hydroxide Alkalinity as CaCO3	DMO-210-001	1	mg/L	<1	<1	<1	<1	<1
Carbonate Alkalinity as CaCO3	3812-32-6	1	mg/L	<1	<1	<1	37	<1
Bicarbonate Alkalinity as CaCO3	71-52-3	1	mg/L	318	304	290	144	325
Total Alkalinity as CaCO3	----	1	mg/L	318	304	290	181	325
ED041G: Sulfate (Turbidimetric) as SO4 2- by DA								
Sulfate as SO4 - Turbidimetric	14808-79-8	1	mg/L	72	63	79	205	56
ED045G: Chloride by Discrete Analyser								
Chloride	16887-00-6	1	mg/L	526	546	645	1640	339
ED093F: Dissolved Major Cations								
Calcium	7440-70-2	1	mg/L	129	120	120	49	99
Magnesium	7439-95-4	1	mg/L	34	37	40	84	29
Sodium	7440-23-5	1	mg/L	256	272	325	821	179
Potassium	7440-09-7	1	mg/L	6	7	9	39	6
EK040P: Fluoride by PC Titrator								
Fluoride	16984-48-8	0.1	mg/L	0.2	0.2	0.3	0.4	0.3
EK055G: Ammonia as N by Discrete Analyser								
Ammonia as N	7664-41-7	0.01	mg/L	<0.01	0.02	0.03	0.02	0.02
EK057G: Nitrite as N by Discrete Analyser								
Nitrite as N	14797-65-0	0.01	mg/L	<0.01	<0.01	<0.01	<0.01	<0.01
EK058G: Nitrate as N by Discrete Analyser								
Nitrate as N	14797-55-8	0.01	mg/L	0.10	0.10	0.03	<0.01	0.08
EK059G: Nitrite plus Nitrate as N (NOx) by Discrete Analyser								
Nitrite + Nitrate as N	----	0.01	mg/L	0.10	0.10	0.03	<0.01	0.08
EK071G: Reactive Phosphorus as P by discrete analyser								
Reactive Phosphorus as P	14265-44-2	0.01	mg/L	<0.01	<0.01	<0.01	<0.01	<0.01

Analytical Results

Sub-Matrix: WATER (Matrix: WATER)			Sample ID	W7AI	W7AO	W7BI	W7BO	W7CI
			Sampling date / time	05-Dec-2022 00:00	05-Dec-2022 00:00	05-Dec-2022 00:00	05-Dec-2022 00:00	05-Dec-2022 00:00
Compound	CAS Number	LOR	Unit	EP2216518-001	EP2216518-002	EP2216518-003	EP2216518-004	EP2216518-005
				Result	Result	Result	Result	Result
EN055: Ionic Balance								
ø **Total Anions**	----	0.01	meq/L	**22.7**	**22.8**	**25.6**	**54.1**	**17.2**
ø **Total Cations**	----	0.01	meq/L	**20.5**	**21.0**	**23.6**	**46.1**	**15.3**
ø **Ionic Balance**	----	0.01	%	**5.01**	**3.98**	**4.03**	**8.06**	**6.02**

Analytical Results

Sub-Matrix: WATER (Matrix: WATER)			Sample ID	W7CO	W7DI	W7DO	W8AI	W8AO
			Sampling date / time	05-Dec-2022 00:00	05-Dec-2022 00:00	05-Dec-2022 00:00	05-Dec-2022 00:00	05-Dec-2022 00:00
Compound	CAS Number	LOR	Unit	EP2216518-006	EP2216518-007	EP2216518-008	EP2216518-009	EP2216518-010
				Result	Result	Result	Result	Result
EA005P: pH by PC Titrator								
pH Value	----	0.01	pH Unit	8.46	8.27	8.32	7.90	8.38
EA010P: Conductivity by PC Titrator								
Electrical Conductivity @ 25°C	----	1	µS/cm	1520	1280	1210	4620	5690
EA016: Calculated TDS (from Electrical Conductivity)								
Total Dissolved Solids (Calc.)	----	1	mg/L	988	832	786	3000	3700
EA065: Total Hardness as CaCO3								
Total Hardness as CaCO3	----	1	mg/L	276	307	264	814	832
ED037P: Alkalinity by PC Titrator								
Hydroxide Alkalinity as CaCO3	DMO-210-001	1	mg/L	<1	<1	<1	<1	<1
Carbonate Alkalinity as CaCO3	3812-32-6	1	mg/L	11	<1	2	<1	9
Bicarbonate Alkalinity as CaCO3	71-52-3	1	mg/L	190	250	194	326	222
Total Alkalinity as CaCO3	----	1	mg/L	201	250	196	326	231
ED041G: Sulfate (Turbidimetric) as SO4 2- by DA								
Sulfate as SO4 - Turbidimetric	14808-79-8	1	mg/L	51	33	33	144	191
ED045G: Chloride by Discrete Analyser								
Chloride	16887-00-6	1	mg/L	362	268	271	1180	1660
ED093F: Dissolved Major Cations								
Calcium	7440-70-2	1	mg/L	66	85	66	181	150
Magnesium	7439-95-4	1	mg/L	27	23	24	88	111
Sodium	7440-23-5	1	mg/L	191	141	146	631	848
Potassium	7440-09-7	1	mg/L	4	3	3	29	40
EK040P: Fluoride by PC Titrator								
Fluoride	16984-48-8	0.1	mg/L	0.3	0.2	0.2	0.3	0.3
EK055G: Ammonia as N by Discrete Analyser								
Ammonia as N	7664-41-7	0.01	mg/L	<0.01	<0.01	0.03	0.03	0.05
EK057G: Nitrite as N by Discrete Analyser								
Nitrite as N	14797-65-0	0.01	mg/L	<0.01	<0.01	<0.01	<0.01	<0.01
EK058G: Nitrate as N by Discrete Analyser								
Nitrate as N	14797-55-8	0.01	mg/L	<0.01	0.52	0.30	0.68	0.04
EK059G: Nitrite plus Nitrate as N (NOx) by Discrete Analyser								
Nitrite + Nitrate as N	----	0.01	mg/L	<0.01	0.52	0.30	0.68	0.04
EK071G: Reactive Phosphorus as P by discrete analyser								
Reactive Phosphorus as P	14265-44-2	0.01	mg/L	<0.01	<0.01	<0.01	<0.01	<0.01

Analytical Results

Sub-Matrix: WATER (Matrix: WATER)				Sample ID	W7CO	W7DI	W7DO	W8AI	W8AO
				Sampling date / time	05-Dec-2022 00:00	05-Dec-2022 00:00	05-Dec-2022 00:00	05-Dec-2022 00:00	05-Dec-2022 00:00
Compound	CAS Number	LOR	Unit		EP2216518-006	EP2216518-007	EP2216518-008	EP2216518-009	EP2216518-010
					Result	Result	Result	Result	Result
EN055: Ionic Balance									
ø **Total Anions**	----	0.01	meq/L		**15.3**	**13.2**	**12.2**	**42.8**	**55.4**
ø **Total Cations**	----	0.01	meq/L		**13.9**	**12.3**	**11.7**	**44.5**	**54.5**
ø **Ionic Balance**	----	0.01	%		**4.67**	**3.51**	**2.30**	**1.91**	**0.81**

Analytical Results

Sub-Matrix: WATER (Matrix: WATER)			Sample ID	W8BI	W8BO	W8CI	W8CO	W8DI
			Sampling date / time	05-Dec-2022 00:00	05-Dec-2022 00:00	05-Dec-2022 00:00	05-Dec-2022 00:00	05-Dec-2022 00:00
Compound	CAS Number	LOR	Unit	EP2216518-011	EP2216518-012	EP2216518-013	EP2216518-014	EP2216518-015
				Result	Result	Result	Result	Result
EA005P: pH by PC Titrator								
pH Value	----	0.01	pH Unit	8.08	8.28	8.30	8.66	8.06
EA010P: Conductivity by PC Titrator								
Electrical Conductivity @ 25°C	----	1	µS/cm	4880	4680	7260	8860	4380
EA016: Calculated TDS (from Electrical Conductivity)								
Total Dissolved Solids (Calc.)	----	1	mg/L	3170	3040	4720	5760	2850
EA065: Total Hardness as CaCO3								
Total Hardness as CaCO3	----	1	mg/L	834	708	758	783	751
ED037P: Alkalinity by PC Titrator								
Hydroxide Alkalinity as CaCO3	DMO-210-001	1	mg/L	<1	<1	<1	<1	<1
Carbonate Alkalinity as CaCO3	3812-32-6	1	mg/L	<1	<1	<1	30	<1
Bicarbonate Alkalinity as CaCO3	71-52-3	1	mg/L	287	240	257	182	271
Total Alkalinity as CaCO3	----	1	mg/L	287	240	257	212	271
ED041G: Sulfate (Turbidimetric) as SO4 2- by DA								
Sulfate as SO4 - Turbidimetric	14808-79-8	1	mg/L	141	140	262	302	136
ED045G: Chloride by Discrete Analyser								
Chloride	16887-00-6	1	mg/L	1270	1160	2030	2370	1140
ED093F: Dissolved Major Cations								
Calcium	7440-70-2	1	mg/L	174	137	104	86	164
Magnesium	7439-95-4	1	mg/L	97	89	121	138	83
Sodium	7440-23-5	1	mg/L	666	649	1110	1280	619
Potassium	7440-09-7	1	mg/L	32	30	54	64	29
EK040P: Fluoride by PC Titrator								
Fluoride	16984-48-8	0.1	mg/L	0.2	0.3	0.4	0.4	0.3
EK055G: Ammonia as N by Discrete Analyser								
Ammonia as N	7664-41-7	0.01	mg/L	0.04	0.11	0.13	0.05	0.48
EK057G: Nitrite as N by Discrete Analyser								
Nitrite as N	14797-65-0	0.01	mg/L	<0.01	<0.01	0.01	<0.01	<0.01
EK058G: Nitrate as N by Discrete Analyser								
Nitrate as N	14797-55-8	0.01	mg/L	0.23	0.14	0.20	0.05	0.76
EK059G: Nitrite plus Nitrate as N (NOx) by Discrete Analyser								
Nitrite + Nitrate as N	----	0.01	mg/L	0.23	0.14	0.21	0.05	0.76
EK071G: Reactive Phosphorus as P by discrete analyser								
Reactive Phosphorus as P	14265-44-2	0.01	mg/L	<0.01	<0.01	<0.01	<0.01	<0.01

Analytical Results

Sub-Matrix: WATER (Matrix: WATER)				Sample ID	W8BI	W8BO	W8CI	W8CO	W8DI
				Sampling date / time	05-Dec-2022 00:00	05-Dec-2022 00:00	05-Dec-2022 00:00	05-Dec-2022 00:00	05-Dec-2022 00:00
Compound	CAS Number	LOR	Unit		EP2216518-011	EP2216518-012	EP2216518-013	EP2216518-014	EP2216518-015
					Result	Result	Result	Result	Result
EN055: Ionic Balance									
ø **Total Anions**	----	0.01	meq/L		**44.5**	**40.4**	**67.8**	**77.4**	**40.4**
ø **Total Cations**	----	0.01	meq/L		**46.4**	**43.2**	**64.8**	**73.0**	**42.7**
ø **Ionic Balance**	----	0.01	%		**2.15**	**3.26**	**2.29**	**2.94**	**2.74**

Analytical Results

Sub-Matrix: WATER (Matrix: WATER)			Sample ID	W8DO	W9AI	W9AO	W9BI	W9BO
			Sampling date / time	05-Dec-2022 00:00	05-Dec-2022 00:00	05-Dec-2022 00:00	05-Dec-2022 00:00	05-Dec-2022 00:00
Compound	CAS Number	LOR	Unit	EP2216518-016	EP2216518-017	EP2216518-018	EP2216518-019	EP2216518-020
				Result	Result	Result	Result	Result
EA005P: pH by PC Titrator								
pH Value	----	0.01	pH Unit	8.16	7.99	8.30	8.10	8.56
EA010P: Conductivity by PC Titrator								
Electrical Conductivity @ 25°C	----	1	µS/cm	4530	4420	5650	3030	3580
EA016: Calculated TDS (from Electrical Conductivity)								
Total Dissolved Solids (Calc.)	----	1	mg/L	2940	2870	3670	1970	2330
EA065: Total Hardness as CaCO3								
Total Hardness as CaCO3	----	1	mg/L	715	801	854	546	430
ED037P: Alkalinity by PC Titrator								
Hydroxide Alkalinity as CaCO3	DMO-210-001	1	mg/L	<1	<1	<1	<1	<1
Carbonate Alkalinity as CaCO3	3812-32-6	1	mg/L	<1	<1	3	<1	16
Bicarbonate Alkalinity as CaCO3	71-52-3	1	mg/L	243	319	301	327	132
Total Alkalinity as CaCO3	----	1	mg/L	243	319	304	327	147
ED041G: Sulfate (Turbidimetric) as SO4 2- by DA								
Sulfate as SO4 - Turbidimetric	14808-79-8	1	mg/L	146	157	213	104	140
ED045G: Chloride by Discrete Analyser								
Chloride	16887-00-6	1	mg/L	1180	1100	1540	752	970
ED093F: Dissolved Major Cations								
Calcium	7440-70-2	1	mg/L	143	197	174	138	80
Magnesium	7439-95-4	1	mg/L	87	75	102	49	56
Sodium	7440-23-5	1	mg/L	658	580	827	386	533
Potassium	7440-09-7	1	mg/L	31	22	42	14	20
EK040P: Fluoride by PC Titrator								
Fluoride	16984-48-8	0.1	mg/L	0.3	0.2	0.2	0.2	0.2
EK055G: Ammonia as N by Discrete Analyser								
Ammonia as N	7664-41-7	0.01	mg/L	0.01	0.02	0.02	0.02	0.02
EK057G: Nitrite as N by Discrete Analyser								
Nitrite as N	14797-65-0	0.01	mg/L	<0.01	<0.01	<0.01	<0.01	<0.01
EK058G: Nitrate as N by Discrete Analyser								
Nitrate as N	14797-55-8	0.01	mg/L	0.44	0.13	0.07	0.02	<0.01
EK059G: Nitrite plus Nitrate as N (NOx) by Discrete Analyser								
Nitrite + Nitrate as N	----	0.01	mg/L	0.44	0.13	0.07	0.02	<0.01
EK071G: Reactive Phosphorus as P by discrete analyser								
Reactive Phosphorus as P	14265-44-2	0.01	mg/L	<0.01	<0.01	<0.01	<0.01	<0.01

Analytical Results

Sub-Matrix: WATER (Matrix: WATER)				Sample ID	W8DO	W9AI	W9AO	W9BI	W9BO
				Sampling date / time	05-Dec-2022 00:00	05-Dec-2022 00:00	05-Dec-2022 00:00	05-Dec-2022 00:00	05-Dec-2022 00:00
Compound	CAS Number	LOR	Unit		EP2216518-016	EP2216518-017	EP2216518-018	EP2216518-019	EP2216518-020
					Result	Result	Result	Result	Result
EN055: Ionic Balance									
ø **Total Anions**	----	0.01	meq/L		**41.2**	**40.7**	**54.0**	**29.9**	**33.2**
ø **Total Cations**	----	0.01	meq/L		**43.7**	**41.8**	**54.1**	**28.1**	**32.3**
ø **Ionic Balance**	----	0.01	%		**2.98**	**1.36**	**0.16**	**3.18**	**1.40**

Analytical Results

Sub-Matrix: WATER (Matrix: WATER)			Sample ID	W9CI	W9CO	W9DI	W9DO	----
			Sampling date / time	05-Dec-2022 00:00	05-Dec-2022 00:00	05-Dec-2022 00:00	05-Dec-2022 00:00	----
Compound	CAS Number	LOR	Unit	EP2216518-021	EP2216518-022	EP2216518-023	EP2216518-024	--------
				Result	Result	Result	Result	----
EA005P: pH by PC Titrator								
pH Value	----	0.01	pH Unit	8.13	8.36	8.17	8.29	----
EA010P: Conductivity by PC Titrator								
Electrical Conductivity @ 25°C	----	1	µS/cm	1980	2060	3470	6100	----
EA016: Calculated TDS (from Electrical Conductivity)								
Total Dissolved Solids (Calc.)	----	1	mg/L	1290	1340	2260	3960	----
EA065: Total Hardness as CaCO3								
Total Hardness as CaCO3	----	1	mg/L	366	371	570	588	----
ED037P: Alkalinity by PC Titrator								
Hydroxide Alkalinity as CaCO3	DMO-210-001	1	mg/L	<1	<1	<1	<1	----
Carbonate Alkalinity as CaCO3	3812-32-6	1	mg/L	<1	6	<1	<1	----
Bicarbonate Alkalinity as CaCO3	71-52-3	1	mg/L	283	265	318	322	----
Total Alkalinity as CaCO3	----	1	mg/L	283	271	318	322	----
ED041G: Sulfate (Turbidimetric) as SO4 2- by DA								
Sulfate as SO4 - Turbidimetric	14808-79-8	1	mg/L	56	54	112	298	----
ED045G: Chloride by Discrete Analyser								
Chloride	16887-00-6	1	mg/L	472	509	900	1660	----
ED093F: Dissolved Major Cations								
Calcium	7440-70-2	1	mg/L	97	91	116	69	----
Magnesium	7439-95-4	1	mg/L	30	35	68	101	----
Sodium	7440-23-5	1	mg/L	235	259	480	1030	----
Potassium	7440-09-7	1	mg/L	10	12	24	62	----
EK040P: Fluoride by PC Titrator								
Fluoride	16984-48-8	0.1	mg/L	0.2	0.2	0.2	0.5	----
EK055G: Ammonia as N by Discrete Analyser								
Ammonia as N	7664-41-7	0.01	mg/L	0.04	0.02	0.04	0.07	----
EK057G: Nitrite as N by Discrete Analyser								
Nitrite as N	14797-65-0	0.01	mg/L	<0.01	<0.01	<0.01	<0.01	----
EK058G: Nitrate as N by Discrete Analyser								
Nitrate as N	14797-55-8	0.01	mg/L	0.28	0.29	0.05	0.16	----
EK059G: Nitrite plus Nitrate as N (NOx) by Discrete Analyser								
Nitrite + Nitrate as N	----	0.01	mg/L	0.28	0.29	0.05	0.16	----
EK071G: Reactive Phosphorus as P by discrete analyser								
Reactive Phosphorus as P	14265-44-2	0.01	mg/L	<0.01	<0.01	<0.01	0.01	----

Analytical Results

Sub-Matrix: WATER (Matrix: WATER)				Sample ID	W9CI	W9CO	W9DI	W9DO	----
				Sampling date / time	05-Dec-2022 00:00	05-Dec-2022 00:00	05-Dec-2022 00:00	05-Dec-2022 00:00	----
Compound	CAS Number	LOR	Unit		EP2216518-021	EP2216518-022	EP2216518-023	EP2216518-024	--------
					Result	Result	Result	Result	----
EN055: Ionic Balance									
ø **Total Anions**	----	0.01	meq/L		**20.1**	**20.9**	**34.1**	**59.5**	**----**
ø **Total Cations**	----	0.01	meq/L		**17.8**	**19.0**	**32.9**	**58.1**	**----**
ø **Ionic Balance**	----	0.01	%		**6.19**	**4.77**	**1.79**	**1.12**	**----**

Appendix II DBCA Research Permits.

DEPARTMENT OF PARKS AND WILDLIFE

Department of
Parks and Wildlife

Enquiries: 17 DICK PERRY AVE, KENSINGTON, WESTERN AUSTRALIA
Telephone: 08 9219 9000
Facsimile: 08 9219 8242

Correspondence: **Locked Bag 30**
Bentley Delivery Centre WA 6983

PAGE NO. 1
CE006749

RECEIPT NO. **AMOUNT**
$0.00

CONSERVATION AND LAND MANAGEMENT REGULATIONS 2002
REGULATION 4

WRITTEN NOTICE OF LAWFUL AUTHORITY

FOR THE PURPOSE(S) DESCRIBED

TO AUTHORIZE A PERSON TO DO AN ACT THAT WOULD, BUT FOR SUCH A NOTICE, BE UNLAWFUL UNDER THE CONSERVATION AND LAND MANAGEMENT REGULATIONS.

DIRECTOR GENERAL

CONDITIONS

1 This authority is a written notice for the purposes of regulation 4(1) of the Conservation and Land Management Regulations 2002 (the Regulations) and it authorises the person named as the authority holder to carry out certain acts as described under "Purpose" (below), that would otherwise be unlawful under the Regulations cited in this authority.

2 Where applicable, licenses issued under regulation 89 or section 15(1) and/or section 23C of the Wildlife Conservation Act 1950 for the taking of flora and/or fauna are required in addition to this authority.

3 This authority does not comprise a lawful authority to enter CALM Act land the subject of division 1 of part 3 of the Regulations unless the land and/or waters is described below. "CALM land" is defined in regulation 2 to mean land, or land and waters, to which the Regulations apply, including caves and parts of caves on, or under that land. The Regulations apply to the land and waters as described in regulation 3.

4 Licensee/authority holder must contact the applicable region/district at least one (1) week prior to activity commencement for site specific instructions. (Contact details provided in the covering letter and/or attached conditions to this licence/authority).

5 No bioprospecting involving the removal of sample aquatic and terrestrial organisms (both flora and fauna) for chemical extraction and bioactivity screening is permitted to be conducted without specific written approval by the Director General.

6 The authorised person is required to ensure that those conditions detailed in the attached document/s are adhered to.

7 Where applicable, a licence issued under the Biodiversity Conservation Regulations 2018 is required in addition to this authority.

LOCATIONS	LEEUWIN-NATURALISTE NATIONAL PARK
PURPOSE	COLLECTION OF FLORA [REGULATION 8(1) ACTIVITY] AND TAKING WATER [REGULATION 30(1) ACTIVITY] FOR RESEARCH PURPOSES WHILE WITH KLOHN CRIPPIN BERGER
AUTHORISED PERSONS	RYAN VOGWILL, GRAHAM UNDERWOOD, TERRY MCGENITY, NATALIE HICKS, ANDREW COOPER, TOM GARNER, GAVIN RISHWORTH, AAN SMITH, JANINE ADAMS, HAYLEY CAWTHRA, CARLY DODD, NICKY SLEE (MUST HOLD VALID FLORA TAKING LICENCE IF TAKING FLORA)

DEPARTMENT OF PARKS AND WILDLIFE

Department of
Parks and Wildlife

Enquiries: 17 DICK PERRY AVE, KENSINGTON, WESTERN AUSTRALIA
Telephone: 08 9219 9000
Facsimile: 08 9219 8242

Correspondence: **Locked Bag 30**
Bentley Delivery Centre WA 6983

DATE OF ISSUE 18/11/2022
VALID FROM 25/11/2022
DATE OF EXPIRY 25/12/2022

LICENSING OFFICER

LICENSEE: DR M FORBES (MATTHEW)
ADDRESS 627-16 BEESLEY STREET
WEST END QLD 4101

- - - - - - - - - - - - - - - - -

Blackwood District

Regulation 4 Authority Additional Conditions:

1. Hygiene – Dieback (*Phytophthora cinnamomi*) and invasive species
    a. The authority holder is to ensure that all activities are carried out under hygienic conditions with respect to vehicles, personal hygiene and equipment used for collection of material to minimise disease risks and negate the spread of invasive species. All equipment must be cleaned between collection sites.
    b. All vehicles, footwear and equipment must be clean prior to entry into CALM Act lands.

2. General
    a. Prior to entry into CALM Act lands the authority holder must discuss planned activities, including permanent markers, with the District Flora Conservation Officer (08 9752 5555).
    b. Blackwood District undertakes prescribed burning and other potentially hazardous activities throughout the year. The authority holder must notify the Blackwood District Office (contact details below) a minimum of one week prior to accessing CALM Act lands with the following information:
        i. Licence number
        ii. Date/s
        iii. Location/s
        iv. Number of people involved
    c. Photographs should be used where possible rather than taking samples, unless a specimen is required to be lodged. Then only the minimum required material is permitted to be collected for identification without detrimental impact to the parent plant.
    d. The project must be undertaken with minimal disturbance to native vegetation and must not interfere with existing projects (eg transects/ plots) already established in the field.
    e. Rootstocks of plants are to remain undisturbed unless specifically indicated.
    f. Any unlawful activities observed on CALM Act lands are to be reported to the Blackwood District Office (08 9752 5555).
    g. Any sightings of threatened or priority listed species or communities are to be reported to the District Flora Officer (08 9752 5555).
    h. Threatened and priority listed species are not to be collected or damaged during research activities.
    i. Any sightings of introduced fauna or flora species is to be reported to the District Conservation Coordinator (08 9752 5555).
    j. The authority holder must provide Blackwood district with a report at the expiry of this authority, detailing the results of the project and a copy of all publications arising from the project. This report must include any outcomes of the research/survey/collection, a map indicating the area collections were made, and GPS locations of all collection sites.
    k. Details of all specimens taken, where lodged and registered numbers in those collections must also be provided.
    l. No vehicles are permitted to be driven off existing tracks and no access to gated areas.

District Contact Details:

Ben Lullfitz Conservation Officer - Flora
Email: ben.lullfitz@dbca.wa.gov.au Ph: 9752 5555

Department of **Biodiversity, Conservation and Attractions**

GOVERNMENT OF WESTERN AUSTRALIA

FLORA TAKING (OTHER PURPOSES) LICENCE

Regulation 61, Biodiversity Conservation Regulations 2018

Licence Number: FT61001164

Licence Holder: Matthew Forbes
627-16 Beesley Street
West End QLD 4101

Date of Issue: 18/11/2022

Date Valid From: 18/11/2022
Date of Expiry: 17/11/2025

LICENSED ACTIVITIES

Subject to the terms and conditions on this licence, the licence holder may –

1. Take flora, other than for a commercial purpose, for research purposes while with Klohn Crippin Berger

LOCATIONS

1. Locations for which written authorisation to undertake the licensed activities has been obtained from the land owner or occupier.

CONDITIONS

1. Flora must not be taken on CALM land, (as defined in the Conservation and Land Management Regulations 2002*),* unless authorised by a written notice of a lawful authority issued under regulations 4 and 8 of the Conservation and Land Management Regulations 2002.
2. Unless authorised by this licence, flora taken under this licence must not be taken in such a manner that constitutes clearing under the *Environmental Protection Act 1986,* and for live flora, in a manner that destroys or is likely to destroy the plant and/or surrounding vegetation, or in the case of annual species or flora taken as scientific samples for the purpose of plant identification, in a manner that affects the viability of the local occurrence of the species.
3. Flora taken under this licence must not be used for a commercial purpose, including bioprospecting activity.
4. For any flora taken by the licence holder where the species is listed as ‘priority flora’ on the Department of Biodiversity, Conservation and Attractions’ Threatened and Priority Flora List https://www.dpaw.wa.gov.au/plants-and-animals/threatened-species-and-communities/threatened-plants, the licence holder must complete and submit a ‘Threatened and Priority Flora Report Form’ (TPRF).
5. Any specimen taken that is significant to the WA Herbarium, or where the species is on the Department of Biodiversity, Conservation and Attractions’ Priority Flora List and the occurrence is not vouchered in the WA Herbarium, must be lodged with the WA Herbarium.
6. The written authorisation of the person in possession or occupation of the land accessed and upon which flora is taken, as required under regulation 101(2) and referred to in “Additional information” below, must:

a) state location details (including lot or location number, street/road, suburb and local government authority);

b) state land owner or occupier name, and contact phone number;

c) specify the time period that the authorisation is valid for;

d) be signed and dated; and

e) be attached to this licence at all times.

7. This licence, and any written authorisation or lawful authority which authorises the take of flora on specified locations must be carried at all times while conducting licensed activities and be produced on demand to a wildlife officer.
8. Any records and information compiled under this licence must be retained for at least two years after the date of expiry of this licence.

Bridgitte Reynolds
LICENSING OFFICER
WILDLIFE PROTECTION BRANCH

Delegate of CEO

ADDITIONAL INFORMATION

1. Regulation 82 empowers the CEO to add, substitute or delete a term or condition of a licence or to correct errors. Such power may be exercised on application of a licence holder or by the CEO's own initiative. If an amendment to a licence term or condition is required, please contact the CEO or the Licensing Section on wildlifelicensing@dbca.wa.gov.au in the first instance. The licence holder, if adversely affected by a condition imposed in this licence, may apply to the State Administrative Tribunal for review of the decision of the CEO to impose that condition on a licence: regulation 89(2) Biodiversity Conservation Regulations 2018.
2. A person must not contravene a condition of a licence. The penalty for an offence involving the contravention of a condition of a licence is a fine of $10 000: regulation 84 of the Biodiversity Conservation Regulations 2018.
3. It is an offence for persons authorised by this licence to enter land that is not in their possession or under their control without first having the *prior* written authorisation of the current owner or occupier of the land to:

   a) enter the land; and

   b) carry out the activity authorised by this licence.

   The penalty for this offence is a fine of $5 000: regulation 101(2) of the Biodiversity Conservation Regulations 2018.
4. CALM Act land are those lands or waters defined under Part II of the *Conservation and Land Management Act 1984* (CALM Act), and include State forest, timber reserves, national parks, conservation parks, nature reserves, marine nature reserves, marine parks, and other lands. Please contact the relevant DBCA district/regional office for clarification on whether a parcel of land is "CALM Act" land or waters.

5. Information on Threatened and Priority Flora Lists as defined in this licence can be found at https://www.dpaw.wa.gov.au/plants-and-animals/threatened-species-and-communities/threatened-plants.
6. Where flora is being taken for identification purposes, please refer to the Environmental Protection Authority (EPA)'s "Technical Guidance- Flora and Vegetation Surveys for Environmental Impact Assessment" document http://www.epa.wa.gov.au/policies-guidance/technical-guidance-flora-and-vegetation-surveys-environmental-impact-assessment.
7. For more information about whether specimens would be considered significant to the WA Herbarium refer to "The Western Australian Herbarium's accessioning and specimen acquisition policy" document https://www.dpaw.wa.gov.au/plants-and-animals/wa-herbarium. Flora should only be taken under this licence where identification in the field is not possible, or where a specimen would be significant to the WA Herbarium, including range extensions or similar significant geographic or ecological value, or where the specimen is thought to be a new taxon or variant.
8. If lodging specimens to the WA Herbarium, please follow the 'Western Australian Herbarium Specimen Lodgement Guidelines' document https://www.dpaw.wa.gov.au/images/documents/plants-animals/herbarium/western_australian_herbarium_specimen_lodgement_guidelines.pdf
9. Unless taken for identification purposes, the licence holder should only take species which have been positively identified and can be taken under this licence. The licence holder should contact the WA Herbarium regarding specimen identification.
10. It is advised that any species taken for human consumption is checked against the listed substances in the *Medicines and Poisons Regulations 2016*.
11. If it is not a condition of this licence to create, compile and maintain records and information as required in a DBCA approved "Return- Flora Licences" of all flora taking activities as they occur, it is advised that the licence holder maintain a record of flora taken under this licence, with details including the species, the quantity, the part, the date that the flora was taken, and the land from which the flora was taken. This information may be requested for DBCA to consider a renewal application.

Appendix III Associated Research Publications

Sedimentary Geology 232 (2010) 52–65

Contents lists available at ScienceDirect

Sedimentary Geology

journal homepage: www.elsevier.com/locate/sedgeo

A characterisation of the coastal tufa deposits of south–west Western Australia

Matt Forbes *, Ryan Vogwill, Kimberly Onton

Department of Environment and Conservation, Locked bag 104 Bentley Delivery Centre, Western Australia 6983, Australia

ARTICLE INFO

Article history:
Received 15 May 2010
Received in revised form 23 September 2010
Accepted 24 September 2010
Available online 29 September 2010

Editor: M.R. Bennett

Keywords:
Coastal tufa
Western Australia
Thin section petrology
Mineralogy
Depositional models

ABSTRACT

Located in the south–west coastal zone of Western Australia are numerous tufa deposits, which are registered as Threatened Ecological Communities (TEC). The tufas occur in near-shore shallow bedrock settings and are associated with local groundwater discharge. Depositional facies, mineralogy, elemental chemistry and water quality were investigated for five key deposits. Two conceptual environmental models are identified. The first, the cascade to barrage pool model is associated with coastal waterfall zones, the second, a perched spring-line and barrage pool model is located predominantly in the supratidal zone. Tufa morphology, texture, mineral composition and elemental chemistry vary within and between sites. Both phytoclast and lithoclast (allochthonous), and phytoherm forms of tufa are identified depending on location within the facies. Calcite, and to a lesser extent, aragonite and Mg-calcite dominate tufa mineralogy, with diagenetic modifications apparent. Tufa water chemistry is generally Na–Cl–HCO_3 dominated; however, Na–Cl concentrations increase at sites situated within the supratidal zone. Currently the most likely potential threat posed to these deposits is increasing nutrient levels in spring waters from agricultural land use within the catchments. This could in the future impact on tufa development.

1. Introduction

1.1. Tufa deposits

Tufa are calcium carbonate-rich deposits, that precipitate in a variety of freshwater settings (e.g. Ford, 1989; Pedley, 1990; Ford and Pedley, 1996; Pedley et al., 1996: Freytet and Verrecchia, 1999; Riding, 2000; Andrews and Brasier, 2005; Carthew et al., 2006; Jones and Renaut, 2010). The complex interplay between physical, chemical and biological factors, which govern tufa formation are reflected in the predominant carbonate mineralogy (Jones and Renaut, 2010). Tufa can develop in waters of different temperatures with high dissolved calcium content and a microbial presence, like bacteria and fungi, resulting in variable morphologies.

Ford and Pedley (1996) developed a tufa classification system for these various morphologies, modeled on ambient temperature spring systems in cool temperate climates. This work has recently been summarised and updated by Jones and Renaut (2010). Many tufa deposits around the world have been described using this system (e.g. Viles and Goudie, 1990a; Pedley, 1990; Ford and Pedley, 1992, 1996; Pentecost and Viles, 1994; Carthew et al., 2003; Arenas et al., 2007; Viles et al., 2007). In many of these studies, the tufa depositional models identified and discussed were a combination of several end-member facies.

Certain environmental conditions, including persistently high water tables, extensive ground cover by macrophytes, spring water with moderate levels of $CaCO_3$ and low nutrient levels, appear most suited to tufa development (Ford, 1989; Pedley, 1990; Pentecost, 1995; Ford and Pedley, 1996; Carthew et al., 2003, 2006; Viles et al., 2007; Jones and Renaut, 2010).

1.2. Tufa composition and characteristics

$CaCO_3$ precipitation in tufa produces a vast array of crystal forms, which can be related to the agency of cyanobacteria, algae, mosses, other plants and/or detritus (Pedley, 1990; Ford and Pedley, 1996; Janssen et al., 1999; Jones and Renaut, 2010). Tufa mineral composition has been widely investigated (e.g. Pedley, 1990; Ford and Pedley, 1996; Freytet and Verrecchia, 1999; Janssen et al., 1999; Pentecost, 2005), calcite predominates in most instances, followed by aragonite, and to a lesser extent Mg-carbonate. Diagenetic processes can alter the tufa's initial mineralogical and textural composition, with micrite and some primary sparite recrystallising into giant radial palisadic secondary sparite (Janssen et al., 1999), similar to speleothems or marine recrystallisations (Freytet and Verrecchia, 1999). Decomposition and subsequent removal of organic matter from the matrix can also occur, resulting in voids, moulds and prints forming within the tufas. The elements Ca, Mg and Sr are common in tufa geochemistry, and have been applied successfully in palaeoclimatic and geomorphologic reconstructions (Chafetz et al., 1991; Janssen et al., 1999; Ihlenfeld et al., 2003; Kano et al., 2003; Garnett

* Corresponding author. Tel.: +61 893340138; fax: +61 893340367.
E-mail address: matt.forbes@dec.wa.gov.au (M. Forbes).

0037-0738/$ – see front matter.
doi:10.1016/j.sedgeo.2010.09.009

et al., 2004; Andrews and Brasier, 2005; Lojen et al., 2009) in order to understand processes that occurred during tufa formation.

1.3. Tufa communities in Australia

Tufa deposits are scattered across the globe, many of which have been studied and characterised (e.g. Ford and Pedley, 1996). This includes several in Australia, located in central and northern Queensland (Dunkerley, 1981, 1987; Drysdale and Head, 1994; Drysdale, 2001; Carthew et al., 2003; Ihlenfeld et al., 2003), northern New South Wales (Carthew and Drysdale, 2003) and north–west Western Australia (Viles and Goudie, 1990b; Wright, 2000; Carthew et al., 2006). Located in the south-western region of Western Australia are numerous coastal tufa deposits that are yet to be described and characterised in any detail. These deposits are associated with carbonate-rich freshwater streams and seeps and are proximal to several waterfalls, as well as coastal limestone scarps. In 2001 these deposits were classified as a Threatened Ecological Community (TEC), with their status being endangered. Main threats to the community at the time were perceived to be physical damage and changes in hydrological regimes. As a result of this classification a robust monitoring program was established in order to firstly understand the functioning of the deposits, and to assess the actual threats to the deposits.

This study discusses and summarises many facets of the monitoring program including detailed examinations of tufa mineralogy, geochemistry and water chemistry. It also provides descriptions of tufa facies and proposes depositional models with the aim of documenting a first detailed account of these deposits. Comparisons of tufa characteristics are also made with other Australian tufa deposits to place the deposits in a regional context.

2. Study area

The tufa deposits characterised in this study are located on the western coastal fringe of the distinctive anvil-shaped promontory, known as the Leeuwin–Naturaliste geographic region, Western Australia (Fig. 1). The tufas are associated with the Leeuwin–Naturaliste Ridge, a strip of karstified coastal dune limestone/calcarenite (Pleistocene Tamala Limestone) that extends from Cape Naturaliste in the north, south to Cape Leeuwin (Playford et al., 1976). The Proterozoic Leeuwin Complex (540–780 Ma), strongly

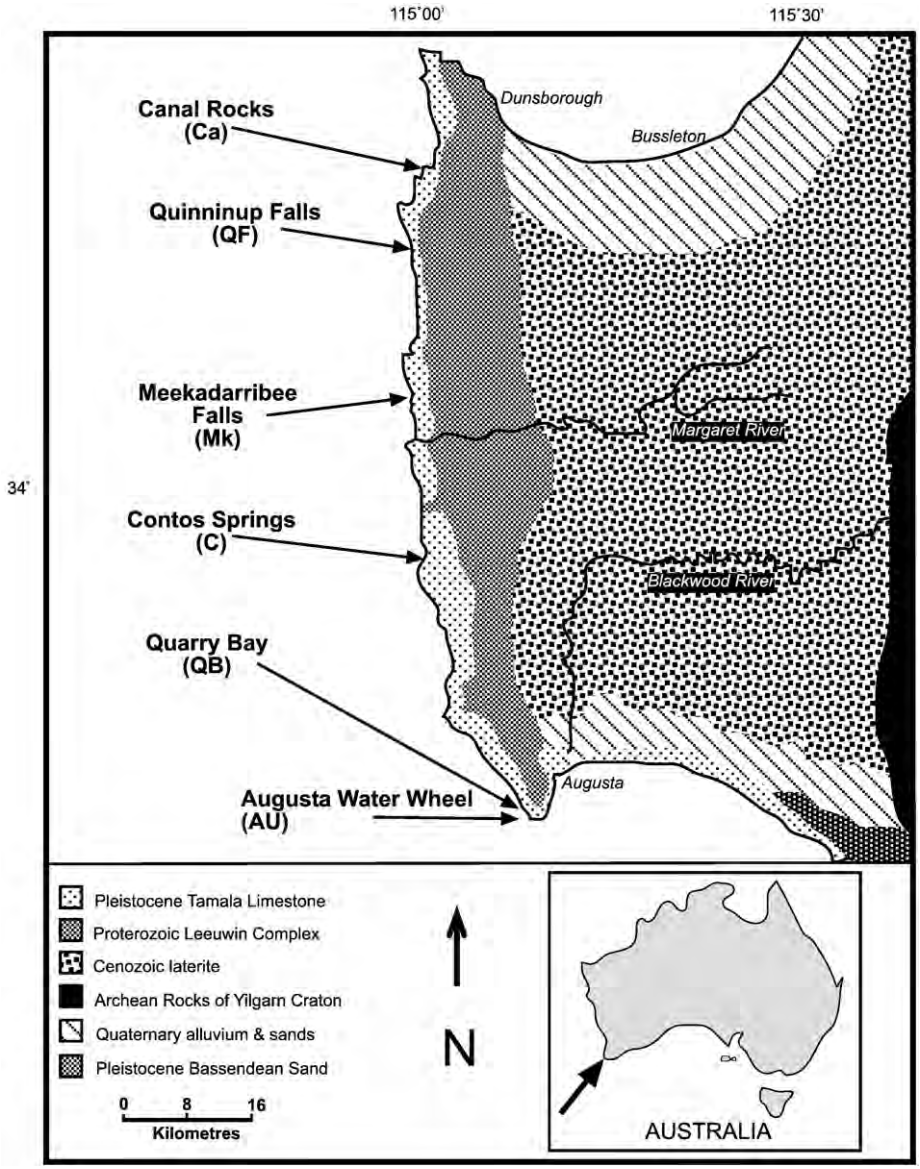

Fig. 1. The location in the south–west of Western Australia of the coastal tufa deposits discussed in this study. Geological features are adapted from Playford et al. (1976) and Hassan (1998).

metamorphosed igneous rocks (granite and anorthositic gneisses), underlies much of the limestone, and outcrops in many areas along the coastal zone (Myers, 1994). The regional climate is Mediterranean, with dry summers and mild, wet winters. Annual precipitation (Cape Leeuwin meteorological station) is approximately 1100 mm, with most rainfall occurring between April and October. Evaporation rates are in the order of 1000 mm yr^{-1} (BOM, 2001).

Five separate tufa deposits are the focus of this study. They are situated north to south along the coast as follows (Fig. 1), Canal Rocks (CR), Quinninup Falls (QF), Meekadarribee Falls (MK), Contos Springs (C) and Quarry Bay (QB). The sites can be separated into two general depositional environments, waterfall settings and spring seeps onto coastal bedrock. Both Meekadarribee and Quinninup are waterfalls, whereas Contos Springs and Canal Rocks are spring seeps onto coastal bedrock. The fifth site at Quarry Bay consists of both types, with waterfalls located at the main Quarry Bay South site and spring seeps onto coastal bedrock at Quarry Bay North. One km farther south of the Quarry Bay South site is the Augusta Water Wheel (AW), where tufa has developed on a flume that was built in the late 1800s to divert spring water. This site will also be discussed in this study.

3. Methods

3.1. Field measurements and water quality

Commencing August 2008, field-water measurements were taken every two months for one year. Water parameters measured included, Temperature, pH, Electrical Conductivity (EC), Oxidation–reduction Potential (ORP), and Dissolved Oxygen (DO), and were measured using a WTW 340i hand-held instrument. Probes used were Blue-line 24 pH electrode (pH), Tetracon 325 (EC), Sentix-Pt (ORP) and CellOx 325 (DO). Note ORP measurements were corrected for the Standard Hydrogen Electron (SHE) relative to water temperature at the time of sampling. Total Alkalinity (TA) was also determined using HACH drop titrator kit. HCO_3^- and CO_3^{2-} ($mg\,L^{-1}$) were calculated based on field TA and pH measurements. Samples for laboratory analysis of major ions (Mg^{2+}, Ca^{2+}, Na^+, K^+, Cl^-, Br^-, F^-, SO_4^{2-}) and nutrients (N and P) were also collected at several monitoring locations at each tufa deposit, every two months. Sites chosen for water sampling were predominantly pools associated with barrage deposits or flows from waterfalls and pools directly below the falls area. HDPE sample bottles including one unfiltered 250 ml and two 125 ml (one filtered through 45 μm) were filled to overflowing and stored at ~4 °C until analysis by Perth Water Chemistry Centre, Bentley, Western Australia. Methods of analysis for major ions and nutrients follow the procedures and guidelines outlined in APHA (1995). Electrical neutrality was determined to check the accuracy of analysis, with a <5% deviation between total anions and cations considered to be acceptable (Appelo and Postma, 2005).

3.2. Petrography

In May 2008 physical tufa samples were collected from all five sites. At all sites samples were collected from the current tufa surface and are thus considered to be recent deposits. After air drying, macroscopic and binocular description, seven samples, representing the different tufa facies identified for the two types of depositional environments were prepared as impregnated thin sections. Thin-section preparation was completed by Pontifex and Associates, Kensington, South Australia.

3.3. Mineralogy

Overall 18 tufa samples were subjected to quantitative mineralogical analysis via X-ray diffraction (XRD). One gram of each sample was ground to <10 μm for 10 min in a McCrone micronizing mill under ethanol. The resulting slurries were oven dried at 60 °C, then mixed thoroughly with an agate mortar and pestle before being lightly pressed into stainless steel sample holders for XRD analysis. XRD patterns were recorded with a PANalytical X'Pert Pro Multi-purpose Diffractometer using Co Kα radiation, variable divergence slit, post diffraction graphite monochromator and fast X'Celerator Si strip detector. The diffraction patterns were recorded in steps of 0.05° 2 theta with a 0.5 s counting time per step, and logged to data files for analysis. Quantitative analysis was performed on the XRD data using the Rietveld method (Rietveld, 1969) with the commercial package TOPAS from Bruker AXS. The results are normalized to 100%, and hence do not include estimates of unidentified or amorphous materials, and depending on the mineral, detection limits of 0.2% or less are achievable.

3.4. Elemental analysis

Major elements in their oxidised state (SiO_2, Al_2O_3, Fe_2O_3, MnO, MgO, CaO, Na_2O, K_2O, TiO_2 and P_2O_5) were determined as a percentage composition (Norrish and Chappell, 1977) on all tufa samples subjected to (XRD) mineralogical analysis. Samples for major elemental analysis were crushed, dried at 110 °C, then combusted at 960 °C overnight, in order to determine Loss of Ignition (LOI), which is indicative of the organic matter and hydrated mineral phases present in the sediment (Craft et al., 1991). The next day, between 1.0 and 1.1 g of the combusted material was weighed and combined with flux (35.3% lithium tetraborate and 64.7% lithium metaborate). Then, using Pt–Au crucibles the mixture was fused at 1150 °C. Samples were analysed at Genalysis Laboratory Services Pty Ltd in Maddington, Western Australia using a Pan Analytical-AXIOS Kw Rhodium tube XRF Spectrometer, with standard/reference materials Sarm1, Sarm2, Sarm 32 and SY-4. Minor or trace element (Cr, Ba, S, As, Cd, Co, Cu, Ni, Pb, Sn, V, Zn, Sr, and U) analysis was undertaken to obtain data in concentrations of one to several thousand parts per million (ppm).

4. Results

4.1. Field observations: tufa facies and site descriptions

4.1.1. Meekadarribee Falls (MK)

Meekadarribee Falls (MK) is located 1.5 km inland from the coast. The tufa deposit itself is situated 10 m north of the junction point between a small tributary that flows over the waterfalls and the main stream channel, which flows west down to the old Ellensbrook homestead site. The extent of the tufa deposit here covers an area of approximately 10 m^2 around the falls site (Fig. 2a). Tufa occurs in and around the waterfall and also within a 5 m radius down gradient of the falls zone. A variety of tufa facies are apparent including microbial laminites as both bubble forms evident within the 8 (1–2 m diameter) barrage pools below the falls, and as flat sheet varieties on the vertical sides of the limestone falls. Phytoherm rimstone-dam tufas dominate the barrage-pool walls, and can reach up to 0.5 m in height. They have a porous and permeable fabric, the likely result of the rapid decay of the carbonaceous framework. Located within the limestone bedrock behind the waterfall is a substantial cave with numerous stalactites and some stalagmites. Microbial laminites and mats are also evident on the cave floor, as well as cave pearls. Moss growing down across the cave entrance is being actively calcified forming a 0.5–1 m long curtain. Mosses and green algae on the vertical faces of the falls are also being actively calcified.

4.1.2. Quinninup Falls (QF)

The Quinninup waterfall tufa deposit is located approximately 500 m inland from the coast. The tufa here is restricted to the 10 m vertical face of the granitic bedrock immediately behind and adjacent to the waterfall (Fig. 2b). Below the falls is a 5 m diameter pool, where tufa development appears to be absent. The tufa on the vertical faces

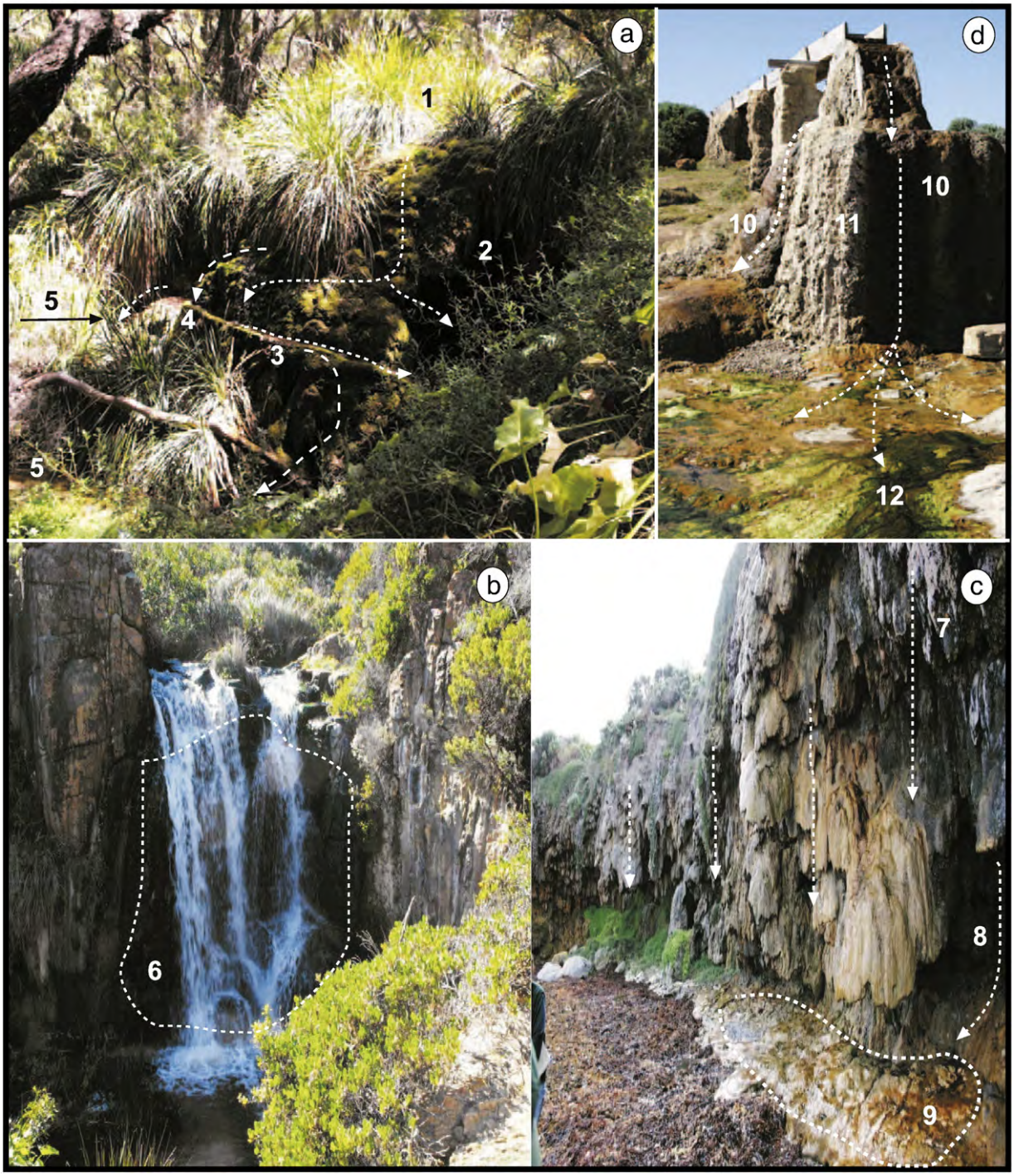

Fig. 2. Site photographs for cascade/waterfall related tufa deposits at Meekadarribee (a), Quinninup (b), Quarry Bay (c) and Augusta Water Wheel (d). White dotted lines indicated general flow patterns of spring water through the area of tufa deposit. 1) Entry point of spring water from stream above where green moss is being actively calcified. 2) Meekadarribee Cave where stalactites and stalagmites have developed and algal curtains have formed across the cave entrance. 3) Narrow barrage pool developed on slope diverting water into cave, moss also actively calcified here and microbial laminites forming within the pool itself. 4) Green moss on spring flow paths above barrage pools being actively calcified. 5) More significant barrage pools containing bubble and sheet form microbial laminites have developed behind rimstone dams, further down from main falls area. 6) Surfaces to either side and behind the immediate falls area covered with growing green moss that is being actively calcified. 7) Stalactite tufa growth on limestone wall merging to form curtain. 8) Overhanging tufa curtain developed on original cliff face, where stalactite type growth is evident. 9) Small discharge apron situated on bedrock below falls where microbial laminites have developed. 10) Surface areas below water wheel discharge covered with growing moss (green) that is being actively calcified. 11) Surface areas below water wheel where discharge and calcification have ceased. 12). Discharge apron below water wheel where growing moss is being actively calcified and microbial laminites are also developing.

of the water fall is both thin (5–10 cm) bubble and sheet form microbial laminites; there is also a green algal component being actively calcified. Tufa abundance appears to vary seasonally at this site with a reduction being observed during the summer periods when lower flows and increased algal growth occur.

4.1.3. Quarry Bay Falls (QB) and Augusta Water Wheel (AW)

The Quarry Bay site is the largest and most diverse of the tufa sites discussed in this study, spanning 2 km of coast-line length and comprising of both waterfall and spring seepage deposits. Approximately 300 m north of the Quarry Bay car park is a distinct limestone

cliff area, where an extensive array of tufa has developed on and below it (Fig. 2c). This tufa is in two main types, firstly a speleothem-like form, existing on the upper and middle overhang areas of the limestone cliff. Below the limestone cliff itself thin sheet and some bubble-shaped microbial laminites have developed in the waterfall splash zone.

The Augusta Water Wheel site is unique to the south–west Australian tufa deposits in that the tufa here has colonized a structure built in the late 1800s. This tufa are generally thin (<5 cm) microbial laminites of bubble form that have developed within the flow duct to the wheel, and in the pools on the ground below the wheel (Fig. 2d). Thin (<5 cm) sheet varieties have developed on vertical walls below the wheel. The pools themselves have no barrage wall features; rather they are just shallow (<10 cm) depressions in the exposed granitic bedrock.

4.1.4. Canal Rocks Barrage Pools (CR)

The Canal Rocks tufa deposit is one of the more minor of those investigated. The deposit consists of less than half a dozen small (<1 m in diameter) barrage pools over granite and limestone (Fig. 3a), which are fed through thin (<10 cm) flow channels by freshwater seepages (Fig. 3b). The location of the barrage pools are restricted to preferential flow paths of the spring seeps, determined by bedrock geomorphology. Autochthonous tufa in the form of phytoherm bubble

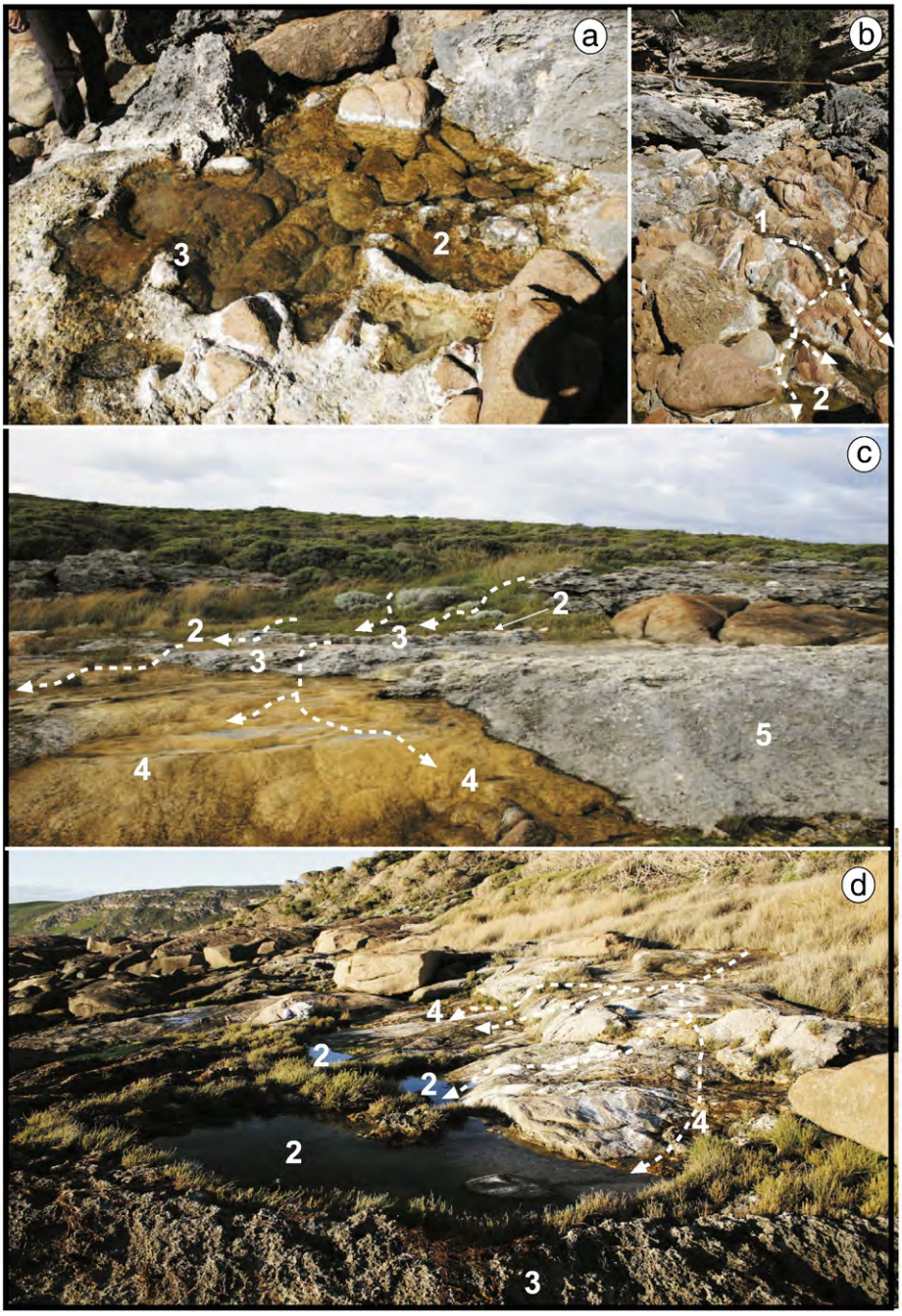

Fig. 3. Site photographs for coastal perched spring line to barrage deposits for Canal Rocks (a) Quarry Bay (b) and Contos Springs (c). White dotted lines indicated general flow patterns of spring water through the area of tufa deposit. 1) Narrow tufa pools in granite bedrock where fine microbial laminites have developed. 2) More significant barrage pools that have developed in larger bedrock depressions. Microbial laminites have developed within these pools and some green algae are being actively calcified. 3) Rimstone dams developing on underlying granite and limestone bedrock 4) Microbial mats associated with current discharge apron covered with shallow terrace pools. 5) Previous discharge apron now inactive due to changes in spring water surface flows.

microbial laminites is identified within the barrage pools, flow channels and bedrock surfaces (as part of small discharge aprons). The barrage-pool walls are lithified rimstone tufa up to 15 cm in height. More thin (<10 cm) lithified tufa, sheets on top of the granite and limestone bedrocks, represent extinct discharge aprons. Minimal amounts of allochthonous intraclast tufa, with calcified sediment grains, are evident within the barrage pools themselves.

4.1.5. Quarry Bay Barrage Pools (QB)

Approximately 300 m north of the main waterfall area at Quarry Bay an extensive network of spring seepages, discharge aprons and barrage pools commences and continues intermittently for another 700 m to the north. These pools and discharge aprons are located on granite bedrock in the supratidal zone and cover an area of approximately 100 m^2. The barrage-pool walls consist of lithified rimstone tufa (<10 cm in height). Bubble microbial laminites of variable thickness (2–8 cm) dominate within the pools themselves. Lithified tufa facies are evident on flat bedrock areas representing inactive discharge apron fans, whereas thin (<4 cm) sheet-like laminite tufa represent the active spring discharge aprons and are closely related to the location of current spring seeps.

4.1.6. Contos Springs Barrage Pools (C)

The Contos Springs tufa deposit consists of a dozen large (1–5 m in diameter) barrage-type pool deposits (Fig. 3d). Spanning an area of over 100 m^2 these pools have developed in large depressions within granite bedrock in the supratidal zone. Spring-water slowly flows into these pools from seeps located at the base of the adjacent steep limestone escarpment. Due to proximity of this site to the ocean mixing of spring and ocean waters occurs in the pools during periods of high swell and large tides. Various tufa facies are identified at the Contos site; the lithified rimstone tufa associated with the barrage pool walls (up to 20 cm high) and lithified sheet tufa on bedrock as part of extinct discharge aprons. Bubble form microbial laminites are evident within the pools, whereas thin sheet laminites are associated with flat bedrock areas. This later variety is in close association with the active groundwater seeps.

4.2. Petrography

Definitions of tufa facies described here are based on the classification system proposed by Ford and Pedley (1996) and revised by Jones and Renaut (2010).

4.2.1. Meekadarribee Falls

A speleothem from the limestone cave ceiling (MKa) and a microbial laminite tufa from the floor directly below the main collection of speleothems (MKb) were examined in thin section (Fig. 4). Sample MKa (Fig. 4a) appears to be completely composed (95%) of large coarse (3–4 mm) calcite crystals, with crystalline intergrowth; the remaining 5% consists of void space. The lack of a biogenic component, either current or previous, suggests this tufa is a lithoclast facies, indicative of flowstone/speleothem type.

Sample MKb (Fig. 4b) also has a dominant carbonate presence (>85%), with minor amounts of quartz, biotite, hornblende and Fe-oxide minerals that constitute the rock fragments (5%). Pisoid-type structures in the form of cave pearls are present; cave pearl nuclei ranges from quartz to calcite crystal intraclasts. The pearls also display isopachous laminae, with some of the earlier laminae poorly crystalline, suggesting that they have been moving quite frequently. There are also calcified microbial/algal tufts present as well. Some of the cave pearls appear to have undergone some level of diagenesis resulting in a conversion to a more massive crystalline structure with only minor remnants of the original texture remaining. This form of tufa is categorised as a phytoherm boundstone facies.

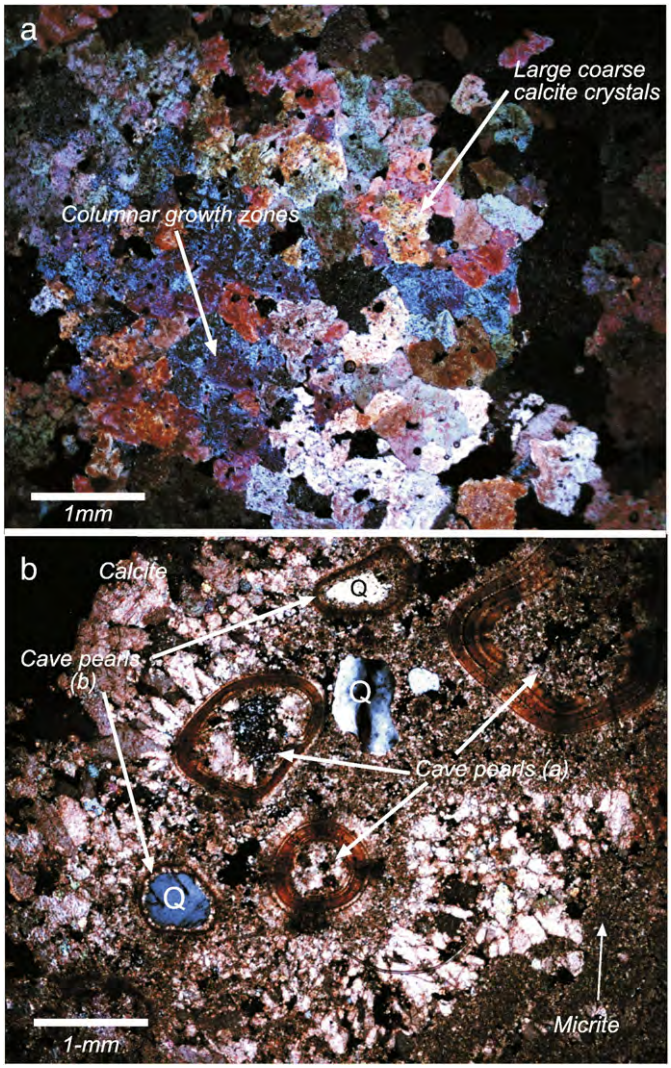

Fig. 4. Petrographic thin sections for the Meekadarribee Falls site. A). A speleothem from the limestone cave ceiling, which is almost entirely large coarse calcite crystals. B). Tufa from the floor directly below the main collection of speleothems. Evident are cave pearls (a) with calcite crystal intraclast as nuclei and (b) others with quartz grains as the nucleus. Scale of thin section is noted on diagram.

4.2.2. Contos Springs

Two Contos Springs samples were examined in thin section (Fig. 5). The first C2 (Fig. 5a) is a non-active discharge fan located 2 m above the barrage pool zone. It contains laminated structures with possible seasonal growth, there are also micritic clots or peloids present in adjacent areas—presumably calcified microbes or microbial clusters. Marine bioclastic material including foraminifera, shell fragments and possibly echinoderm spine fragments are also evident, presumably added during storm events. In some cases calcified domal structures have nucleated on these shell fragments. This tufa can be classified as a phytoherm framestone facies.

C3 (Fig. 5b) is tufa located on the wall of one of the barrage pools; its composition consists of predominantly of carbonate (85%), with rock fragments (10%) and void space. The carbonates are predominantly abiotic calcite (in the form of sparite and micrite). However, there is also a micro-biotic component in the form of thick calcified filaments—perhaps green algae (like *Vaucheria*). This tufa is classified as autochthonous phytoherm framestone.

4.2.3. Quarry Bay

Two tufa samples from the Quarry Bay waterfall site were examined in thin section (Fig. 6). QBa (Fig. 6a) is a thin sheet

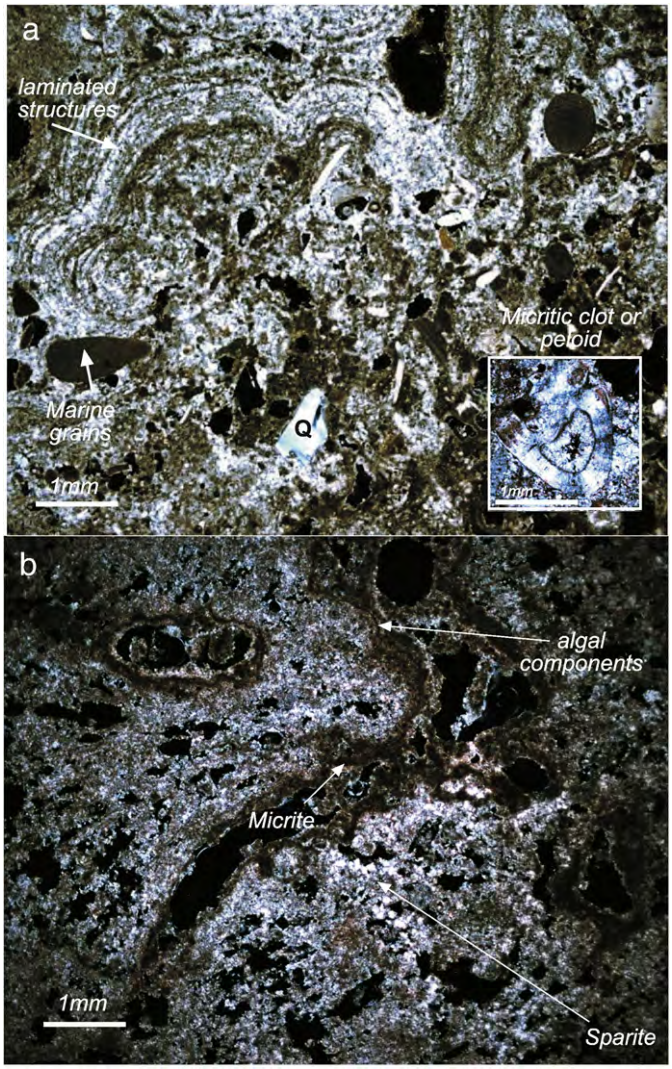

Fig. 5. Petrographic thin sections for the Contos Springs site. A). Tufa from bedrock above the barrage pool area, consists of laminated structure with possible seasonal growth, bioclastic shell material and micritic clots or peloids (see inset). B). Tufa taken from the rimstone dam wall of one of the barrage pools. It consists of predominantly micrite and sparite and an active algal component possibly green algae. Scale of thin section is noted on diagram.

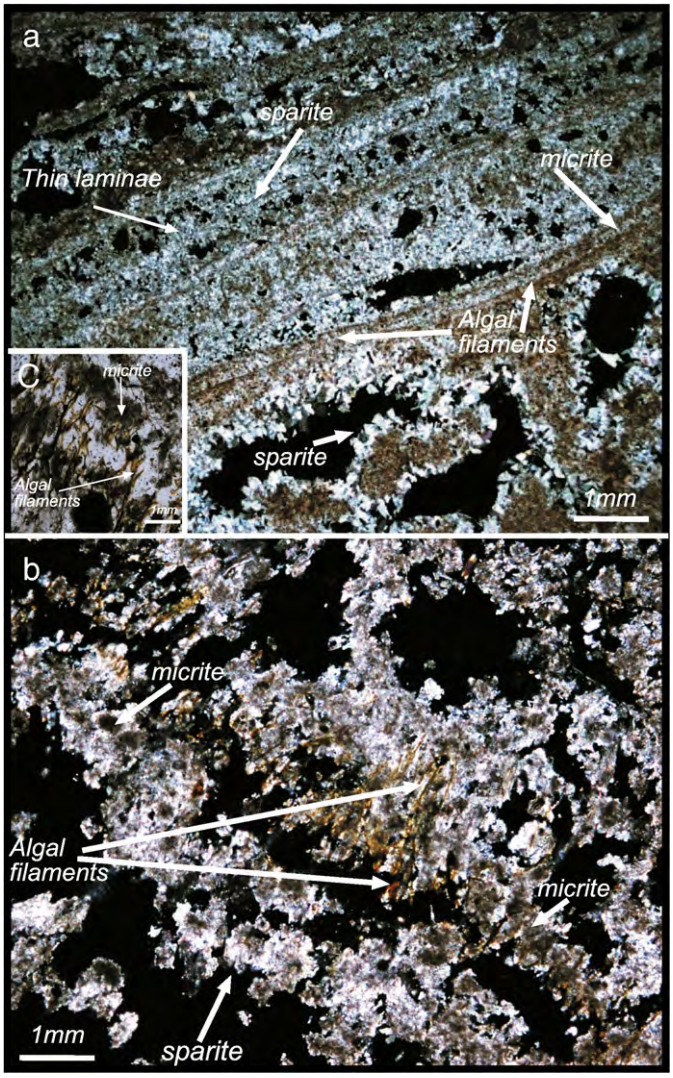

Fig. 6. Petrographic thin sections for Quarry Bay. A). is a tufa stalactite type from the limestone cliff overhang falls area. It is predominantly calcite (micrite/sparite), with an active algal filament component that has been calcified. B). Phytoherm sheet form microbial laminite tufa directly below the stalactite is also predominantly calcite/micrite. It has an algal component that has been calcified but lacks any ooids/pisoids. Scale of thin section is noted on diagram.

microbial laminite located on the ground immediately below the speleothems, whereas QBb (Fig. 6b) is a speleothem-type tufa that has developed down the overhanging limestone cliff. Sample QBa has thin laminae probably formed from microbial sheets which have then been calcified, with much thicker peloidal micro-sparitic calcite laminae in between. There are also some poorly calcified microbial tufts growing on the laminae surfaces. This microbial laminite tufa can be classified as micritic peloidal facies.

Sample QBb is a combination of both micro-biotic and abiotic carbonate components (calcite), with both sparite and micrite identified. The micrite occurs in association with long filamentous cyanobacteria or green algal strands; there are rare quartz grains within the filaments. Peloidal areas, possibly calcified microbial clots, are also evident. Approximately half of the matrix is porous/void space representing areas of possible diagenesis. This tufa can be classified as a phytoherm framestone facies.

4.3. Water chemistry

Field (Table 1) and laboratory (Table 2) analysis identified variations in water chemistry between seasons and across sites. Water quality was monitored on a bi-monthly basis; however, water chemistry end members were evident at the winter (August) and summer (February) peaks, as such these two months are discussed here only. Water temperature ranged between 24° and 20 °C in summer to 16° to 13 °C in winter. The highest water temperatures (>22 °C) were observed in the coastal pools in summer and the lowest (<15 °C) temperatures were observed in spring discharges in winter. Electrical conductivity (EC) ranged from fresh (0.5 mS.cm^{-1}) to saline (70 mS cm^{-1}). The saline EC values were identified at barrage pool sites within the supratidal zone, whereas the waterfall sites over 1 km inland from the coast were fresh (<1 mS cm^{-1}). EC concentrations also varied between seasons with higher concentrations observed at the end of summer compared to winter, this trend was most significant for sites within the supratidal zone. In some instances greater EC variations were observed in winter than in summer, most particularly in the Contos Springs barrage pools. This variation is more than likely reflecting seawater influx and mixing in the tufa pools during winter storm surge periods of high swell and large tides.

Slightly alkaline conditions (pH 7 to 9) were observed consistently, oxidation–reduction potentials (ORP) of 600 to 100 mV indicate likely oxidising conditions and Total Nitrogen (TN) and Total Phosphorous

Table 1
Site description and field water chemistry.

Location	Site code	Type	Site[a] #	Latitude	Longitude	Temp[b] °C	pH[b]	EC[b] mS/m
Canal Rocks	CR	Coastal spring and barrage	3	−33.669	115.001	16–23	7–9	48–1
Meekadarribee	MK	Cascade falls and barrage	4	−33.911	114.997	13–20	7–9	1–0.5
Quinninup	QF	Casacade falls	2	−33.746	114.995	14–25	7–9	2–0.5
Contos	CO	Coastal spring and barrage	5	−34.088	115.000	14–25	7–9	70–2
Quarry Bay Pools	QB P	Coastal spring and barrage	3	−34.362	115.134	13–28	7–9	35–2
Quarry Bay Falls	QB F	Casacade falls	2	−34.364	115.137	16–27	7–9	6–1
Augusta waterwheel	AW	Construted spring fed flume	2	−34.369	115.135	14–24	7–9	2–0.5

[a] Site # refers to the number of sub-sites at each tufa deposit where a water sample was collected.
[b] Ranges shown relate to the data collated from a number of sub-sites.

(TP) concentrations were generally low (<1 mg L^{-1}). An exception was at Meekadarribee Falls, where higher TN concentrations (2 to 5 mg L^{-1}) were observed; however, TP levels were not seen to be elevated.

Hydrologically all tufa sites are Na–Cl–HCO_3 dominated systems (Fig. 7). Na–Cl–Ca–HCO_3 for spring waters at Meekadarribee and Quinninup Falls, and Na–Cl–HCO_3 at the coastal barrage pool sites. At various times of the year, predominantly during the winter months (June to September) some coastal barrage pools exhibit Na–Cl levels equal to that of seawater. Other cation concentrations are in the order of Ca>Mg>K and are an order of magnitude less than Na. SO_4^- is at similar concentrations to Mg and K. Water chemistry changes seasonally, in particular a shift at all sites to greater HCO_3^- concentrations during summer are evident.

4.4. Mineralogy

Tufa mineralogical composition (Table 3) is clearly dominated by calcite and to a lesser extent aragonite and Mg-calcite (>90%). This large presence of calcite in favour of aragonite is expected in most temperate water tufa deposits (Jones and Renaut, 2010). Minor amounts of quartz (<2%) are also observed, as with the evaporative minerals halite and gypsum (<2%). Halite is only identified at the three supratidal zone sites (Quarry Bay, Contos Springs and Canal Rocks), gypsum is evident only at Quarry Bay. It's possible that the formation of these minerals is the result of evaporation after sample collection; however, the fact that they are found only at the coastal sites suggests that they are more likely ocean derived.

Table 2
Average ions and nutrient concentrations at the six tufa sites for Winter (Aug) 2008 and Summer (Feb) 2009.

	# sites	Ca	Cl	K	Mg	Na	SO_4	HCO_3	TN	TP
Winter 2008										
CR	3	43.6	549.7	12.5	34.8	304.3	60.5	340.3	0.64	0.02
QF	2	26.6	280.0	4.2	21.2	140.5	58.6	101.9	0.62	0.03
MK	3	45.5	76.7	1.9	9.8	49.8	13.1	318.5	3.40	0.02
CO	5	145.7	2313.3	29.1	103.6	908.3	243.7	401.3	0.81	0.02
QB F	2	52.4	317.0	3.1	20.6	123.0	26.5	368.5	1.10	0.02
QB P	3	98.8	781.0	8.0	44.2	360.7	83.0	422.8	0.25	0.06
WW	2	62.2	286.0	3.2	23.3	135.0	24.7	341.3	0.24	0.03
Summer 2009										
CR	3	82.0	323.7	6.5	26.3	190.0	37.5	687.5	0.83	0.03
QF	2	76.0	358.5	7.0	31.7	192.5	8.6	864.0	0.24	0.02
MK	3	81.9	81.0	6.8	9.7	49.2	16.9	723.3	7.27	0.33
CO	5	149.0	1174.3	19.3	80.5	605.3	126.1	746.4	1.09	0.74
QB F	2	94.6	324.0	3.4	25.5	151.0	31.1	798.1	0.46	0.02
QB P	3	112.7	452.7	4.1	34.6	235.7	48.4	893.5	0.18	0.01
WW	2	92.2	257.0	2.3	23.7	131.0	26.0	572.1	0.18	0.03

sites refers to number of sub-sites at each tufa location.
All values are in mg/L.

4.5. Elemental analysis

Elemental analysis reveals an expected dominance by CaO (45–60%) due to the high carbonate contents. Loss on Ignition (LOI; 42 to 52%) is also significant and reflects the combined presence of organic matter, carbonates and hydrated mineral phases in the sample (Craft et al., 1991). SiO_2 and MgO are the next most abundant elements, but do not exceed 5%. NaO and Cl concentrations are minimal, although slight increases (>1%) are observed in supratidal barrage pool sites (i.e. Contos and Canal Rocks). Minor levels of Al_2O_3 and Fe_2O_3 (~1%) are identified at Quinninup Falls. The concentration of strontium is significant (800–1500 ppm), whereas arsenic is the only other trace element to be detected at any appreciable level (20 ppm).

5. Discussions and conclusions

Mineralogical, elemental and physical investigations of tufa composition, as well as associated spring water chemistry have shed insight into the key environmental parameters, which have driven their deposition and continued existence in the south–west coastal region of Western Australia. Furthermore these data has allowed for the development of depositional models and insights into their Ecological Water Requirements (EWRs).

5.1. Tufa depositional models

Geomorphological and hydrological characteristics investigated in this study identify two distinct depositional models for the south–west Australian tufa deposits, based on the Ford and Pedley (1996) classification scheme. The first model is a combination of perched springline and fluvial barrage deposits identified at the supratidal sites of Contos Springs, Canal Rocks and Quarry Bay North. A combination of perched springline and cascade models are identified at the Quinninup, Meekadarribee and Quarry Bay South waterfall sites. Meekadarribee Falls is atypical in that it exhibits a mixture of both at the same locality.

The perched spring and cascade (waterfall) depositional model contains several tufa facies (Fig. 8). Geomorphological variations in terms of surface gradients and thus stream flow velocities are a key factor in which facies predominates at each of the waterfall sites. Tufa facies identified at Meekadarribee include curtains of moss that build down and out from the limestone overhang (a), becoming entombed in steeply inclined sheets of slow-flowing carbonate-rich water. This facies of tufa is not evident at either Quinninup or Quarry Bay falls sites, more than likely due to the greater flow velocities experienced at these sites. Speleothem-like tufa (b), are evident in the cave at Meekadarribee and also the cliff overhang at the Quarry Bay waterfall. Speleothem composition varies between the two sites from the inorganic-dominated facies at Meekadarribee to the organic derived boundstone and framestone facies at the Quarry Bay waterfall. The dominance by inorganic tufa within the

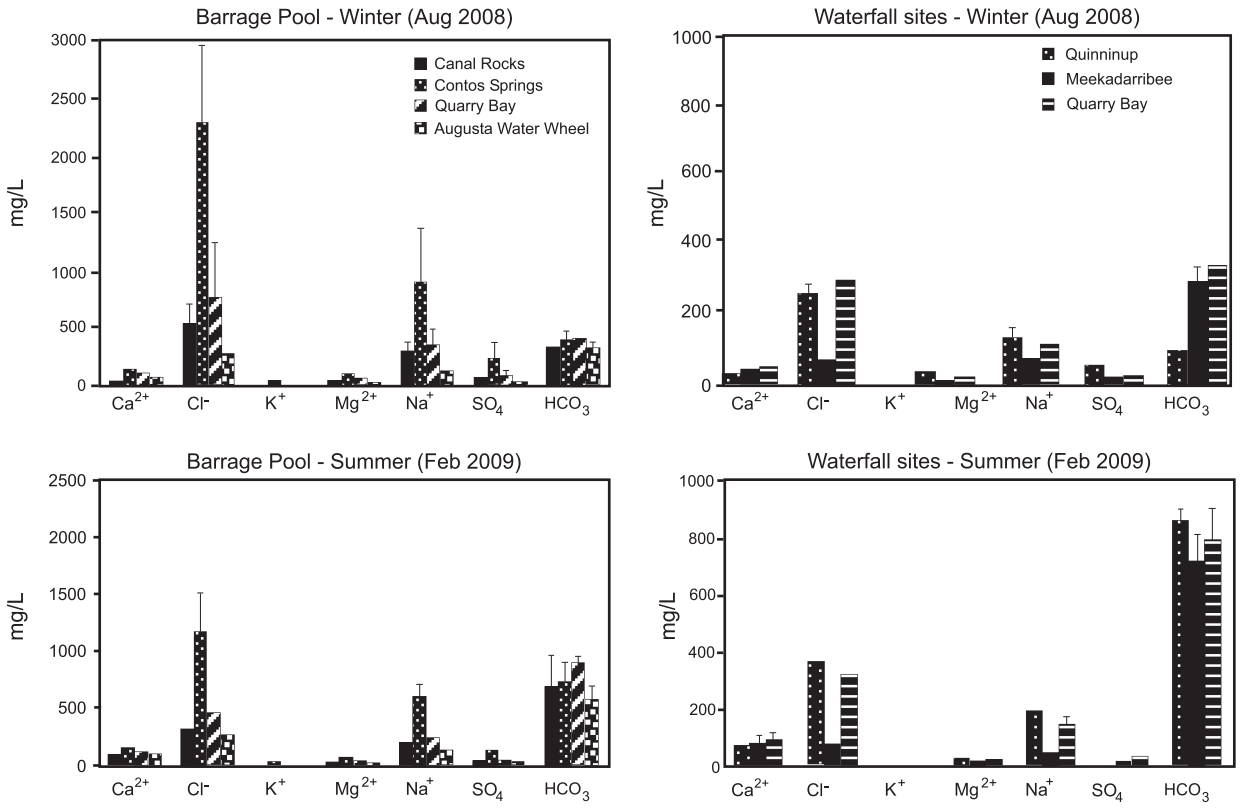

Fig. 7. Water chemistry averaged for all six sites for the peak winter (a) and summer (b) periods for the year 2008/09. All waters for tufa sites are characterised as varying forms of Na–Cl–HCO_3 systems. Data presented here are averages of a number of monitoring sites at each tufa deposit. The number of sites is detailed in Table 1.

Meekadarribee Falls cave is due likely to a combination of constant and moderate flow of spring water (hence ample CO_2 degassing) down through the cave and a lack of direct sunlight (inhibiting algal growth). In comparison greater light exposure at the Quarry Bay waterfall sites has allowed for the establishment of the biotic boundstone and framestone speleothem-like tufa evident there. At Quinninup Falls the significant flow regime and non-porous nature of the granitic bedrock are the likely reasons for the absence of either abiotic or biotic speleothem tufa there. At waterfall sites with higher velocity flows tufa development is predominantly driven by enhanced inorganic CO_2 outgassing rather than biotic processes, restricting tufa colonisation to the falls zone (Chen et al., 2004), which is apparent at Quinninup.

Various forms of bulbous, vertically stacked, phytoherm boundstone tufa facies are identified directly around all the falls areas (c). At Quinninup Falls this tufa facies is thin (<5 cm) and minor in abundance, restricted to just the side walls of the waterfall. At Quarry Bay this tufa facies is located directly on the beach in the tidal zone. This has resulted in some mixing with seaweed and sand, and secondary weathering, creating interclast and Phytoclast tufa. Over time, the flat tops of the older deposits that have not been altered by secondary weathering become dominated by impervious, thick coarse

Table 3
Elemental and mineralogical analysis of tufa.

Code	Location	Type	CaO	LOI	SiO2	MgO	NaO	Cl	Sr	Cal.	Arag.	Mg-cal.	Qtz.	Halite
			%	%	%	%	%	%	ppm	%	%	%	%	%
QB1	Quarry Bay North	Sheet tufa	50.7	46.4	1.5	1.2	0.3	0.3	832	93.4	0.8	5.4	0.4	–
QB2	Quarry Bay North	Rimstone dam tufa	52.0	46.2	1.5	1.2	0.6	1.0	1133	95.5	0.2	2.8	0.4	0.9
QB3	Quarry Bay South	Speleothem tufa	52.8	44.9	1.4	1.0	0.8	1.2	1106	92.2	0.2	4.4	0.3	0.6[a]
QB4	Quarry Bay South	Sheet tufa	45.8	51.6	2.0	1.1	0.1	0.1	1488	97.4	–	2.0	0.6	–
AW1	Augusta	Sheet tufa	46.7	50.9	1.8	1.1	0.2	0.1	1140	99.0	–	–	1.0	–
C01	Contos Springs	Bubble-sheet tufa	46.0	51.5	1.6	1.9	0.4	0.2	952	99.4	–	–	0.6	–
C02	Contos Springs	Rimstone dam tufa	53.3	44.9	1.6	1.9	0.1	0.1	966	74.9	5.5	18.5	1.1	–
C03	Contos Springs	Sheet tufa	53.7	45.5	1.3	1.2	0.3	0.3	651	95.6	0.2	3.4	0.5	0.2
C04	Contos Springs	Tamala Limestone	50.5	44.0	3.3	2.2	1.4	1.6	1540	58.7	18.5	19.1	2.5	1.1
C05	Contos Springs	Sheet tufa	52.7	45.1	1.5	1.4	0.6	0.7	815	94.5	0.6	3.9	0.8	0.2
MK01	Meekadarribee Falls	Speleothem tufa	57.3	44.5	1.4	0.3	0.0	0.0	153	96.0	0.5	3.1	0.4	–
MK02	Meekadarribee Falls	Sheet tufa	55.5	44.9	1.4	0.4	0.0	0.0	270	95.2	0.2	4.1	0.6	–
MK03	Meekadarribee Falls	Bubble-sheet tufa	55.4	44.4	1.8	0.2	0.0	0.0	127	96.0	0.1	2.8	1.1	–
QF01	Quininnup Falls	Sheet tufa	50.1	43.5	4.2	1.9	0.2	0.2	868	85.1	1.7	10.8	2.3	–
Ca01	Canal Rocks	Sheet tufa	50.9	45.8	2.0	2.0	0.9	1.0	810	91.0	1.6	6.0	0.9	0.5
Ca02	Canal Rocks	Sheet tufa	49.8	46.8	1.9	1.4	1.1	1.2	817	86.2	5.5	6.9	0.7	0.6
Ca03	Canal Rocks	Rimstone dam tufa	46.2	50.8	1.8	1.5	1.2	1.0	890	83.1	8.2	7.7	0.6	0.4

[a] QB3 also has 2.3% gypsum identified.

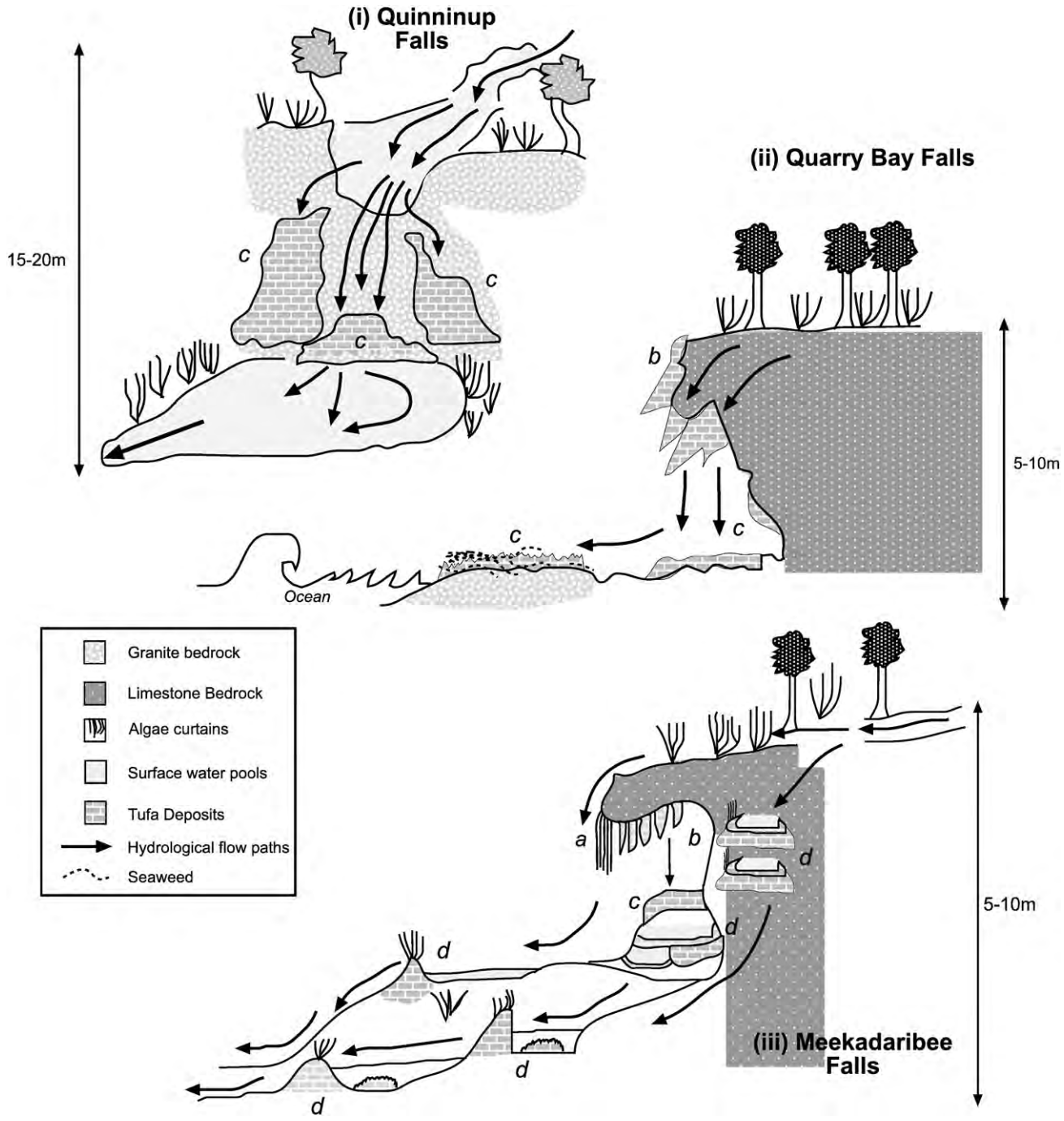

Fig. 8. The various models of cascade and barrage tufa deposits evident at (i) Quinninup Falls, (ii) Quarry Bay Falls, (iii) Meekadarribee Falls. At Meekadarribee Falls algal curtains have developed above the cave entrance (a) and speleothem tufa have developed within the cave. In comparison the North Quarry Bay falls site does not possess a cave system and the tufa there are less like abiotic speleothem, rather having a substantial algal component (b) Active sheet form microbial laminites (c) exist as discharge aprons at all sites on flat bedrock areas below and adjacent to the water fall areas. At Quarry Bay much of this sheet tufa is mixed with seaweed and other ocean biota as a result of its location within the tidal zone. Numerous tufa barrage pools (d) exist at Meekadarribee Falls where the flow regimes are not as vigorous and more constant compared to the two other falls sites. Within these pools are bubble and sheet form microbial laminites and large amounts of algae.

spar layers. Only Meekadarribee Falls has tufa facies associated with the fluvial barrage depositional model. The small (20 to 50 cm high) barrage tufa are phytoherm framestone (d), whereas within their associated pools fine peloidal intraclast tufa and microdetrital tufa exist. The presence of the barrage facies at Meekadarribee Falls and their absence at the other waterfalls is due to the constant medium flow velocity observed there; Such constant flows are not seen at either Quinninup or Quarry Bay waterfalls, where high velocities are evident in winter, reducing dramatically in summer.

The perched springline and fluvial barrage depositional model evident at Contos Springs, Canal Rocks and North Quarry Bay contains various tufa facies (Fig. 9). Phytoherm framestone to boundstone tufa represent barrage pool walls, where spring water discharge is concentrated into depressional areas within the underlying bedrock (a). Bubble type microbial laminite in the form of both peloidal and micro-detrital tufa facies exist within the pools themselves. These tufas have developed either solely from biomediation (macrophytic framestone) or the biomediation of carbonate encrusted sediment

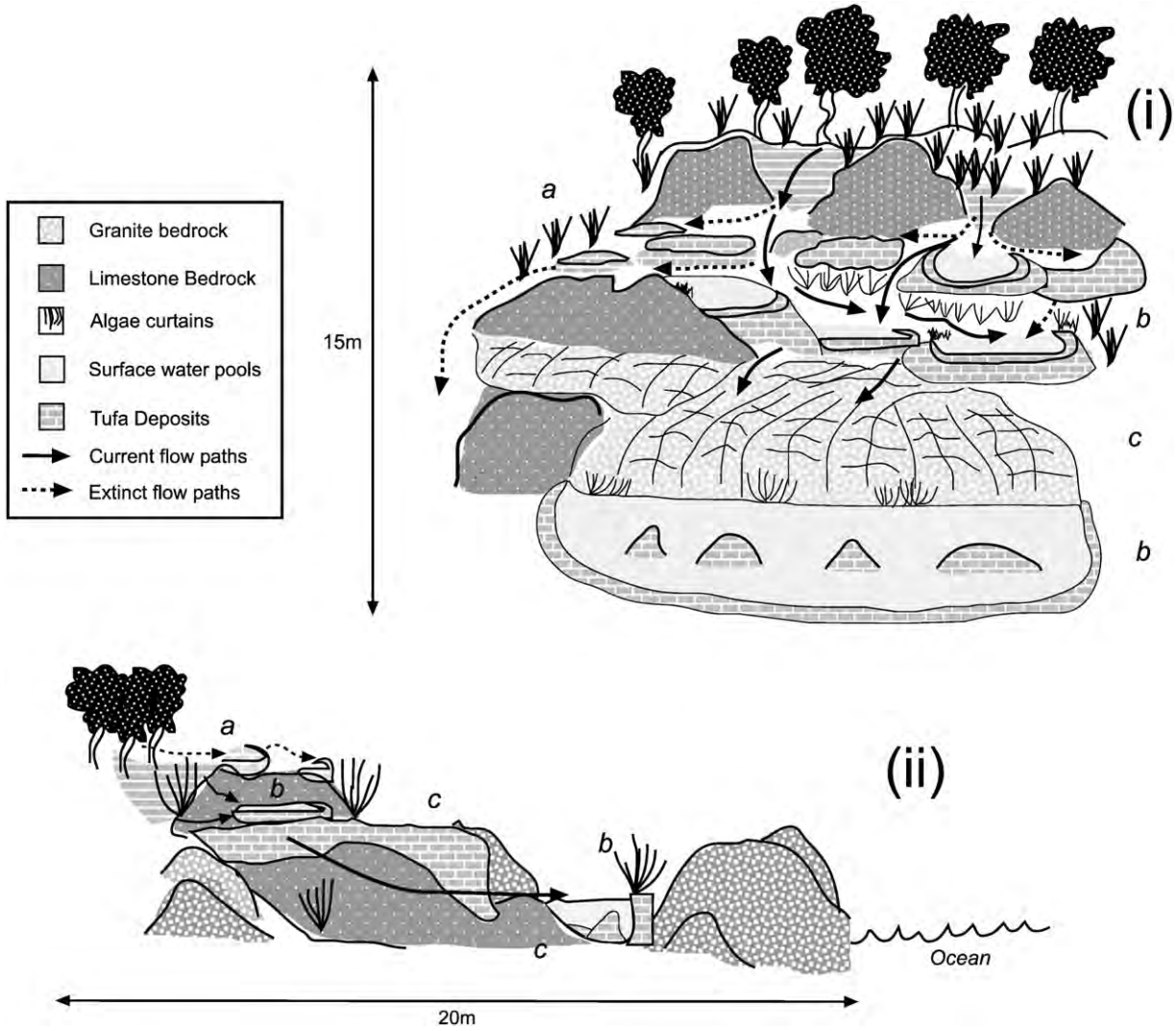

Fig. 9. Frontal (i) and side (ii) views representing the perched spring line and barrage tufa deposits situated at Contos Springs, Canal Rocks and Quarry Bay. These systems typically include an area of transitional or extinct barrage pools (a), where spring flow has ceased, and active tufa rimstone barrage and pool areas, where flows currently congregate and pass through (b). The extinct flow paths result from reduction and or diversion of the flow. Flow from these active barrage pools is across large relatively flat areas of bedrock creating discharge aprons (c), where active sheet form microbial laminites develop. In many instances these systems have coastal granites acting as barriers between pools and the ocean or as surface water conduits to the bigger pools. These are located closer to water's edge and can be partially filled with seawater.

grains (peloidal and microdetrital) that have been transported into the pools. The bubble microbial laminite tufas result from the microbial production of gas bubbles on the floor of the pools, which are in turn encased with precipitated calcite and/or aragonite (e.g. Jones and Renaut, 2010). These coated bubbles are easily broken and hence the vast majority is not preserved.

Barrage pool size and life span is highly dependent on bedrock geomorphology, position in the intertidal/supratidal zone and the volume of water input into the pool. Over time clastic materials can be transported into the pool via spring waters and rain runoff, causing fill behind the rimstone barrier. The result is an alteration in surface flow, thus inhibiting tufa growth within that particular pool. In turn, spring flow is diverted to a new bedrock depression allowing for the creation of a new barrage system (c) further down the flow gradient. This altered flow regime also impacts on the bubble and sheet forms of microbial laminites, which are micritic peloidal framestone facies. They primarily develop as spring discharge aprons on flat areas of bedrock (b). Altered flow results in some becoming non-active and the creation of new discharge aprons along a new flow path. Alterations or reductions to these spring flow paths could also occur from changes in local hydrology, the result of factors like reduced annual rainfall or increased groundwater extraction.

5.2. Water chemistry

The Na–Cl–HCO_3 characteristics for tufa spring waters are representative of variable mixtures of seawater and spring water across the five sites. HCO_3 concentrations fluctuate seasonally and are generally greatest, towards the end of summer. This summer peak is likely the result of reduced CO_2 degassing and in turn a decrease in carbonate precipitation, relating to generally lower flow velocities, causing the higher HCO_3 concentrations. Examination of HCO_3/Cl ratios combined with Cl concentrations provides further insight into HCO_3 fluctuations (Fig. 10). From winter to summer the coastal barrage pool sites (including the Augusta Water Wheel) exhibit increases in HCO_3/Cl ratios combined with decreasing Cl concentrations (Fig. 10a). This observed increase in HCO_3 into summer is the result of decreased degassing of CO_2 due to reduced spring flows, whereas the reduced barrage pool Cl concentrations represents a decrease in the mixing of Cl rich seawater from winter storm events.

All three waterfall sites (Fig. 10b) display an increase in HCO_3/Cl ratios from winter to summer; however, Meekadarribee and Quarry Bay have no significant increase in Cl concentrations, while Quinninup does. Hence it is likely that the HCO_3 increases at both Meekadarribee and Quarry Bay reflects reduced flows and as such a reduction in CO_2

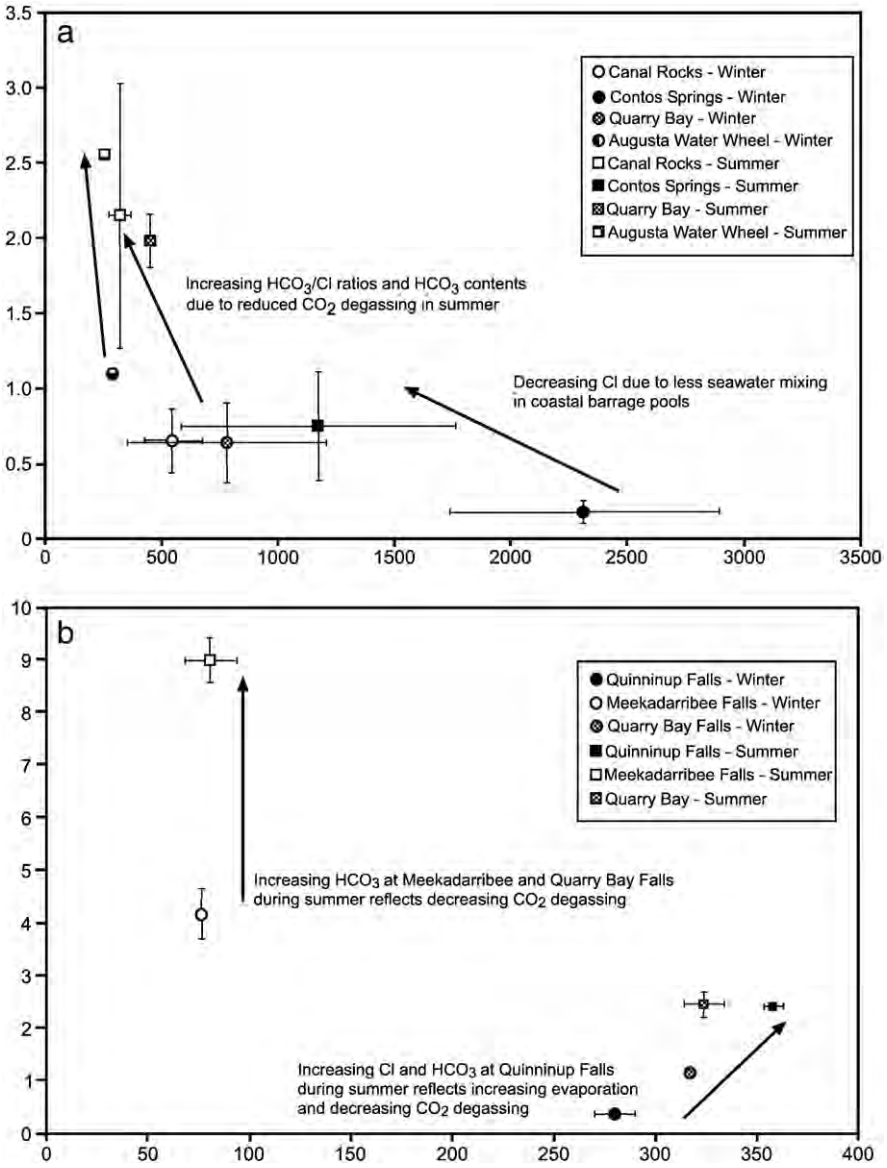

Fig. 10. Seasonal variations in HCO_3/Cl v Cl for barrage pool (a) and waterfall (b) tufa sites. Decreasing Cl concentrations combined with increasing HCO_3/Cl ratios from winter to summer in the barrage pools indicates a reduction in CO_2 degassing and less seawater mixing during storm events. Increasing HCO_3/Cl from winter to summer with no change in Cl concentrations suggests reduced CO_2 degassing. At Quinninup increased Cl due to evaporation during summer.

degassing, while at Quinninup a combination of reduced flows (and CO_2 degassing) and increased evaporation is evident.

5.3. Mineral and elemental composition

X-ray diffraction (XRD) results and petrographic thin sections identify subtle variations in the dominant carbonate minerals in the south–west Australian tufa deposits. Tufa have experienced various stages of growth and decline, evident by banding and layering, cementation, dissolution, and recrystallisation. Diagenesis has affected much of the tufa, algal degradation via natural decay and its subsequent removal from the matrix is evident; a key indicator of tufa diagenesis (e.g. Janssen et al., 1999). Furthermore, sparry cement (or sparite), particularly in the columnar type tufa has substituted the original micrite, also suggesting the occurrence of diagenesis (Freytet and Verrecchia, 1999; Janssen et al., 1999). The conversion to more massive crystalline structures around peloidal structures (including cave pearls) and the creation of radial $CaCO_3$ grains, some with original quartz grain cores is also apparent indicating diagenesis. Spring water flow through the initially porous deposits is a likely driver of this form of diagenesis (Jones and Renaut, 2010).

The Meekadarribee Cave tufa resemble the common calcite speleothem, which are frequently encountered as a fill to pre-existing tufa deposits (Ford and Pedley, 1996). These speleothems form in poorly lit cavities and inter-particle sites via ambient temperature waters dripping from cavity walls and seepage through the tufa. They rarely contain any biological material, forming by physico-chemical precipitation of calcium carbonate. These speleothems are considered to be the inorganic facies end-member, opposite to the bio-mediated tufa, which represents the other facies end member (Ford and Pedley, 1996). Unlike the cave ceiling speleothems, the Meekadarribee Cave floor tufa contain algal filaments, high microbial content, distinct laminae, as well as cave pearls, with both quartz and crystal intraclasts as nuclei. These characteristics are due likely to location on the cave floor providing greater exposure to more light from the cave entrance, as well as spring water runoff containing sedimentary and biological debris.

The evaporite mineral halite (and to a lesser extent gypsum) is only identified within tufa located at supratidal zone sites (Quarry

Bay, Contos Springs and Canal Rocks). Their presence is the likely result of these pools being affected by seawater inundation via sea sprays and wave action during storm surge events. Subsequent evaporation of this mixed pool water would allow for the incorporation of halite into the tufa. Greater concentrations of Na^+ and Cl^- and saline EC values within the coastal barrage pool waters is further evidence of seawater mixing with spring water.

The parent spring water temperatures of 10–20 °C at the south–west Western Australia tufa sites are known to promote calcite precipitation over aragonite (e.g. Jones and Renaut, 2010), which is evident in many of the tufa samples investigated. However, greater amounts of aragonite are seen in the coastal barrage pool sites at Contos Springs and Canal Rocks, which still display similar water temperatures. Marine influences may be the reason for this, with skeletal material such as bivalves and gastropod shells present at these sites being dominated by aragonite. These materials are brought into the tufa environment by storm events, allowing them to incorporate into developing tufa. Mg-calcite in tufa is regarded as a key identifier of diagenesis (Ford and Pedley, 1996; Jones and Renaut, 2010), thus as expected greater Mg-calcite concentrations appear in the lithified tufa rather the microbial laminites, which are seen to have experienced diagenesis via thin section petrography. Mg-calcites have been linked to high Mg/Ca ratios (e.g. Jones and Renaut, 2010); however, this relationship cannot be confirmed in this study due to the either small number samples analysed and/or the heterogeneous nature of the tufas sampled.

Elemental concentrations within the tufa are as expected considering the mineralogy. CaO represents over 50% in all cases reflecting the dominance by carbonate minerals. LOI which is a representation of both hydrated mineral phases and organic matter content (Craft et al., 1991) ,is in the case of the south–west Australian tufa indicative of the large amounts of carbonate present, probably more so than organic matter content. SiO_2 content, while minimal (<5%) is seen to increase in tufa at barrage pool sites where mixing with sedimentary products, transported by spring waters has occurred.

Despite dominating the spring water chemistry both NaO and Cl (<2%) are minimally represented within the tufa itself. This suggests that tufa does not readily incorporate these elements. However, investigations into the tufa biological composition (Onton and Forbes, 2009), identified a combination of cyanobacteria, diatoms and green algae, whose relative abundances fluctuated between unique combinations of fresh and saline water species. Hence NaO and Cl levels in tufa waters would appear to be more of an influence on the biological composition of the tufa rather than its chemical composition. Strontium (Sr) concentrations identified in tufa (800–1500 ppm) are significant. This is to be expected as Sr^{2+} can easily substitute with Ca^{2+} in calcite and aragonite (Capo et al., 1998); yet, no direct correlation is identified in this study between carbonate minerals and Sr abundance.

5.4. The south–west Australian coastal tufa in broader context

Comparisons of the south–west Australian tufa deposits with other Australian sites where active/modern tufa sites have been studied identify obvious differences. This can be attributed to different environmental settings. These other Australian sites are predominantly located in the northern part of the continent in tropical, seasonally arid monsoonal karst environments (e.g. Dunkerley, 1987; Viles and Goudie, 1990b; Drysdale and Head, 1994; Wright, 2000; Carthew et al., 2003; Drysdale et al., 2003), and thus can experience potential evaporation up to 5 times annual precipitation (Wright, 2000). This means the dry season evaporation processes play a major role in the concentration or re-precipitation as tufa, of carbonates dissolved from limestone bedrock during the monsoon. In comparison, the coastal south–west Australia tufa are not subjected to such extreme climatic variations with annual evaporation and precipitation approximately equal. Hence evaporation is unlikely to be as significant an influence on the type of tufa that develops, compared to the northern Australian sites. Tufa facies relating to evaporative processes, such as upstream-dipping ramps, detailed at northern Australian sites (e.g. Dunkerley, 1987; Wright, 2000), are not observed at the south–west Australian sites.

The size of the tufa deposits in south–west Australia are generally of a smaller scale than those observed in the northern part of the continent. Greater volumes of tufa and larger facies size can be related to different hydrological regimes, the larger volumes of water evident in the northern Australian sites obviously allows for larger stream systems and consequently more extensive tufa deposits. For example the tufa in the Gregory River system have barrage pool dam walls that can be up to 5 m in height and associated pools up to 20 m in diameter (Carthew et al., 2003). Some sites like the stream systems in the Napier Range region in north–west Australia (Wright, 2000) contain tufa sheets (5 mm thick) and dams (50 cm high) that are of a similar scale to those studied in south–west Australia. However, these streams are over 8 m wide and several kilometres in length meaning the overall amount of tufa in these systems is far greater than that examined in this study.

One other study within Australia that investigated spring water chemistry provides similar results to those observed at the south–west Australian sites. The Queensland spring waters analysed display similar pH (6.5 to 8.5), slightly higher temperatures (30 °C) and similar HCO_3 (400–500 ppm), Ca_2^+ (50–70 ppm) and Mg^+ (40–80 ppm) concentrations. However, the substantial differences in environmental setting between such sites and the south–west tufa makes it difficult to make any real inferences between data sets, other than generally similar conditions appear necessary for tufa development to occur. Generally other cases geochemical analysis of tufa in Australia has been restricted to fossil varieties (e.g. Ihlenfeld et al., 2003) as part of palaeoclimatic studies, also making significant comparisons problematic.

5.5. Ecological water requirements (EWR) for tufa

Tufa development is reliant on the presence and distribution of biotic elements, such as plants, algae, fungi and prokaryotes, throughout a spring system (e.g. Ford and Pedley, 1996; Pentecost, 2005; Jones and Renaut, 2010). Environmental parameters, which can affect these biotic elements, and hence limit tufa development include water composition, temperature, pH, CO_2 degassing, and water toxicity. Ecological Water Requirements (EWRs) relating to such parameters can be derived for the south–west tufa from hydrological and geochemical data discussed here. The most obvious EWRs centre on the precipitation of carbonate and nutrient levels. For carbonate precipitation, suitable concentrations of CO_3/HCO_3 and/or sufficient CO_2 degassing processes are required. HCO_3 concentrations are currently observed at between 200 and 600 mg L^{-1}; and can get as high as 1000 mg L^{-1}. Of interest is HCO_3 levels of below 100 mg L^{-1} observed at Quinninup Falls, the site where tufa is the least developed. This lack of tufa development maybe a reflection of the lower HCO_3 concentrations there and that 100 mg L^{-1} could thus be below the threshold required for sustained tufa development. It would be anticipated that relatively low nitrogen and phosphorous levels are required to limit the growth of undesirable algal forms, which would impede tufa development. The fact that the highest TN levels (3–5 mg/L) observed were at the Meekadarribee Falls site, where tufa development appears unaffected indicates that current nutrient levels are likely not an issue at any of the sites. However, the region has a well established and expanding agricultural and viticulture industries, meaning future increases in the immediate catchments, thus potentially impeding tufa development are possible. Furthermore increasing groundwater extraction by the same industries may reduce spring flows impacting on tufa development via reduced CO_2

degassing. A photogrammetry exercise assessing accretion rates of tufa at several sites (Onton and Forbes, 2009) observed very slow to almost unnoticeable growth over the course of 2008 to 2009. Hence the south–west Australian tufa deposits maybe very vulnerable to the previously mentioned potential alterations in hydrology.

Acknowledgements

The authors would like to thank the following; Prof. Maurice Tucker of Durham University, UK for thin section interpretations and editorial comments on manuscript, Mr. Mark Raven at CSIRO Land and Water Adelaide, South Australia for mineralogical preparation and analysis. Thanks to Dr. Ian Pontifex at Pontifex and associates, Adelaide, South Australia for thin section preparation. Assoc. Prof. Jacob John is thanked for microbial interpretations of tufa. Final thanks to Assoc. Prof. Heather Viles and Dr. Matt Leybourne for their contributions to the manuscript during the review process.

References

Andrews, J.E., Brasier, A.T., 2005. Seasonal records of climate change in annually laminated Tufas: short review and future prospects. Journal of Quaternary Science 20 (5), 411–421.
APHA, 1995. Standard Methods for the Examination of Water and Waste Water, 19th Edition. American Public Health Association, USA.
Appelo, C.A.J., Postma, D., 2005. Geochemistry, Groundwater and Pollution. A.A. Balkema, Amsterdam.
Arenas, C., Cabrera, L., Ramos, E., 2007. Sedimentology of Tufa facies and continental microbialites from Palaeogene of Mallorca Island (Spain). Sedimentary Geology 197, 1–27.
BOM, 2001. Bureau of Meteorology climate data. available at http://www.bom.gov.au.
Capo, R.C., Stewart, B.W., Chadwick, O.A., 1998. Strontium isotopes as tracers of ecosystem processes: theory and methods. Geoderma 82, 197–225.
Carthew, K.D., Drysdale, R.N., 2003. Late Holocene fluvial change in a tufa-depositing stream: Davys Creek, New South Wales, Australia. Australian Geographer 34 (1), 123–139.
Carthew, K.D., Taylor, M.P., Drysdale, R.N., 2003. Are current models of tufa sedimentary environments applicable to tropical systems? A case study from the Gregory River. Sedimentary Geology 162, 199–218.
Carthew, K.D., Taylor, M.P., Drysdale, R.N., 2006. An environmental model of fluvial tufas in the monsoonal tropics, Barkly Karst, Northern Australia. Geomorphology 73, 78–100.
Chafetz, H.S., Utech, N.M., Fitzmaurice, S.P., 1991. Differences in the $\delta^{18}O$ and $\delta^{13}C$ signatures of seasonal laminae comprising travertine stromatolites. Journal of Sedimentary Petrology 61, 1015–1028.
Chen, J., Zhang, D.D., Wang, S., Xiao, T., Huang, R., 2004. Factors controlling tufa deposition in natural waters at waterfall sites. Sedimentary Geology 166, 353–366.
Craft, C.B., Seneca, E.D., Broome, S.W., 1991. Loss on ignition and Kjeldahl digestion for estimating organic carbon and total N in estuarine marsh soils: calibration and dry combustion. Estuaries 14, 175–179.
Drysdale, R.N., 2001. Factors controlling the hydrochemistry of Louie Creek, a travertine-depositing stream in the seasonally wet tropics of northern Australia. Marine and Freshwater Research 52, 793–804.
Drysdale, R.N., Head, J., 1994. Geomorphology, stratigraphy and ^{14}C-chronology of ancient tufas at Louie Creek, northwest Queensland, Australia. Earth Science Processes and Landforms 22, 1037–1051.
Drysdale, R., Lucas, S., Carthew, K., 2003. The influence of diurnal temperatures on the hydrochemistry of a tufa-depositing stream. Hydrological Processes 17 (17), 3421–3441.
Dunkerley, D.L., 1981. Chemistry of a tropical tufa-depositing spring near Mt. Etna, Queensland: a preliminary analysis. Helictite 19, 15–21.
Dunkerley, D.L., 1987. Deposition of tufa on Ryans and Stockyard Creeks, Chillagoe Karst, North Queensland: the role of evaporation. Helictite 25, 30–35.
Ford, T.D., 1989. Tufa: a freshwater limestone. Geology Today 5 (2), 60–63.
Ford, T.D., Pedley, H.M., 1992. Tufa deposits of the world. Journal of the Speleological Society of Japan 17, 46–63.
Ford, T.D., Pedley, H.M., 1996. A review of tufa and travertine deposits of the world. Earth Science Reviews 41, 117–175.
Freytet, P., Verrecchia, E.P., 1999. Calcitic radial palisadic fabric in freshwater stromatolites diagenetic and recrystallized feature on physicochemical sinter crust. Sedimentary Geology 126, 91–102.
Garnett, E.R., Andrews, J.E., Preece, R.C., Dennis, P.F., 2004. Climatic change recorded by stable isotopes and trace elements in a British Holocene tufa. Journal of Quaternary Science 19, 251–262.
Hassan, L.Y., 1998. Mineral occurrences and exploration potential of southwest Western Australia. Western Australian Geological Survey Report 65.
Ihlenfeld, C., Norman, M.D., Gagan, M.K., Drysdale, R.N., Maas, R., Webb, J., 2003. Climatic significance of seasonal trace element and stable isotope variations in a modern freshwater tufa. Geochimica et Cosmochimica acta 67 (13), 2341–2357.
Janssen, A., Swennen, R., Podoor, N., Keppens, E., 1999. Biological and diagenetic influence in recent and fossil tufa deposits from Belgium. Sedimentary Geology 126, 75–95.
Jones, B., Renaut, R.W., 2010. Calcareous spring deposits in continental settings. Developments in Sedimentology 61, 177–224.
Kano, A., Matsuoka, J., Kojo, T., Fujii, H., 2003. Origin of annual laminations in Tufa deposits, southwest Japan. Palaeogeography, Palaeoclimatology, Palaeoecology 191, 243–262.
Lojen, S., Trkov, A., Ščančar, J., Vázquez-Navarro, J.A., Cukrov, N., 2009. Continuous 60-year stable isotopic and earth-alkali element records in a modern laminated tufa (Jaruga, river Krka, Croatia): implications for climate reconstruction. Chemical Geology 258 (3–4), 242–250.
Myers, J.S., 1994. Late Proterozoic high-grade gneiss complex between Cape Leeuwin and Cape Naturaliste. Geological Society of Australia (WA Division) Excursion Guidebook 6. 26pp.
Norrish, K., Chappell, B.W., 1977. X-ray fluorescence spectrometry. In: Zussman, J. (Ed.), Physical Methods in Determinative Mineralogy, 2nd Ed. Academic Press, pp. 201–272.
Onton, K., Forbes, M.S., 2009. Augusta microbial threatened ecological community monitoring report. Technical report Department of Environment and Conservation, Bunbury, Australia.
Pedley, H.M., 1990. Classification and environmental models of cool freshwater tufas. Sedimentary Geology 68, 143–154.
Pedley, M., Andrews, J., Ordonez, S., Garcia del Cura, M.A., Gonzales Martin, J.-A., Taylor, D., 1996. Does climate control the morphological fabric of freshwater carbonates? A comparative study of Holocene barrage tufas from Spain and Britain. Palaeogeography, Palaeoclimatology, Palaeoecology 121 (3–4), 239–257.
Pentecost, A., 1995. Quaternary travertine deposits of Europe and Asia Minor. Quaternary Science Reviews 14, 1005–1028.
Pentecost, A., 2005. Travertine. Springer, Berlin.
Pentecost, A., Viles, H.A., 1994. A review and reassessment of travertine classification. Geographie Physique et Quaternaire 48, 305–314.
Playford, P.E., Cockbain, A.E., Low, G.H., 1976. Geology of the Perth Basin, Western Australia. Western Australian Geological Survey Bulletin 124.
Riding, R., 2000. Microbial carbonates: the geological record of calcified bacterial algal mats and biofilms. Sedimentology Supplement 1–47, 179–214.
Rietveld, H.M., 1969. A profile refinement method for nuclear and magnetic structures. Journal of Applied Crystallography 2, 65–71.
Viles, H.A., Goudie, A.S., 1990a. Tufas, travertines and allied carbonate deposits. Progress in Physical Geography 14 (1), 19–41.
Viles, H.A., Goudie, A.S., 1990b. Reconnaissance studies of the tufa deposits Napier Range, NW Australia. Earth Science Processes and Landforms 15 (5), 425–443.
Viles, H.A., Taylor, M.P., Nicoll, K., Neumann, S., 2007. Facies evidence of hydrological regime shifts in tufa depositional sequences from the arid Naukluft Mountains, Namibia. Sedimentary Geology 195, 39–53.
Wright, J.S., 2000. Tufa accumulations in ephemeral streams: observations from the Kimberly, north–west Australia. Australian Geographer 31, 333–347.

Marine Geology 481 (2025) 107496

Contents lists available at ScienceDirect

Marine Geology

journal homepage: www.elsevier.com/locate/margo

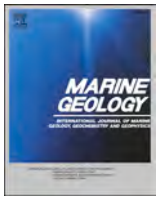

Research Article

Marginal marine spring carbonates defining an emergent rocky shoreline at Cape Freycinet, Western Australia

Thomas W. Garner [a,*], J. Andrew G. Cooper [a,b], Alan Smith [b]

[a] School of Geography and Environmental Science, Ulster University, Coleraine BT52 1SA, Ireland
[b] Discipline of Geology, School of Agriculture, Earth and Environmental Sciences, University of KwaZulu-Natal, P. Bag X54001, Durban 4000, South Africa

ARTICLE INFO

Editor: Edward Anthony

Keywords:
Carbonate
Microbialite
Rocky shoreline
Emergent
Marginal Marine

ABSTRACT

Modern and Holocene tufa microbialites have been documented globally on groundwater spring-fed supratidal rock coasts. Here, we document the first emergent facies assemblage and demonstrate its utility as a palaeo-shoreline (and sea-level) indicator. At Cape Freycinet, Western Australia, discrete palaeo-spring-associated deposits comprise five distinct facies that collectively define a Quaternary shoreline on a granitic rock coast similar to the contemporary coast. A palaeosol facies, passes laterally seaward into tufa microbialite on sub-horizontal bedrock, associated with oncoids. The most seaward facies is a microbially-cemented sand representing deposition in the upper-intertidal to supratidal zone of a sandy embayed beach, flanked by prominent headlands. A tufa-lithoclast breccia indicates occasional high-energy events. Facies distributions are controlled by bedrock topography in relation to palaeo-sea-level and the distinct suite of marginal marine, springline-associated facies define a Quaternary palaeo-shoreline at ca. +13 m above sea-level. The approach demonstrates the utility of marginal marine microbialite and related carbonate deposits as indicators of Quaternary sea-level on rock coasts.

1. Introduction

Modern tufa microbialites and associated carbonate deposits have been documented in the peritidal zone of rock coasts in southern Africa (Perissinotto et al., 2014; Smith and Uken, 2003; Smith et al., 2011), Southern and Western Australia (Forbes et al., 2010; Lipar and Webb, 2015) and Great Britain and Ireland (Cooper et al., 2022; Cooper et al., 2013; Faulkner and Crae, 2018; Smith et al., 2018). They are associated with spring discharges of carbonate-saturated groundwater and develop on high intertidal to supratidal locations in rock coast environments affected by sea spray and occasional marine storms (Cooper et al., 2022). Previous work on supratidal rock coast tufa facies has investigated groundwater spring hydrology (Dodd et al., 2018; Rishworth et al., 2017b), their microbial genesis (Rishworth et al., 2016b), wider ecology (Rishworth et al., 2019; Rishworth et al., 2017a; Rishworth et al., 2016a; Weston et al., 2018) and landform geomorphology (Edwards et al., 2017; Forbes et al., 2010; Rishworth et al., 2020a; Cooper et al., 2022).

Rock coast microbialites share many similarities with continental carbonate deposits but form in a distinct transitional, marginal marine, depositional setting (Garner et al., 2024). Supratidal rock coast tufa microbialites are regarded as potential archives of palaeo-climate, palaeo-shorelines and palaeo-sea-level (Rishworth et al., 2020a, 2020b), but investigations to date have been limited to active and remnant (Holocene) localities and potential submerged deposits (Rishworth et al., 2020a). Palaeo-rocky shorelines are only occasionally preserved in the geological record (Johnson, 1992; Johnson, 1988; Manikam et al., 2022) and their inherently erosional nature is often reflected in stratigraphic signatures as a single unconformity surface. Palaeo-rocky shores are usually only definitively identified via fossil associations (Johnson, 1992; Johnson, 1988; Sheppard, 2006), as the coastal morphology of erosion-resistant lithologies (e.g., granitic) in particular is negligibly affected by erosion at sea level (Kennedy et al., 2014). Consequently, preservation of these marginal marine tufa facies holds much potential for the delineation of former rocky shorelines.

Based on observations at Cape Freycinet, Western Australia this paper describes an emergent, Quaternary marine shoreline delineated by inactive microbialite and associated facies on a granitic rock coast. The aims are: (i) to describe and interpret microbialite-associated lithofacies and associations at the macro- to micro-scale; (ii) propose a depositional model; and (iii) assess post-depositional influences on preservation potential. A palaeo-shoreline is then delineated, and its age is inferred by comparison with dated proximal shorelines and

* Corresponding author.
E-mail address: Garner-T@ulster.ac.uk (T.W. Garner).

https://doi.org/10.1016/j.margeo.2025.107496
Received 6 November 2024; Received in revised form 31 January 2025; Accepted 1 February 2025
Available online 4 February 2025

observations from other far-field sites.

2. Geographical and geological context

Cape Freycinet is located in the Leeuwin-Naturaliste region, in the southwest of Western Australia (Fig. 1A). The site comprises a bedrock headland, of highly deformed Mesoproterozoic garnet-biotite granite gneiss (Collins, 2003; Janssen et al., 2003). Bedrock forms large joint-controlled elongate domal outcrops (Fig. 1D, E, F).

The surrounding area hosts outcrops of bioclastic calcarenite of Middle to Late Pleistocene-age 'Tamala Limestone' (Geoscience Australia and Australian Stratigraphy Commission, 2017; Logan et al.,

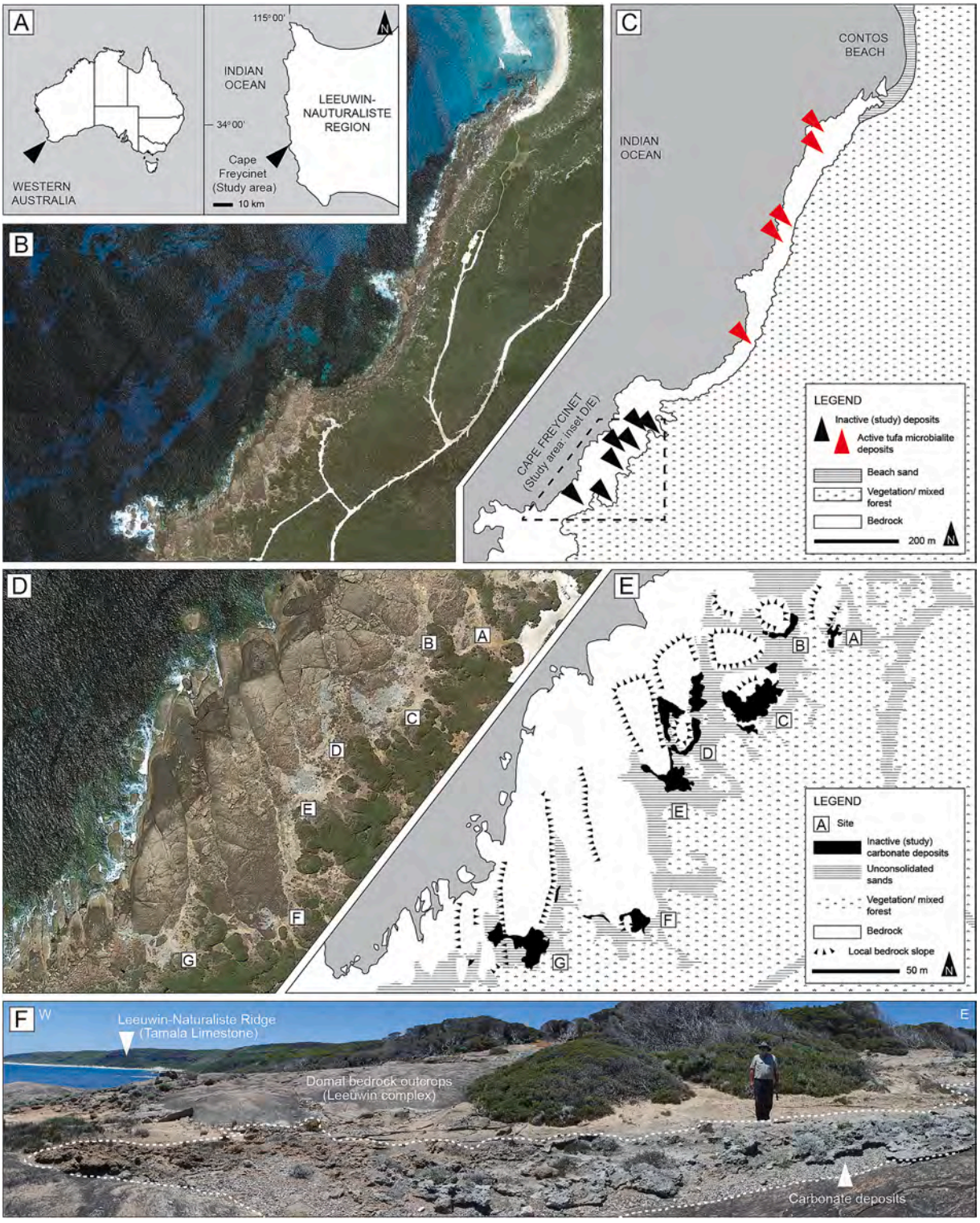

Fig. 1. A: Location of study area within Western Australia and Leeuwin-Naturaliste Region; B/C: Map of inactive (study) carbonate deposits and active tufa microbialite deposits within wider area north to Contos Beach (aerial imagery: Google Earth Pro (2017)); D/E: map of inactive (study) carbonate deposits showing individual study sites (aerial imagery: Google Earth Pro (2017)); F: photograph of the study site (from site B) due north; showing dominant regional geomorphological features.

1974; Logan et al., 1970) that forms the Leeuwin-Naturaliste ridge (Playford et al., 1976) that exhibits a number of karst features (Eberhard, 2004). Mineralised groundwater springs are present close to sea level and support actively accreting groundwater-fed supratidal tufa and tufa microbialite deposits occur along the modern coast (Forbes et al., 2010; Rishworth et al., 2020b)(Fig. 1B, C). No active spring discharges were noted at higher elevations in the jointed granitic terrain.

The regional climate is warm-summer Mediterranean, and the study area mean annual precipitation is 1013 mm (Bureau of Meteorology, 2024). The annual evaporation is 1069 mm (Luke et al., 1987). Regionally, mean daily wind speed varies from 2.58 ms^{-1} (May), to 3.32 ms^{-1} (January) (Bureau of Meteorology, 2024); with sea breeze dominating, up to 15 ms^{-1} (Fahner and Pattiaratchi, 1994; Pattiaratchi et al., 1997).

The coast is microtidal (diurnal tidal range 0.6 m (Pattiaratchi and Eliot, 2009)). Fluctuations in the Leeuwin Current cause mean sea level to vary on an annual cycle averaging 0.22 m. Continental shelf waves, coastal-trapped waves and meteorological effects cause additional water level variability (Cresswell and Golding, 1980; Fahner and Pattiaratchi, 1994; Feng et al., 2009; Feng et al., 2004; Pattiaratchi and Eliot, 2009). Data from the Cape Naturaliste Buoy (1998–2006) (Hemer et al., 2008) indicate significant winter wave height ca. 2.7 m and mean peak period of 13.76 s. Waves are unidirectional centred on ca. 225 °N (Hemer et al., 2008). Extreme wave events are largely attributed to extra-tropical cyclones (Hemer et al., 2008). Tsunamis have been recorded regionally in tide gauge data (Pattiaratchi and Eliot, 2009) and movement of coastal boulders >10 m asl and 100 m inland have also been attributed to tsunamis (Scheffers et al., 2008).

3. Methods and materials

Following the serendipitous discovery of this locality while prospecting for modern spring-fed supratidal microbialites, the deposits were mapped and sampled. Representative hand samples of carbonate deposits were cut, polished and thin sections prepared. The description of carbonate and microbialite facies follows Flügel (2010) and Grey and Awramik (2020); mixed siliciclastic-carbonates follows Flügel (2010) and palaeosol facies follows Bullock et al. (1985) and Kemp (1985). Facies classifications were defined following Pedley (1990), Ford and Pedley (1996), Riding (1991) and rock-coast-tufa-specific nomenclature (Garner et al., 2024).

Elevation data was derived from the Copernicus DEM (Global and European Digital Elevation Model (COP-DEM, 2024)) with a Height Error Mask (HEM) quality layer representing the corresponding height error standard deviation.

4. Results

4.1. Outcrop: Occurrence and distribution

Inactive deposits of tufa and related carbonate facies occur in a linear series of discrete sites (A-G) arranged parallel to the modern shoreline at

Table 1
Summary of facies characteristics.

Code	Facies name	Macro-geometry/ -structure	Lithology/ Textural characteristics of components	Sedimentary structures and biological content	Common associated facies	Depositional environment	Post-depositional (diagenetic features)
F1	Oncoid	Unattached to oncolite sheet; one-clast thick sheets up to 3 m^2	Microbial boundstone	External: pustular Internal: concentric undulatory layered with discontinuities; transitioning to domal-columnar Laminae-perpendicular microbial filaments	Merge into F2 vertically and horizontally. Associated with F4, F5 on erosional surfaces.	Shallow bedrock depressions; on discharge aprons and unconsolidated sands	Chemical weathering (etching)
F2	Tufa microbialite	F2.1 Crusts and sheets; ca. 330 m^2 in area; < 20 cm thickness F2.2 Small barrages F2.3 Cascades F2.4 Basin rims	Microbial boundstone	External: F2.1: pustular-colloform; F2.3: microterraces and microridges Internal: variable structure (stratiform/ undulatory layered/ bulbous domical/ linked columnar/thrombolitic) Microbial multifurcate shrubs; microbial filaments; marine mollusc shell	Merge with F1 and F3. Merge with F4 dependent on lithic content.	Discharge apron (sub-horizontal bedrock) Barrages (sub-horizontal bedrock) Cascade (sub-vertical bedrock) Basins (bedrock and karst)	Cements: spar infilling of fracture pore Karren features
F3	Tufa-lithoclast breccia	Irregular karren/ micro-karstified; ca. 1 m^2 in area	Micrite matrix-supported breccia with clast type 1: granule-cobbles of micrite; and clast type 2: laminated platy granules of spar	Shell fragments, echinoid spine; clast type 1: burrow porosity; clast type 2: microbial rip up clasts	Associated with F2.	Storm/high swell deposit within barrage pool or depression	Cements: coatings, gravitational, pendent, and bridging
F4	Microbially-cemented sand	Irregular karren/ micro-karstified; ca. 20m^2 in area; < 30 cm thickness	Micritic sandstone; coated grains interlaminated with laminated boundstone	Variable structure: undulatory layered/ linked columnar	Merge with F2 (inter-digitates F2.1, sharply F2.2). Erosional contact with F2.4.	Inter- to supratidal sand beach	Cements: gravitational, dripstone and meniscus cements
F5	Palaeosol	Irregular karren/ micro-karstified; ca. 30 m^2 in area; < 23 cm thickness	Peloidal wackestone	Ubiquitous rhizoliths, charcoal, gastropods (terrestrial), clast type 2: microbial rip up clasts	Merge with F4.	Vegetated soil (groundwater calcrete)	Cements: spar coating of pores and rhizoliths Karren features

a consistent elevation and separated from each other by topographic highs of granite bedrock (Fig. 1D, E). Deposits are primarily situated at between 18.92 ± 0.48 m (top of site A) to 11.5 ± 0.44 m (bottom of sites C and D) ASL; although site G extends to 4.98 ± 1.58 m ASL.

Carbonate build-ups range in thickness from thin veneers (< 1 mm) on bedrock to ca. 25 cm in topographic lows. Each site contains a complex suite of five adjoining facies (F1–5) which are summarised below (Table 1).

4.1.1. F1: Oncoids

Oncoids (F1) occur on the landward side of all sites forming in loose 'patches', and thin surficial beds, up to 3 m^2 (Fig. 2A) on flat-lying bedrock and lithoclastic sand. While most oncoids are unattached (Fig. 2B, C) some are attached to the substrate (Fig. 2D). Oncoids typically form patches one oncoid thick, however, where they merge with F2, some imbrication and vertical development is present. Individual oncoids vary in size from 1.5 to 15 cm in diameter and are platy with a distinct discoidal shape. Intra-site accumulations are uniform in size.

4.1.2. F2: Tufa microbialite

Tufa microbialite (F2) is present at all sites as expansive (up to 330 m^2) sheet-like deposits up to 20 cm thick resting directly on bedrock (Fig. 3A) and typically grading into F4 seaward. Four distinct macromorphologies/−structures occur:

- F2.1: Extensive sheet-like crusts on a gently dipping sub-horizontal surface (Fig. 3B). These vary from thin veneers (< 1 mm) to 20 cm thick deposits.
- F2.2: Small barrage structures forming on moderate gradients (Fig. 3C).
- F2.3: Cascades and shelves on complex bedrock topographies with steeply dipping surfaces, forming a thick waterfall-like deposit (Fig. 3D).
- F2.4: Thin (<2 cm) discontinuous rims around bedrock depressions (Fig. 3E).

The surface of F2 frequently displays karren or microkarstic solution features including trittkarren (Fig. 4B, C) and microkarren features including microrills and micro-grikes.

4.1.3. F3: Tufa-lithoclast breccia

Tufa-lithoclast breccia (F3), covers ca. 1.5 m^2 within an outcrop of F2 with an obscure contact (Fig. 5A). It has an irregular, weathered and microkarstic surface texture.

4.1.4. F4: Microbially-cemented sand

F4 forms up to 30 cm thick, expansive (up to 20 m^2) deposits of carbonate-cemented sand (Fig. 5B) at the most seaward extent of sites on the margins of elongate depressions flanked by bedrock outcrops (Fig. 6A, B). At sites B and E, this facies is present at similar elevations of 15.45 ± 0.48 m to 12.86 ± 0.39 m and 15.54 ± 0.43 m to 13.1 ± 0.39 m respectively.

Mid-orange to brown in colour, it rests directly upon bedrock, and within more extensive areas of unconsolidated sand (Fig. 6). Weathered outcrops preserve cm-scale parallel bedding that dips gently seaward at 5-10° with occasional granitic boulder intraclasts (Fig. 5B). At site B, it inter-digitates with F2, and has occasional erosional contacts such as weathered outcrops with tufa microbialite rims (Fig. 4A).

4.1.5. F5: Palaeosol

Palaeosol (F5), occurs as a thick deposit, up to 23 cm and up to 30 m^2 in area. It is dark–mid grey in colour, has an irregular, weathered texture, and rests directly on bedrock (Fig. 5C, D). It occurs landward of F1 and F4 with which it has a gradational contact. The surface morphology of F5 includes three notable karren features: cavernous (alveoles) weathering (Fig. 4E), pans and pit-like structures (Fig. 4D, F), and wells and shafts (Fig. 4F, G).

4.1.6. Carbonate facies distribution

The distribution of facies varies between sites (Fig. 6), with sites (A, C, E, F and G) with sub-horizontal bedrock comprised of F2 (tufa

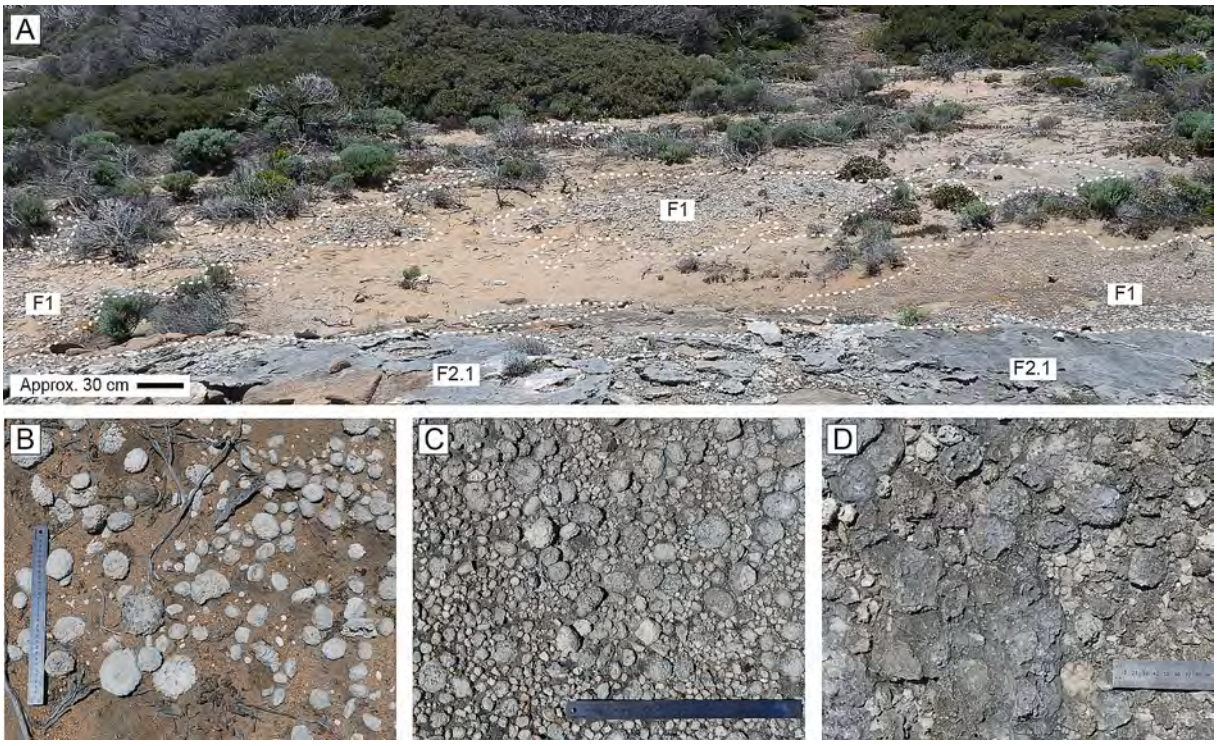

Fig. 2. Oncoid macrostructure. A: discrete patches (white dashed lines) on the landward side of site D; B-D: variety of oncoid attachment in plan view: B: 'unattached' oncoids lying on unconsolidated siliceous sand (site D); C: oncoid 'pavement' (site F); D: in situ oncoids merging with F2 (site C). Scale: 30 cm metal ruler.

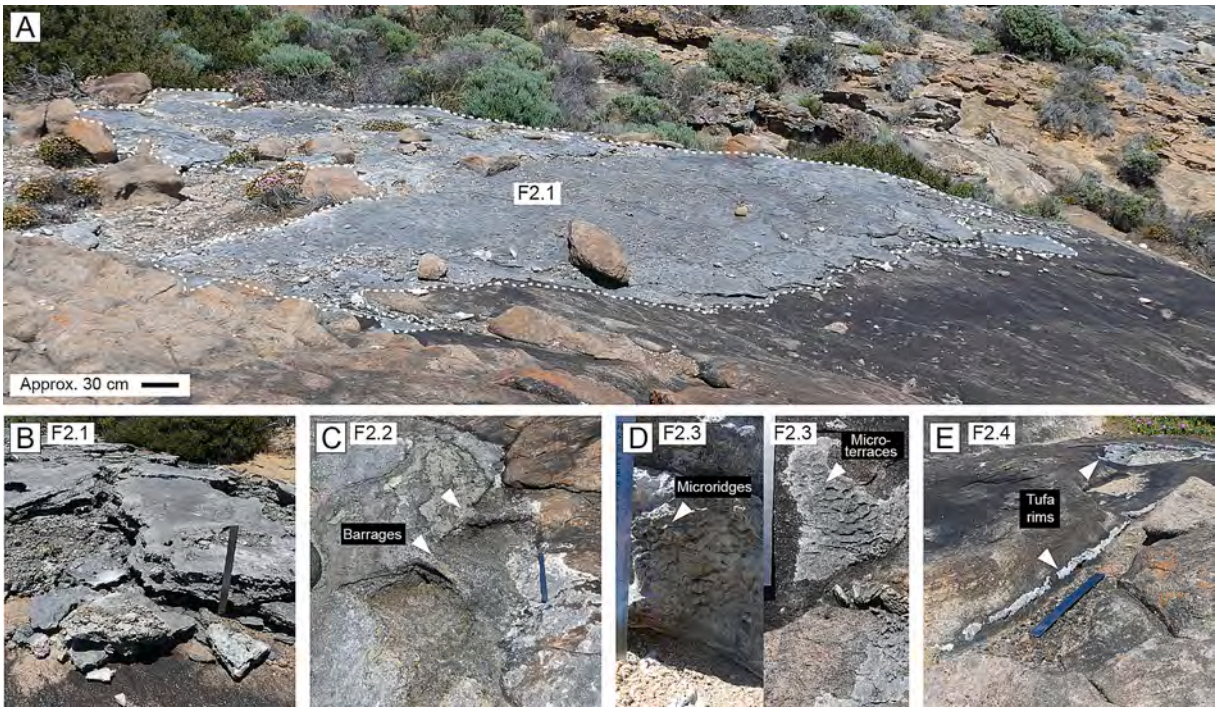

Fig. 3. Tufa microbialite macrostructure. A: expansive sheet-like deposit accreting directly on bedrock (site C) (white dashed lines), B: F2.1 crusts and sheets (site D); C: F2.2 small barrages (site G); D: F2.3 cascades on sub-vertical bedrock, with microridges and microterraces (site F); E: F2.4 thin rims surrounding bedrock depressions (site F). Scale: 30 cm metal ruler.

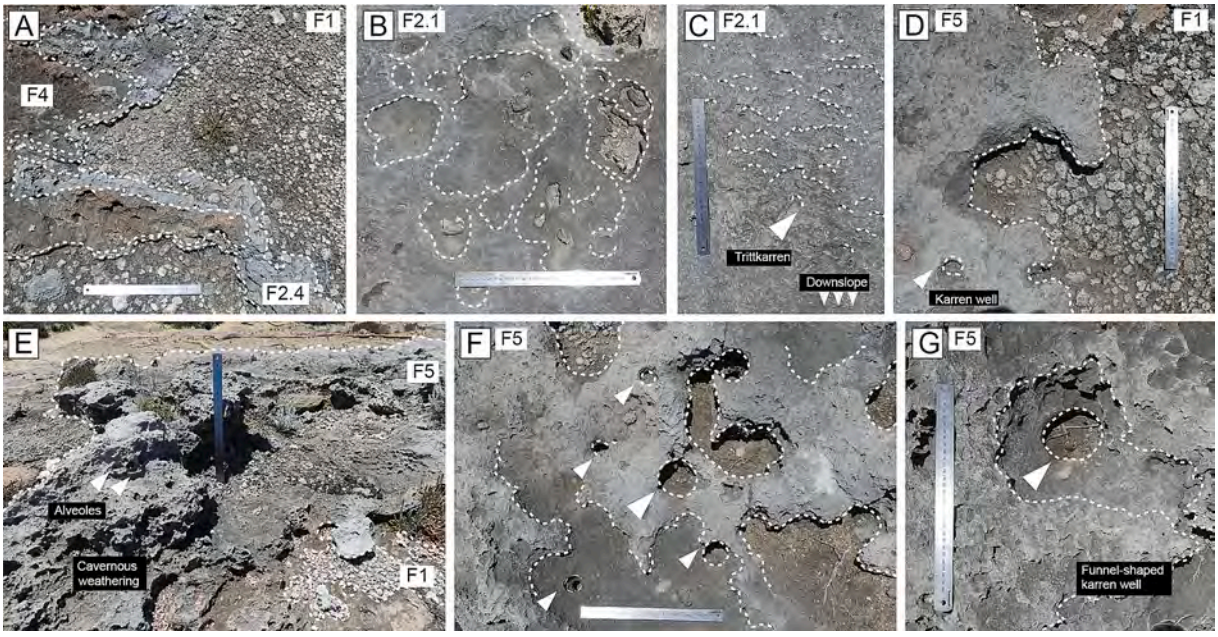

Fig. 4. (A-C) karren features of F2 tufa microbialite facies in plan view: (A) erosional margin of F4 with later deposition of F2 facies; (B) shallow depressions; (C) shallow semi-circular depressions or trittkarren; (D) karren wells with erosional margin of the deposit; (*E*-G) karren features of F5 palaeosol facies (white dashed lines): (E) cavernous weathering with alveoles; (F) karren wells in plan view; (G) funnel-shaped karren well in plan view. Scale: 30 cm metal ruler.

microbialite) which forms a large sheet-like deposit (Fig. 6D). The carbonate deposits occur a series of in elongate depressions along strike from each other and separated by large bedrock domes, resulting in horseshoe-shaped deposits (Fig. 6B, C). Where present, F5 occurs at the highest elevation (landward), and grades seaward into F2 and then F4 with decreasing elevation. Where F5 is absent F1 and F2 grade seaward into F4 (Fig. 6C).

4.2. Sedimentology: Macro- and meso-structure

4.2.1. F1: Oncoids

Oncoids have a cortex surrounded by concentric lamination of microbial boundstone, with markedly different upper and lower surfaces (Fig. 7). The paler coloured upper surface is typically rounded and pustular (Fig. 7A-C). The darker, lower surfaces are commonly etched

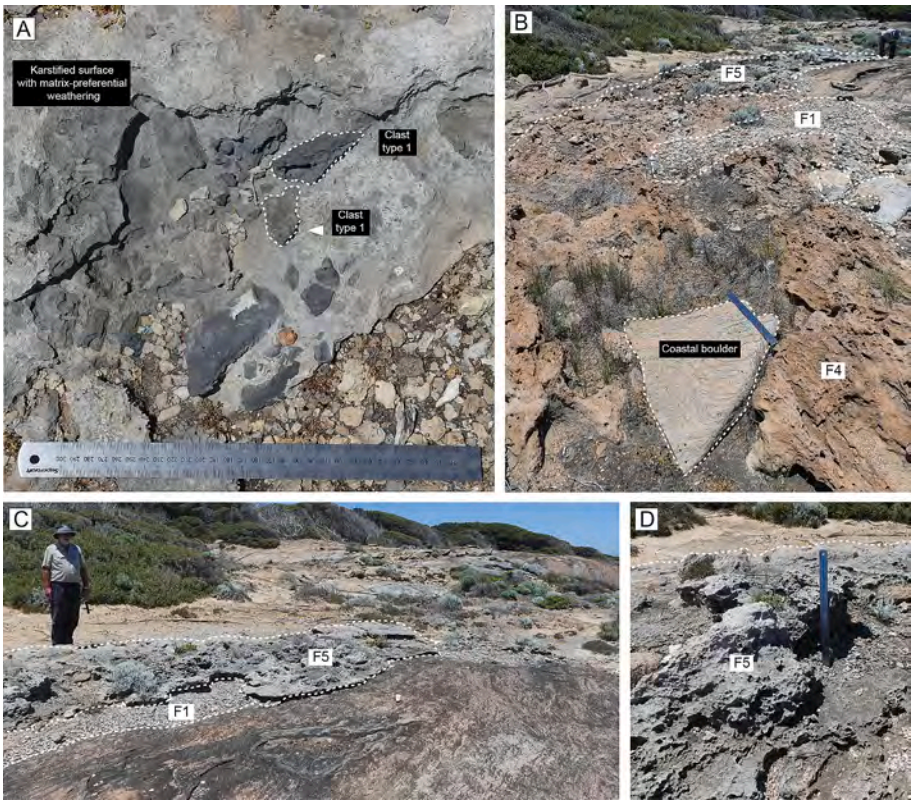

Fig. 5. Outcrops of F3–5: A: Tufa-lithoclast breccia outcrop showing macrostructure with weathered matrix and clasts (clast type 1) (white dashed lines); B: outcrop showing irregular, karstified surface and distribution of F4 (white dashed lines), and boulder clast; plus associations with F1 within elongate embayment surrounding domal bedrock outcrop (site B); C, D: distribution and highly karstified surface topography of F5 (white dashed lines) (site B), scale: 30 cm metal ruler.

with a large central cavity and small coalescing pits (Fig. 7A.). The internal mesostructure comprises an undulatory to columnar cortex, developed around a nucleus, of carbonate-cemented detrital grains (Fig. 7E). Siliciclastic detrital grains are also present in inter-column spaces (Fig. 7D, G).

Undulatory layered laminae envelop a nucleus primarily in mode I, inverted hemisphere, growth patterns (Logan et al., 1964) (Fig. 7E). The oncoids show concentric undulatory laminae with variable continuity and thickness and are smooth-wavy with a moderate degree of inheritance. They transition outwards to more complex linked, closely-spaced slender columns to bulbous domes (Fig. 7D, G), manifesting as pustules. This columnar growth develops directly on older laminae and detrital bedrock grains. Intercolumnar shelter pores are frequently infilled by lithic grains that are enclosed by laminae forming coalesced and anastomosing structures (Fig. 7D, G). These columns and domes demonstrate some degree of growth variability (constringed) and have variable degrees of branching, from single columns to multifurcate and anastomosed (Fig. 7D, G). Laminae are of variable thickness (ca. 10–150 μm) and are harmonized between adjacent columns and domes with a high degree of inheritance (Fig. 7G). Laminae are highly variable in shape with wrinkled and smooth laminae, often in succession (Fig. 7D-G).

Undulatory layered laminae are disrupted by erosive discontinuities, evident in section where discontinuities cross-cut oncoid lamination (Fig. 7D, E). Minor discontinuity surfaces are also present on the oncoid upper surfaces between pustules (Fig. 7E).

4.2.2. F2: Tufa microbialite

F2 is a microbial boundstone with a variable surface texture. Crusts and sheets (F2.1), have a smooth surface with some domal to flat-topped pustules and colloform topography, while the surfaces of cascades (F2.3) frequently have microterraces and microridges (Fig. 3D).

F2 is predominantly composed of precipitated carbonate with rare detrital grains. The mesostructure is predominantly stratiform-undulatory layered, with some bulbous domical and linked-columnar structures with contacts between growth structures are delineated by intra-head fractures and pores (Fig. 8G, H). Lamination is defined by colour variation, shrubs capped by fenestral pores and inter-laminae porosity. Small shrub-like structures are visible at the mesoscale as thick laminae and branching features, commonly multifurcate (Fig. 8E, H). A thrombolitic (clotted) mesostructure was noted, in the upwall of a small barrage feature (F2.2). The clots are irregular with interparticle and burrow-like porosity (Fig. 8C, D). Inclusions are common, with lithic bedrock-derived and exotic clasts varying from boulders (that protrude above the enclosing microbialite) to sand, and occasional marine gastropod shells.

4.2.3. F3: Tufa-lithoclast breccia

F3 is a poorly-sorted matrix-supported breccia with carbonate clasts (large cobbles to very fine sand), within a pale grey matrix (Fig. 5A). Two types of coarse carbonate clasts, both with a thin spar coating are common within the matrix: type 1 comprises angular granules to large cobbles of micrite (Fig. 9B, D-E) while type 2 is characterised by sub-angular, platy granules of laminated spar with alternating dark and light laminae parallel to the clast long axis (Fig. 9A, C-E).

The matrix comprises granules to fine sand in a micrite matrix and includes fine detrital lithic grains, carbonate grains, and compound grains. Compound grains are well- rounded to rounded grains of micrite (Fig. 9D). The meso-porosity is complex, dominated by interparticle pores between compound grains, and shelter pores beneath clasts. The latter are infilled or partially cemented with spar cement that forms partial coatings and gravitational (pendant and bridging) cements on the underside of grains or matrix (Fig. 9C). Marine gastropod and echinoid spine fragments are also present.

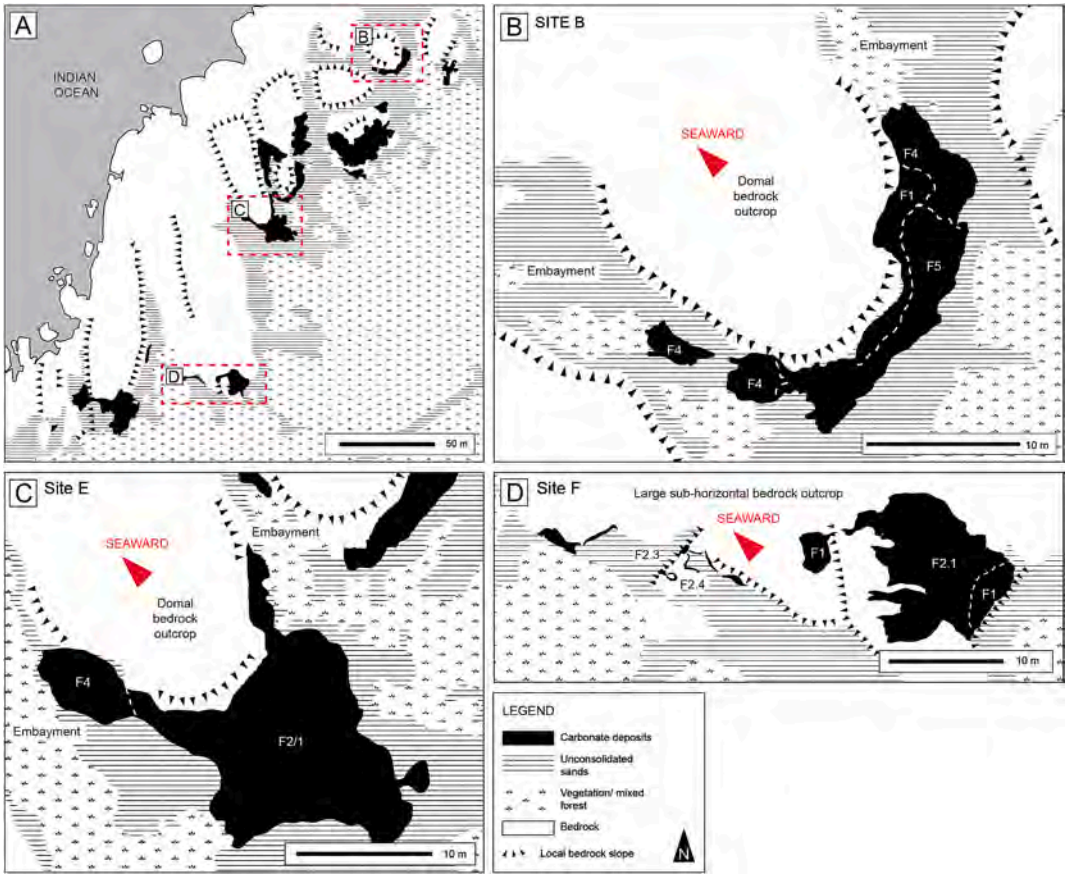

Fig. 6. Maps of carbonate deposit distribution: A: All inactive (study) deposits; with insets A, B and C: Site facies maps for sites B, F, and E.

4.2.4. F4: Microbially-cemented sand

F4 is a clast-supported micritic sandstone, with two distinct microfacies distinguished by differing lithic-carbonate ratios: a coated lithic grain-dominated and a laminated carbonate microfacies (Fig. 10C).

The coated grain-dominated microfacies contains well-rounded to sub-angular, and moderately sorted, medium to very coarse detrital sand grains (dominated by quartz but rich in orthoclase feldspar). These grains are micrite-coated (Fig. 10) and some grains have a 'double' coating (Fig. 10B). This microfacies is highly porous with dripstone and meniscus cements (gravitational fabric) often occurring at the sharp contact between microfacies (Fig. 10B).

The laminated carbonate microfacies is composed of encrusting micrite (Fig. 10). The laminated micrite is undulatory layered to linked columnar (Fig. 10B) with irregular (non-couplet) laminar patterns and a high degree of inheritance. This microfacies has low porosity, containing interparticle or breccia pores where laminae are not continuous but brecciated. Intercolumn spaces are typically infilled with carbonate and coated lithic debris and interparticle or shelter pores containing gravitational or dripstone cements, forming microstalactites.

4.2.5. F5: Palaeosol

F5 is a peloidal wackestone with the fabric supported by carbonate mud, comprising a detrital component and a dark micrite matrix. There is little meso-porosity or large-scale structure (Fig. 5C, D). Rhizoliths (channel infills of plant roots) of microsparite are ubiquitous on weathered surfaces (Fig. 11A). F5 contains numerous bioclasts and inclusions including charcoal particles; involute and lenticular gastropod shells (Fig. 11C, D.) and clasts of type 2 (platy, laminated spar) breccia clasts (F3).

4.3. Sedimentology: micro-scale and petrography

4.3.1. F1: Oncoid

Thin sections (Fig. 12) confirm the undulatory layered and columnar structures seen in hand specimen but also reveal numerous microbial filaments perpendicular to lamination (Fig. 12B, C).

4.3.2. F2: Tufa microbialite

Thin sections display similar mesostructure features to polished sections. Two microstructures are evident: a) subtle undulatory laminae, with convex laminae over pores and voids; and (b) stubby bulbous structures with smooth-wavy laminae (Fig. 13). Dome initiation is from the undulatory layering and lithic grains. The contact between the various growth forms is typically gradational, but some sharp erosional contacts were observed. Whole spar infilling of pores was observed at the microscale (Fig. 13F). Bundles of small (4–6 μm wide; 115 μm long) dark rods within darker lamina in the basal undulatory layering are orientated near perpendicular to lamination are interpreted as algal or cyanobacterial filaments (Fig. 13D, E).

4.3.3. F3: Tufa-lithoclast breccia

In thin section, clast type 1 within F3 is mid-dark brown and is dominated by micrite (Fig. 14). It is composed of massive, irregular blocky grains (280–1200 μm diameter) and small irregular grains (50–80 μm diameter). Rounded to sub-rounded grains are interpreted as micrite peloids. The complex porosity is dominated by zones of burrow pores, merging with indistinct channel pores, interparticle pores and a single fracture pore. Pores are coated or fully infilled with spar cement (Fig. 14C).

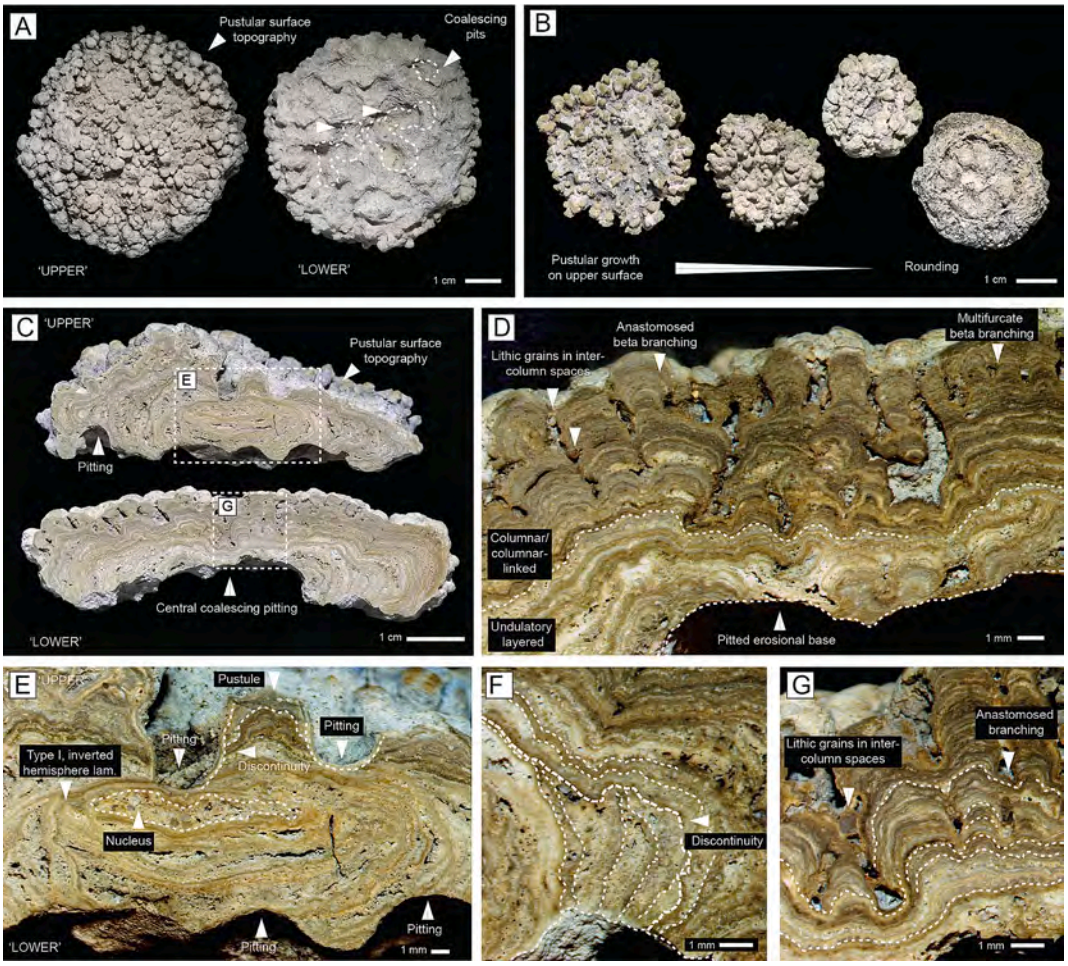

Fig. 7. Oncoid macro−/ meso-structure; unattached oncoids from site D. A: upper and lower surface of a representative oncoid, showing pustular upper surface and coalescing pits on the lower surface (plan view); B: variable degree of rounding of oncoids (plan view); C: cross section through oncoids; D: showing columnar/ columnar-linked and undulatory layered mesostructure (cross section); E; showing oncoid nucleus, and frequent discontinuities (cross-section); F: frequent discontinuities in laminae (white dashed lines; in cross section); G: detail of columnar structure (cross section).

4.3.4. *F4: Microbially-cemented sand*

In thin section, F4 exhibits with the same two distinct facies seen in hand specimen (Fig. 15). Coated grains are composed of sub-rounded and sub-angular siliciclastic detrital grains (predominantly orthoclase feldspar and quartz). In the laminated carbonate microfacies, erect turbinate stubby columns (microstromatolites) are evident with inter-column infill of lithic grains and disaggregated micrite (Fig. 15C). Laminae are typically continuous and non-couplet. Thin cement rims of spar are observed in voids, and dripstone or gravitational cements are also present.

4.3.5. *F5: Palaeosol*

In thin section, F5 has an intergrain microaggregate structure composed of coarse lithic grains and a fine microaggregate of particles around 15–60 μm which form a crumb-like structure (Fig. 16). The groundmass comprises coarse (< 2 mm; > 100 μm) and fine (<100 μm) fractions distributed heterogeneously. The coarse fraction is dominated by well-rounded to sub-angular, bedrock-derived grains and compound of medium to fine sand grains with a partial or complete coating of micromass or forming aggregated compound grains. The fine fraction has a mottled appearance due to the occurrence of small, 20–40 μm diameter, ellipsoid pellets and smaller undifferentiated particles interpreted as peloidal micrite. Channels, vugs, complex packing voids and planar voids (cracks) are present (Fig. 16). Nearly all voids are partially or wholly infilled by spar forming a void coating. The largest macro- and meso-channels (Fig. 16) equate to the rhizoliths visible on weathered surfaces (Fig. 11A).

5. Interpretation and discussion

5.1. *Facies interpretation and depositional environment*

5.1.1. *F1: Oncoids*

Oncoids commonly form through the activity of cyanobacteria involving both biomineralization (Dupraz et al., 2009; Freytet and Verrecchia, 1998; Jones and Renaut, 2010; Riding, 1983), and inorganic mineralization (Beeler et al., 2020; Gomez et al., 2014; Kano et al., 2003). This facies is interpreted as having formed in shallow basins of sub-horizontal bedrock or unconsolidated sands within or adjacent to a groundwater spring. The basins were impounded by tufa microbialite barrages (F2.2) or occupied low bedrock topography, impounding groundwater. The discoidal shape of oncoids suggests vertical growth was limited by water depth, and uniformity in size within each site indicates that morphology is controlled by local factors.

Nucleation of oncoids occurred as a microbial community developed around a nucleus of detrital bedrock grains and undulatory layered laminae indicate successive microbial activity. Mode I lamination (inverted hemisphere with discontinuities) suggests occasional overturning. Concentric lamination within oncoids is classically attributed to sub-aqueous rolling of spheroidal and rounded morphologies

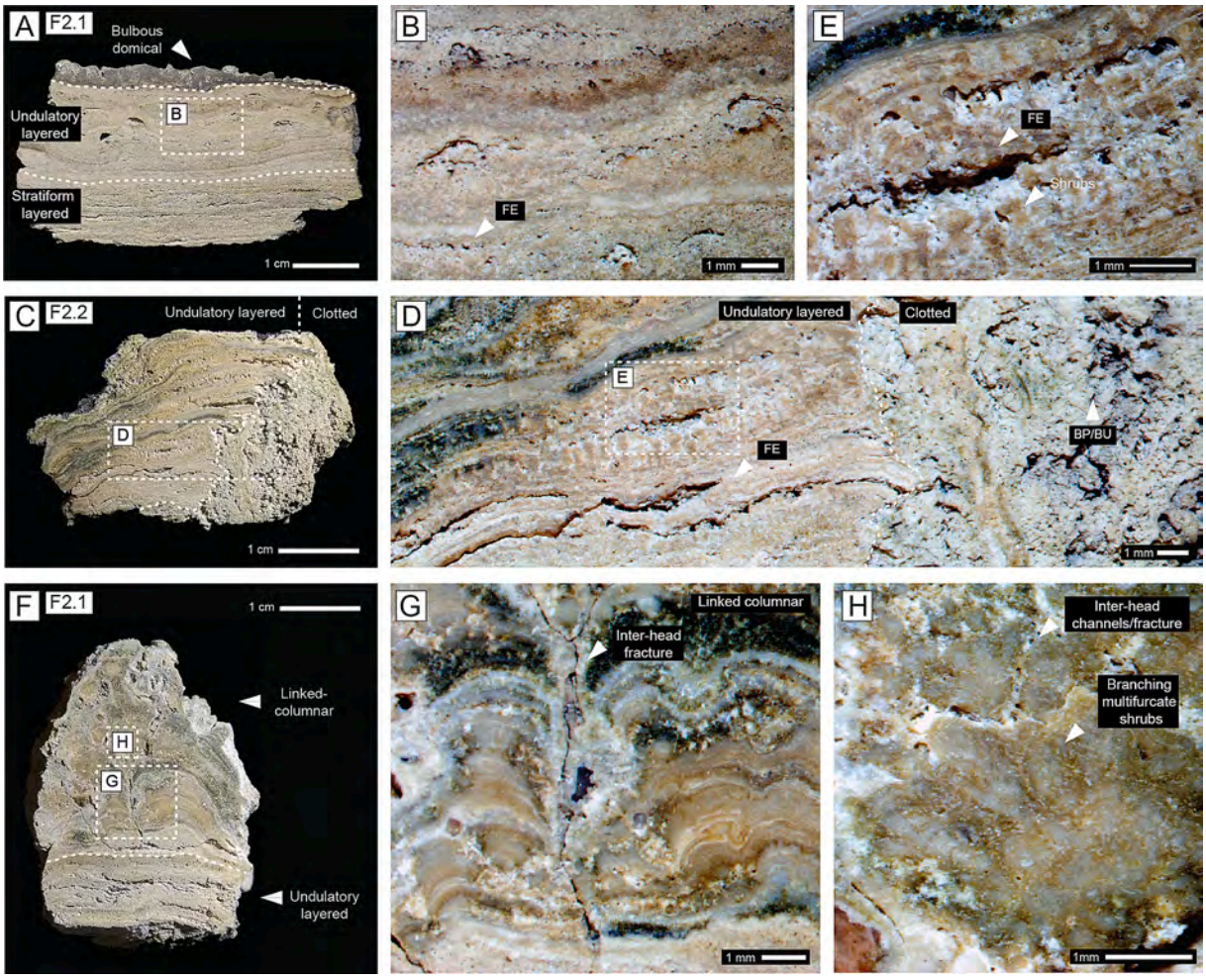

Fig. 8. Tufa microbialite internal mesostructure in section. A: stromatolite (F2.1; site F) showing stratiform layered, undulatory layered and bulbous domes in section with inset B: fenestral (FE) porosity; C: small barrage (F2.2; site G) with undulatory layered (stromatolitic) and clotted (thrombolitic) mesostructure with inset D: interparticle/burrow (BP/BU) porosity and inset E: porosity and shrub structure; F: stromatolite (F2.1; site G) showing layered and bulbous domical/columnar mesostructure with inset G: stromatolitic columnar growth and inset H: shrub structures.

(Dahanayake, 1978; Flügel, 2010; Logan et al., 1964). However, in situ growth without particle overturning has been recognised (Hägele et al., 2006; Jones, 2011; Leinfelder and Hartkopf-Fröder, 1990; Lencina et al., 2023; Zatoń et al., 2012; Zhang et al., 2015), with this facies comparable to reported oncoids with pustular surface and characteristic underside cavity (Leinfelder and Hartkopf-Fröder, 1990).

Discontinuities suggest of periods of dissolution, weathering, or erosion alternated with microbial growth. Present in the undulatory layered microstructure, it suggests this was frequent when oncoids were smaller and required less energy to be overturned, and their absence in the domal/columnar microstructure suggests stabilisation when larger.

The occurrence of coalescing pits in the centre of the lower side and minor etching between pustules on the upper side points to chemical weathering (etching). This suggests that large oncoids were not overturned, and the absence of later accretion in these pits suggests that some weathering occurred post-deposition or the basal hollow is a primary feature (Leinfelder and Hartkopf-Fröder, 1990). Microbial growth on the underside of in situ oncoids is suggested to result from reflected light penetration through inter-pustular gaps accessing the lower surface (Hägele et al., 2006; Leinfelder and Hartkopf-Fröder, 1990; Rodrigues et al., 2022). The central coalescing pits in Cape Freycinet oncoids are interpreted as being formed through a primary hollow formed due to light constraints and subsequently exploited by chemical weathering.

5.1.2. F2: Tufa microbialite

F2 is a phytoherm boundstone facies (Ford and Pedley, 1996; Pedley, 1990) or tufa microbialite (Garner et al., 2024; Riding, 1991), that forms as a discharge apron on bedrock. The variable macro-morphologies reflect local bedrock topography and discharge flow conditions. Crusts on gently-dipping, sub-horizontal surfaces (F2.1) are attributed to deposition by sheet flow of water. The variable thickness of laminae and erosional contacts (e.g., between basal undulatory lamina and the upper bulbous domes) suggest episodic flow that creates growth hiatuses. Small barrage structures (F2.2) develop on moderately dipping bedrock where flow was channelised and barrages impounded water in bedrock depressions. On sub-vertical bedrock the thick accumulations with surface microterraces and microridges (F2.3) are regarded as hydrodynamic features, related to the formation of barrages (Edwards et al., 2017; Hammer et al., 2007; Pentecost, 2005). Thin rims surrounding depressions (F2.4) are interpreted as developing in in bedrock depressions or basins. Tufa rims form at the water-air interface and represent the palaeo-water-level in these pools. Their precipitation may be linked to degassing of carbonate saturated groundwater enhanced by microbial activity.

A microbial genesis for F2 is supported by the fenestral and inter-laminae porosity, associated with supratidal-intertidal algal and microbial-related sediments (Flügel, 2010), and the presence of multifurcate shrubs and pustular-colloform surface topography. The clotted mesostructure is interpreted as a thrombolite (Fig. 17). While

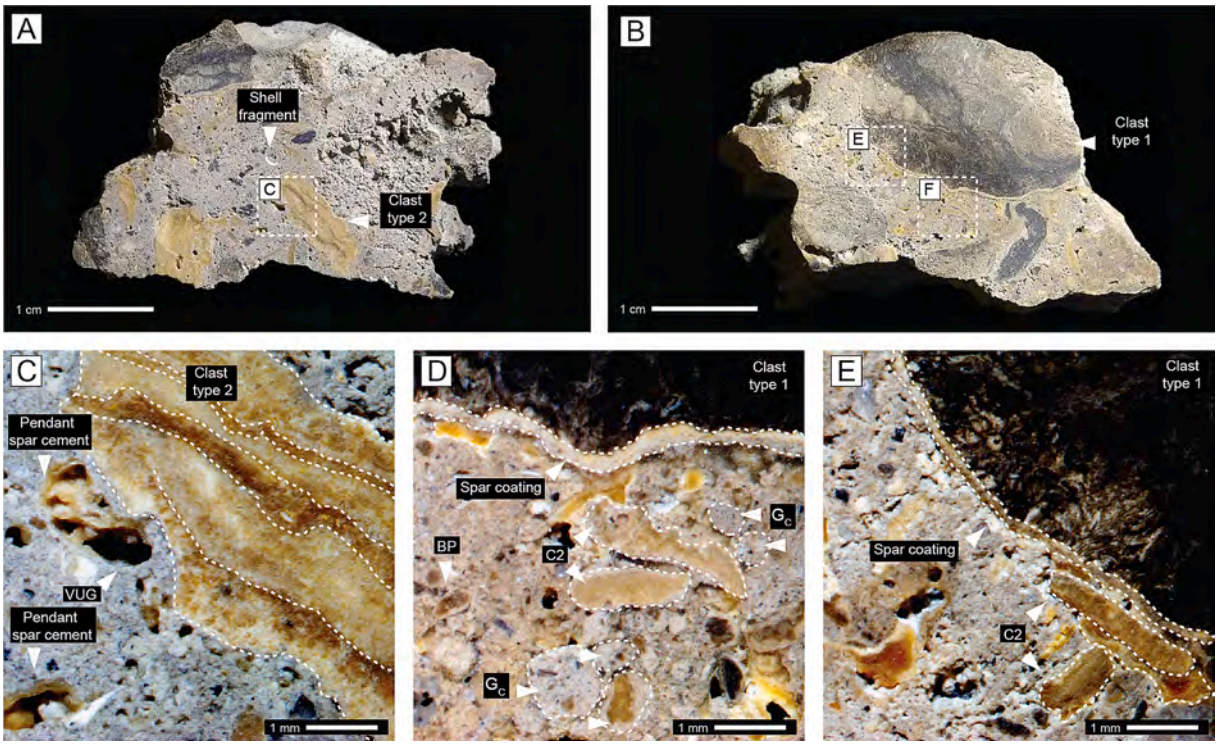

Fig. 9. Tufa-lithoclast breccia macro−/meso-scale (site G): A, B: tufa-lithoclast breccia showing clast type 1 and 2, and insets C: detail of clast type 2 with couplet lamination, and pendant spar cement within vugs (VUG); D: detail of clast type 2, compound grains (Gc), interparticle pores (BP) and spar coating of clast type 1; E: detail of both clast types with spar coating.

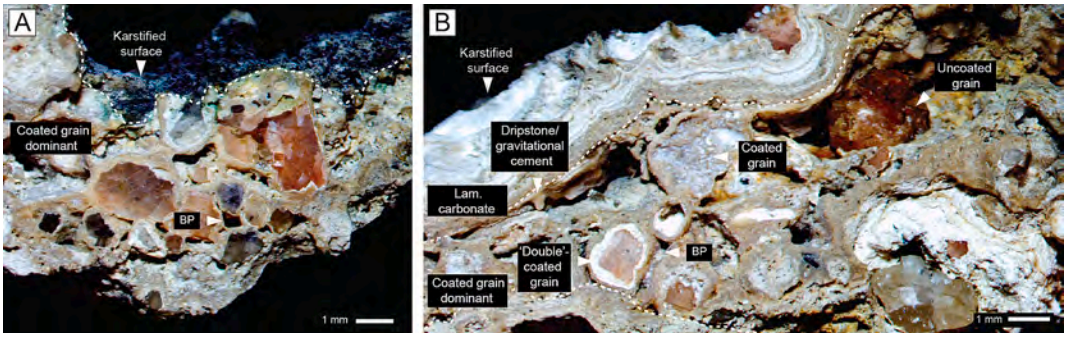

Fig. 10. Microbially-cemented sand macro−/meso-scale: mesostructure showing laminated carbonate and coated grain dominant microfacies with interparticle (BP) pores.

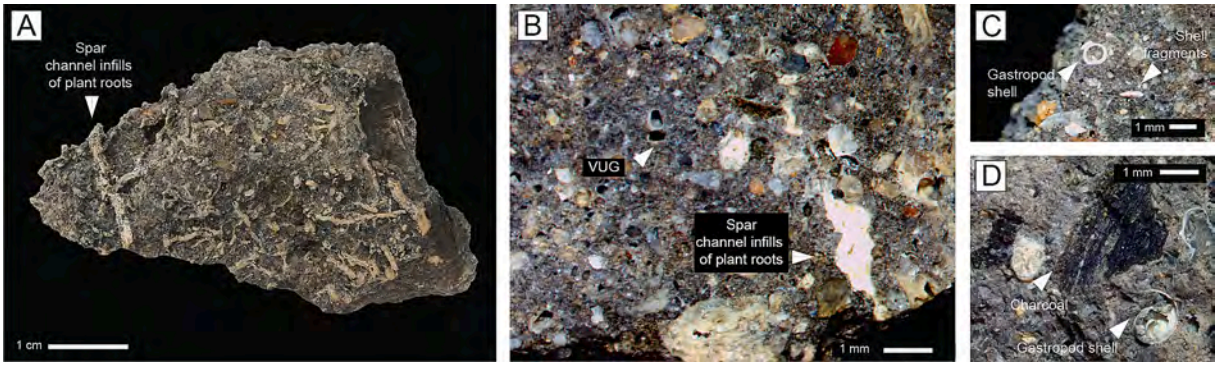

Fig. 11. Palaeosol macro−/meso-scale: A: spar channel infills of plant root cast pores on the surface of a hand specimen; B: Palaeosol in section showing channel infills and lithic content; C: gastropod shell and shell fragment inclusions; D: blocky charcoal and gastropod shell inclusions on broken face of sample.

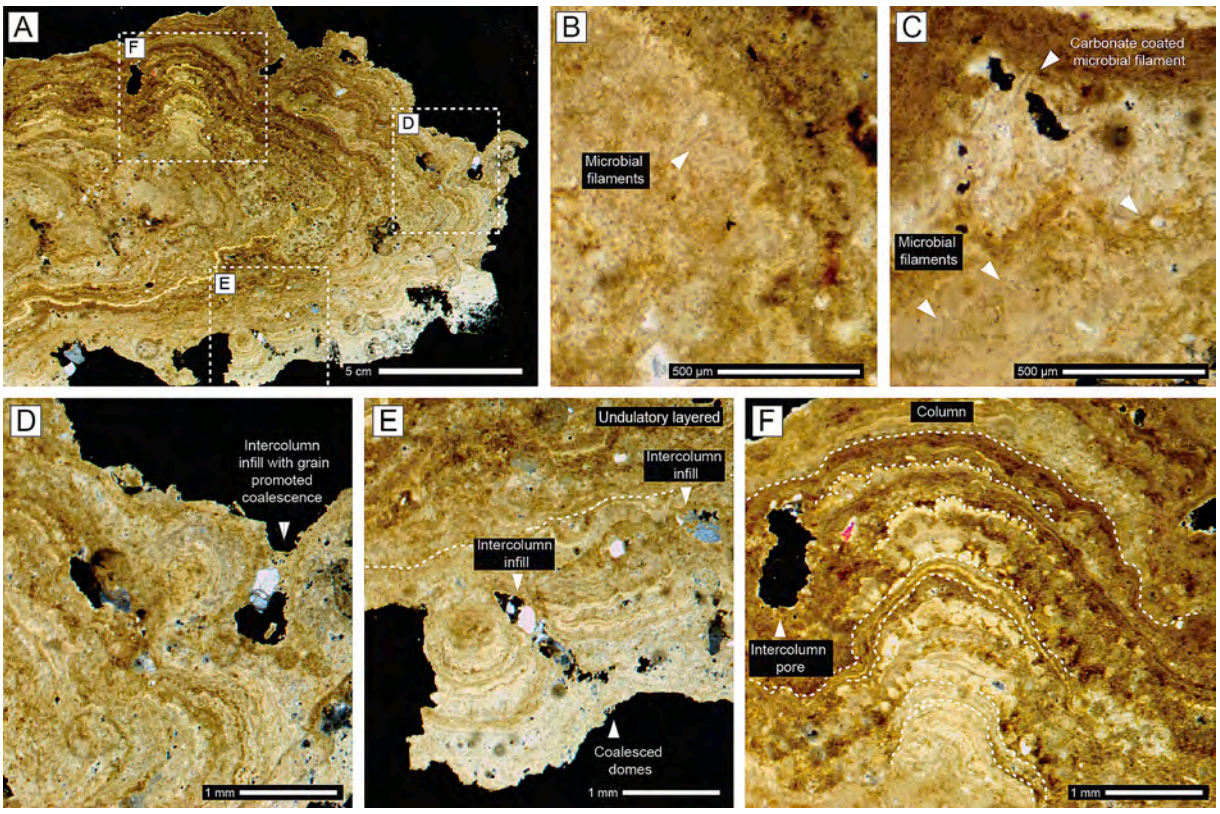

Fig. 12. Oncoid microstructure in thin section under XPL (site F): A: large scale scan of thin section showing concentric lamination; B, C: microbial filaments; carbonate coating visible around microbial filament within vug; D, E: intercolumn infills with detrital grains; F: detail of some column lamination (white dashed lines).

thrombolites may form through distinct microbial communities or the bioturbation of an original stromatolitic fabric (Burne and Moore, 1987; Harwood Theisen and Sumner, 2016; Shapiro, 2000; Walter and Heys, 1985) the latter genesis is suggested by the adjacent undisturbed stromatolitic texture. The restriction of thrombolitic structure to the upwall of a small barrage feature (Fig. 17) suggests bioturbators were present within the barrage pool, while the dropwall was subaerially exposed.

5.1.3. F3: Tufa-lithoclast breccia

F3 is an intraclast or macrodetrital tufa (Ford and Pedley, 1996; Pedley, 1990). The presence of large clasts suggests deposition under periodic high-energy conditions and the poorly-sorted mixture of constituent grains points to event-based sedimentation (i.e., storms and high swell events). The source of clasts is variable: clast type 1 (generally structureless large cobbles of micrite, with burrow porosity) is likely to be locally sourced lithified pool infill, with benthic metazoans forming burrow porosity in a marl-like calcareous mud. Clast type 2, (laminated platy clasts) are interpreted as indurated microbial mats detached through wave action (wave-rip-up clasts) or subaerial desiccation that were then deposited in the intertidal and supratidal zones during storms (Eriksson et al., 2007; Flügel, 2010; Smith et al., 2020). The fine matrix of micrite and compound grains may have accumulated as a calcareous mud. F3 is thus attributed to deposition in a micrite-accumulating barrage pool in the supratidal zone, into which locally sourced angular clasts were periodically deposited by marine wave influences. Marine gastropod shell fragments and echinoid spines confirm an occasional marine influence.

5.1.4. F4: Microbially-cemented sand

The variability in coating thickness and mineralogy in the coated grain microfacies of F4 indicates that coated grains were initially developed on mobile nuclei. This was followed by further cementation forming meniscus, pendulous and microstalactic gravitational cements. These suggest that F4 was cemented by carbonate-rich spring water flowing through unconsolidated sands that were periodically colonised by a biofilm or microbial mat. The coated grains and meniscus cements indicate a vadose zone setting, and the alternating microbe- carbonate cements suggest regular changes in energy conditions. Contemporary supratidal sand beaches in the study area (Fig. 20B, C), plus others documented by Edwards et al. (2017) contain microbially-cemented beach sands comparable to this facies. The seaward dipping bedding, moderately well-sorted, and well-rounded to subangular nature of the sands are also consistent with deposition in a beach environment. This contention is supported by their distribution in small joint parallel embayments in the granitic topography and their consistently seaward-most location in each locality. (Fig. 6).

Cementation in F4 is attributed to (i) the mixing of marine and meteoric waters and (ii) microbial activity. The former promotes cementation as $CaCO_3$ water solubility decreases with salinity, and the mixing of these waters results in carbonate saturation and precipitation (Vousdoukas et al., 2007). Microbial action in F4 is indicated by the irregular, non-gravitationally controlled microbialite microcolumns.

5.1.5. F5: Palaeosol

F5 is interpreted as a calcisol palaeosol (Mack et al., 1993), formed as shallow groundwater flows through a soil profile with vegetation. While the occurrence of vugs and complex packing voids have no single significant genetic interpretation, the occurrence of channels can be ascribed to plant root growth and faunal bioturbation (Kemp, 1985). Circumgranular cracks and rhizolith root casts suggest a pedogenic origin, with the latter demonstrating a vegetated exposure surface. The larger ellipsoid grains within the micromass resemble excrement pedofeatures, potentially of oribatid mites, however, they are not readily distinguishable from the micrite peloids that form the majority of the

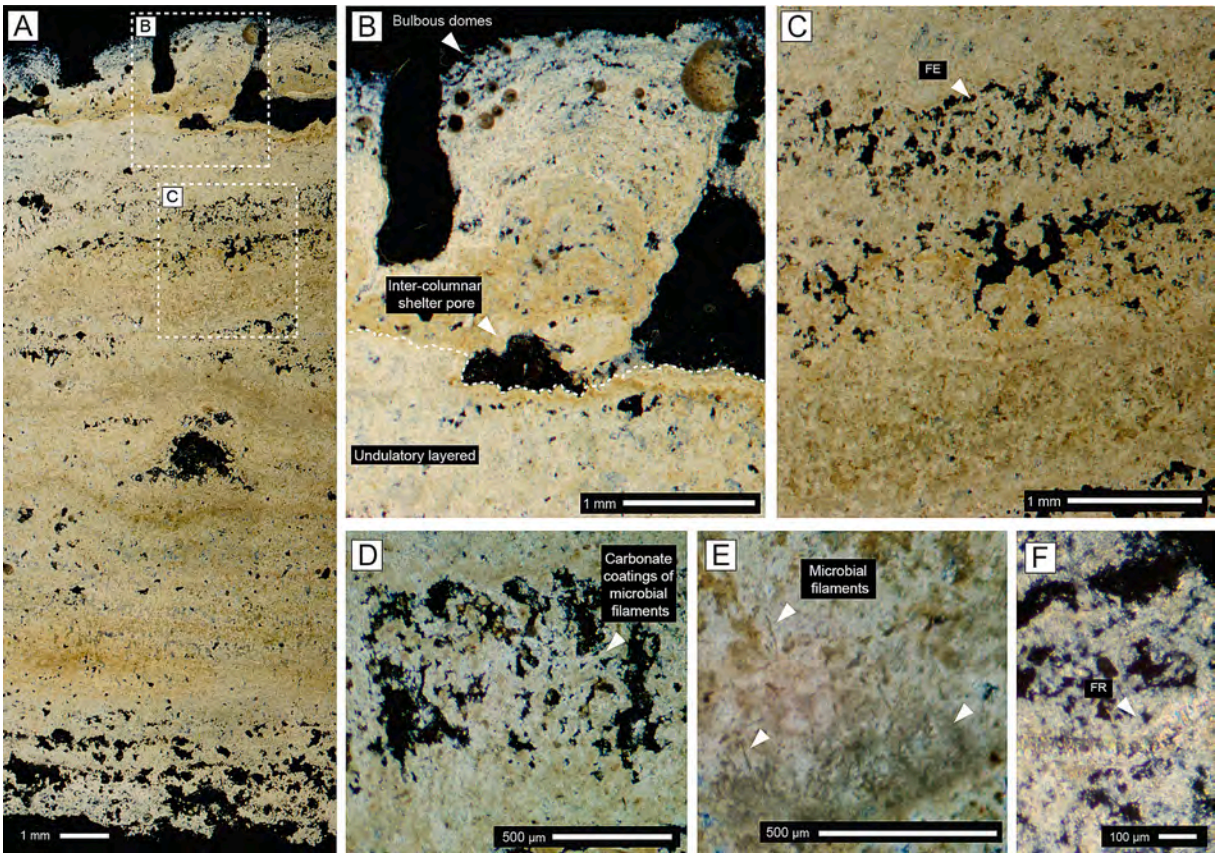

Fig. 13. Tufa microbialite microstructure in thin section under XPL (F2.1; site F): A: large scale scan of thin section showing inter-columnar shelter porosity; inset B: detail of contact between undulatory lamina and bulbous domical structures; inset C: detail of fenestral (FE) porosity between macrolaminae; D: carbonate coatings of poorly preserved microbial filaments with parallel orientation, perpendicular to laminae; E; microbial filaments within organic material-rich lamina; F: spar cement within fracture (FR) void.

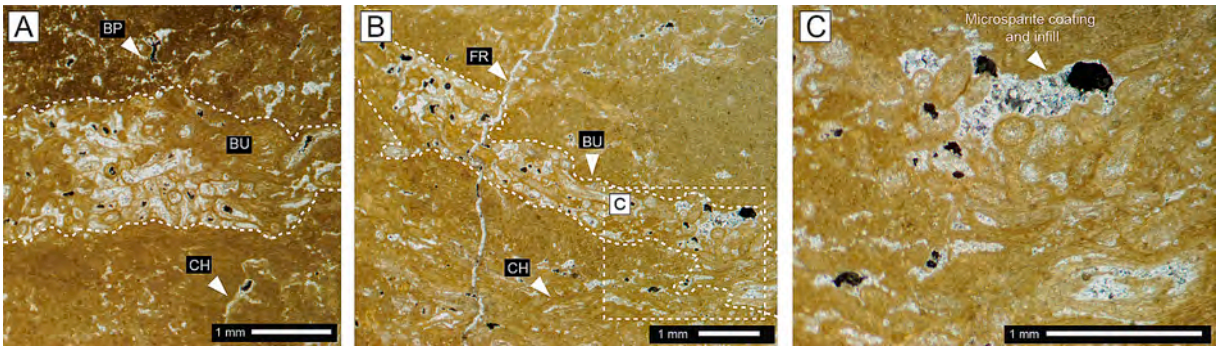

Fig. 14. Clast type 1 microstructure in thin section under XPL (F3; site G): A: large scale scan of thin section showing pore types (BP: interparticle; BU: burrow; CH: channel; FR: fracture) within the micrite matrix; B: detail of pore structure, with large fracture pore with inset C: detail of microsparite coatings and infill of burrow pores.

micromass. The blocky charcoal with a foliated surface texture suggests a wood origin (Courtney Mustaphi and Pisaric, 2014), demonstrating burning of woody plants on the landscape. While pedogenic carbonates form via several mechanisms, the depositional setting suggests a *per ascendum* model with pedogenic carbonate forming through capillary action or through variations in shallow groundwater (Alonso-Zarza and Tanner, 2010; Zamanian et al., 2016).

5.2. Comparison with contemporary rock coast microbialite systems

Active Holocene tufa microbialite deposits including actively accreting groundwater-fed supratidal tufa and tufa microbialite deposits occur close to the study site (Fig. 18A) (Forbes et al., 2010; Rishworth et al., 2020b). These contemporary rock coast tufa microbialite systems offer a partial modern analogue.

The tufa microbialite facies have clear analogues in modern spring-fed supratidal rock coast microbialites (Cooper et al., 2022; Edwards et al., 2017; Forbes et al., 2010; Perissinotto et al., 2014) (Fig. 18). F2.1, expansive sheet like deposits; F2.2, small barrage structures; F2.3, waterfall and cliff face deposits and F2.4 rock pool facies all have direct modern analogues on rock coasts. While the tufa-lithoclast breccia facies is poorly documented in modern systems, microbial mat rip up clasts have been recognised in modern systems (Cooper et al., 2022; Forbes et al., 2010; Smith et al., 2020) and are equivalent to clast type 2 in the

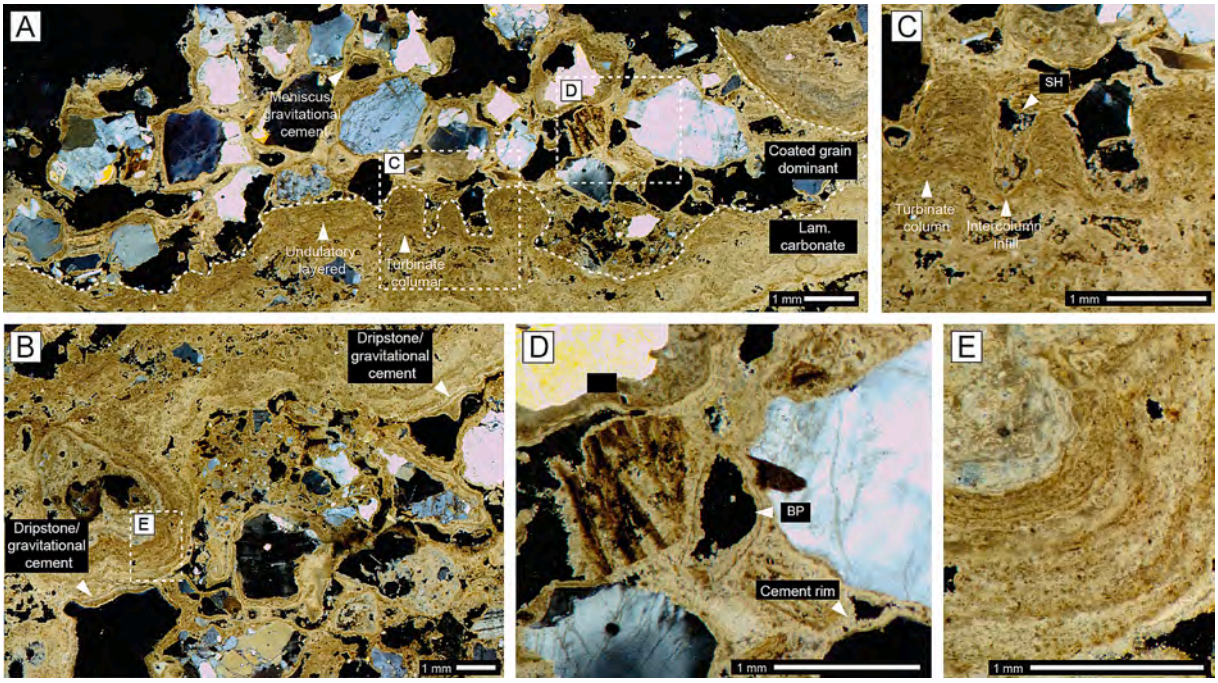

Fig. 15. Microbially-cemented sand microstructure in thin section under XPL (F4; site C): A: large scale scan of thin section showing coated grain dominant microfacies with gravitational cement and laminated carbonate microfacies with undulatory layered and turbinate columnar microstructure; B: detail of dripstone/ gravitational cements at microfacies interface; inset C: detail of columnar structure with shelter (SH) pore; inset D: detail of vegetative material and interparticle (BP) pores and cement rims); E: detail of laminated carbonate microfacies.

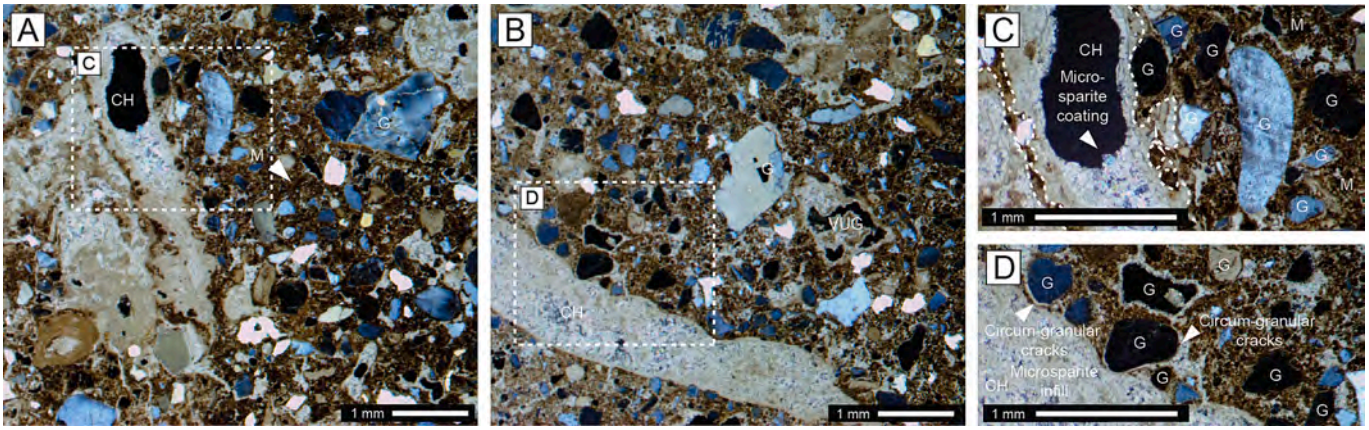

Fig. 16. F5 thin section under XPL: A: three dominant components (channel voids (CH), lithic grains (G) and micromass (M); B: channel voids with complete infilling vugs (VUG); C: detail of B showing spar coating of channel voids and distribution of lithic grains and micromass; D: detail of B showing complete infilling of channel voids with spar; and circum-granular cracks.

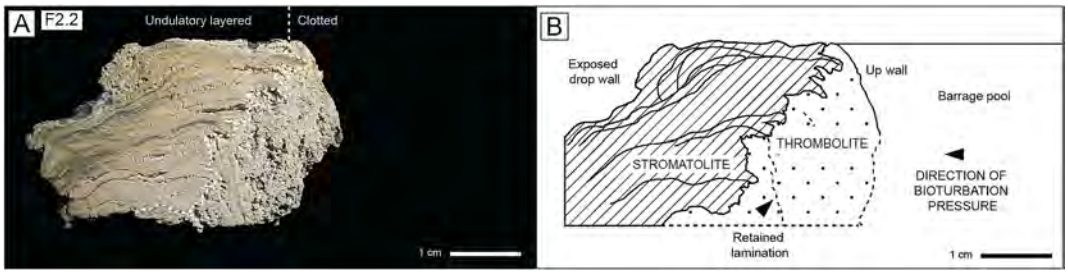

Fig. 17. A: small barrage (F2.2) with undulatory layered (stromatolitic) and clotted (thrombolitic) mesostructure (divided by white dashed line); B: interpretative sketch showing direction of bioturbation from a barrage pool.

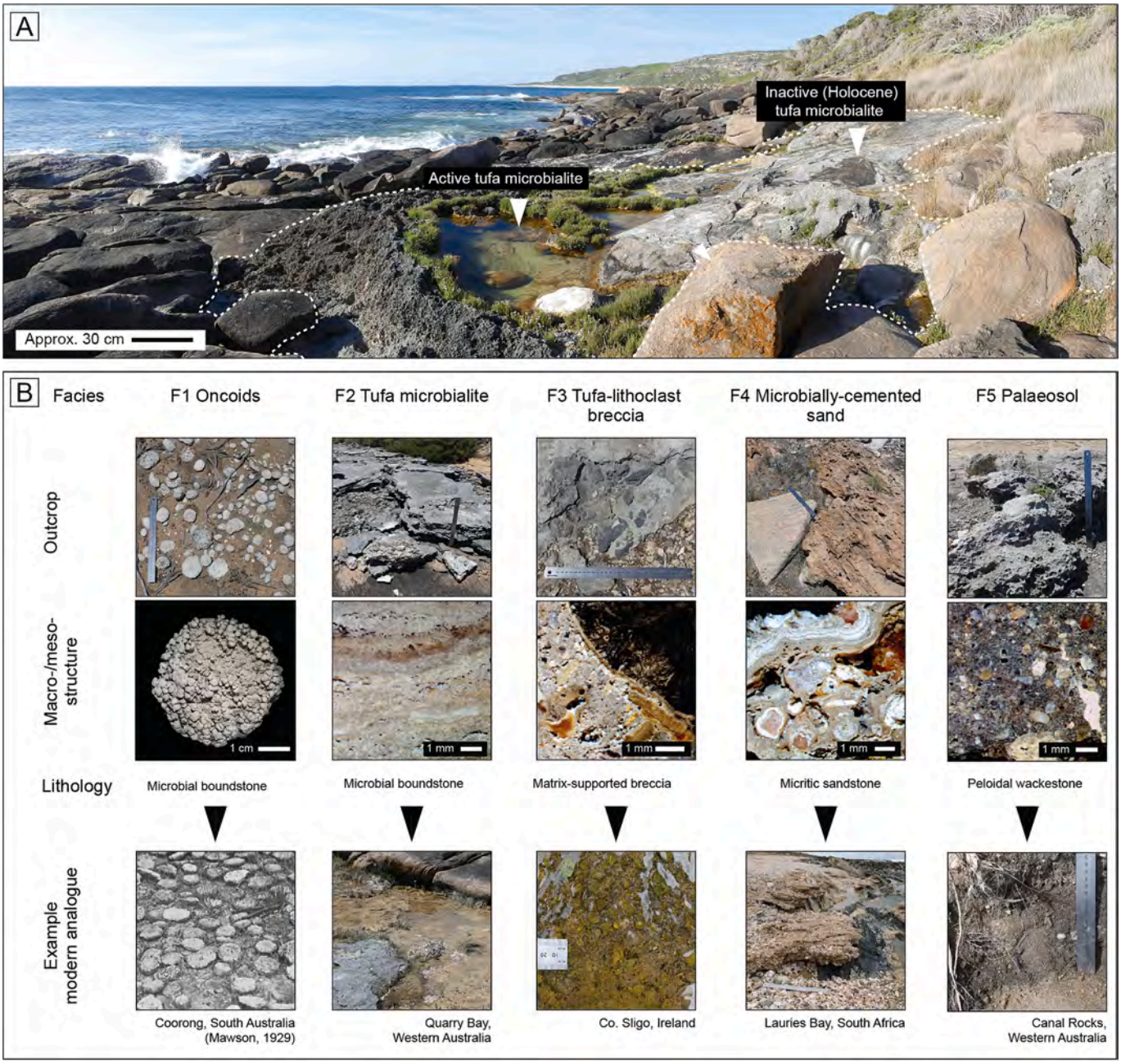

Fig. 18. Comparison with modern analogues: A: active tufa microbialite system, with inactive (Holocene) deposits, proximal to Cape Freycinet deposits (see active deposits in Fig. 1); B: Facies summary with outcrop (in-field photograph), macro/mesostructure and lithological summary; and modern analogue examples.

tufa-lithoclast breccia and palaeosol facies. The microbially-cemented sand facies is comparable to modern microbialite-associated "beach-rock" (Cooper et al., 2022; Edwards et al., 2017; Perissinotto et al., 2014) (Fig. 18), incipient back-beach deposits (Howie, 2009; Howie and Ealey, 2010; Kneale and Viles, 2000) and microbialite/microbially-cemented beachrock (Webb et al., 1999). These form in a range of zones from upper intertidal (Webb et al., 1999) to low supratidal (Cooper et al., 2022). Edwards et al. (2017) describe initial biomineralization of microbialite horizons in unconsolidated beach sands that is followed by further cementation by percolating groundwater. Although the palaeosol facies is scarcely described in the rock coast microbialite literature, unconsolidated calcareous soils have been observed at contemporary spring-fed rock coast microbialite sites in the immediate area (e.g. Canal Rocks, Western Australia) (Fig, 18).

Oncoids described from modern rock-coast microbialite systems, involve simple microbialite encrustation around scattered nuclei (rock or microbialite fragments) in bedrock basin or barrage pools (Cooper et al., 2022; Smith et al., 2020), which are not perfect analogues. Nonetheless, during the mid-19th century European exploration of South Australia several authors (Angas, 1847; Burr and Grey, 1845; Jukes, 1850) made reference to apparently similar deposits. For example (Angas, 1847, p. 155) described "*spongy plains, covered in shells and tufa biscuits, and subject to occasional inundations*". The first formal description of the 'biscuit flat' of the Coorong, near Robe, South Australia (Mawson, 1929), characterises thin discs ranging in size from small 'particles' to 20 cm in diameter (Fig. 18) composed of calcium carbonate with a smooth to warty upper surface, etched underside and internal concentric lamination. These occurred in low-lying shallow inter-dune slacks, inundated during the wet season forming pools around 3 in. (7.6 cm) in depth. Pigmentation of the upper surface was attributed to

the presence of *Gloeocapsa* and like-*Schizothrix fasciculata* (currently a synonym of *S. semiglobosa*) alga, indicating a microbial genesis. The original 'biscuit flat' site has since been destroyed through land development and drainage (Pentecost, 2005; Walter et al., 1973) but the biscuit tufa from coastal dune slacks offer a good coastal (supratidal with occasional inundation) analogue for F1 from Cape Freycinet.

5.3. Depositional model

The carbonate deposits at Cape Freycinet represent deposition from a palaeo-groundwater-spring in the supratidal zone as low as mean high-water level on a former rock coast. The facies distribution is dependent on a complex suite of formative drivers but is predominantly controlled by bedrock topography and elevation above palaeo-sea-level. Modern springs emerge only in the supratidal zone in the study area, and it seems probable that they similarly emerged along the palaeoshoreline when the microbialite deposits described here were being formed. Bedrock topography can be used to reconstruct the palaeo-shoreline, notably through the distribution of F4, (microbialite-cemented sand) and the bounding headlands within which these units accumulated.

Domal bedrock outcrops are reconstructed as small headlands, and the gullies between them as small beach-filled embayments on a former rock coast (Fig. 19A). Landward of the beaches, a variety of carbonate facies developed in topographic lows. The distribution and nature of tufa microbialite depends on the elevation and topography of the bedrock substrate. A hard substrate is important for the growth and preservation of tufa microbialites, as noted in modern freshwater tufa microbialites (Roche et al., 2019) and a variety of other settings (Benson, 1994; Casanova, 1994; Della Porta, 2015; Ginsburg and Planavsky, 2008; Winsborough et al., 1994) including high energy-supratidal environments (Rishworth et al., 2020b).

A clear and distinctive spatial facies sequence is present that reflects elevation in relation to palaeo-sea-level. The F5 palaeosol occurs at the highest elevations (landward), closest to the palaeo-spring emergence, and is interpreted as a cemented vegetated soil. Seaward, this transitions into F2, tufa microbialite, and F4, microbialite-cemented sand at the lowest elevation representing upper intertidal-supratidal (marginal marine) deposition (Fig. 19B). This spatial succession demonstrates the progression from the groundwater spring flowing seaward from the supratidal zone into the upper-intertidal zone where cementation occurs at the meteoric-marine water interface. On sub-horizontal bedrock, this sequence is replaced by F2 discharge aprons. The facies sequence in embayments (Fig. 19B) is comparable to the perched springline model of Pedley (1990), and involves thick proximal deposits, of paludal and tufa barrages; and distal fine intraclast/microdetrital tufa and thin, discontinuous tufa sheets (Pedley, 1990). Application of this model to supratidal sites (Forbes et al., 2010), allows the identification of this model and fluvial barrage models. A modified supratidal springline model is presented here (Fig. 19A).

5.4. Shoreline deposits: Evidence, dating and correlation

5.4.1. Evidence for a proposed shoreline

Like other contemporary supratidal groundwater springs in Western Australia (Forbes et al., 2010), the palaeo-springs that formed the Cape Freycinet site occur as a line or cluster, and show some evidence of

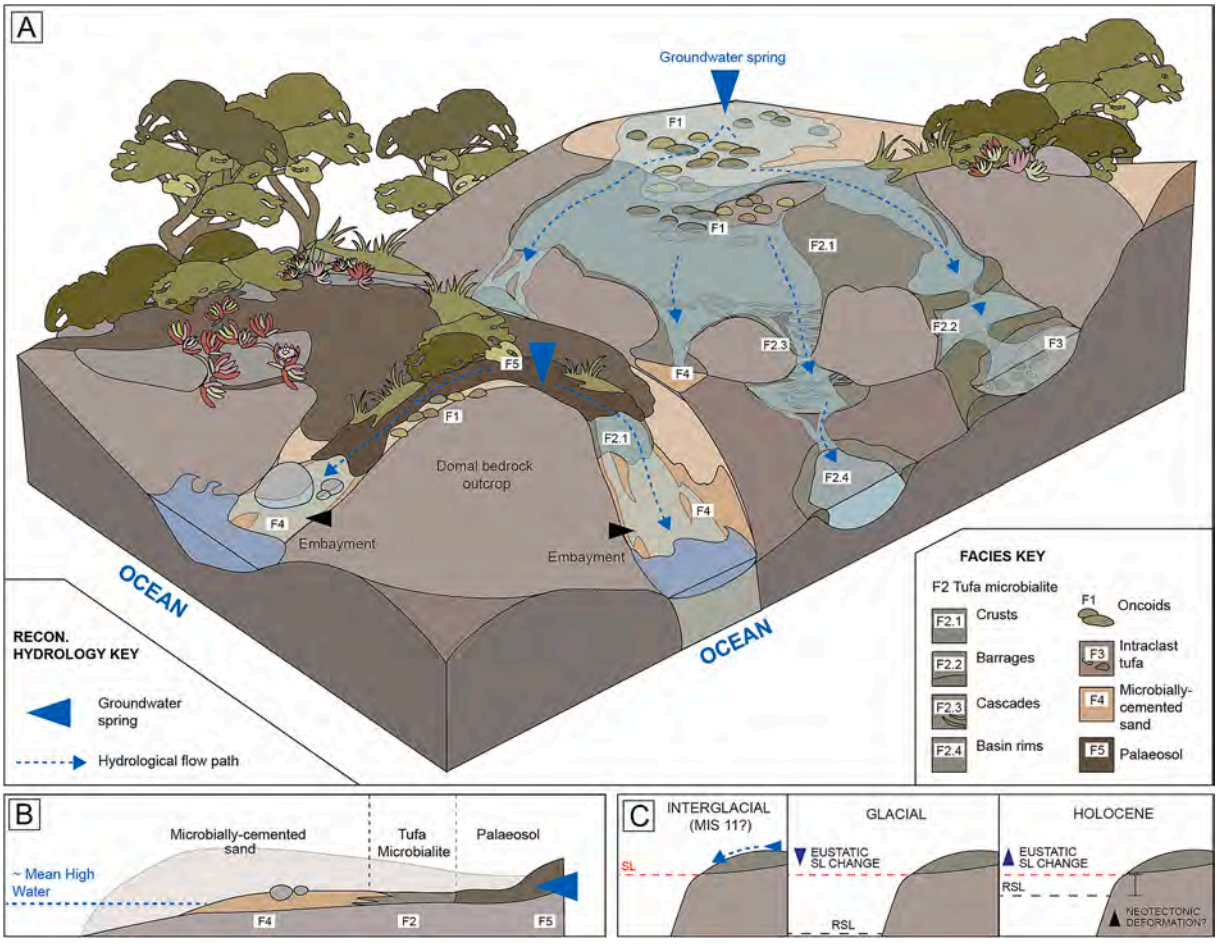

Fig. 19. A: Depositional model of terrestrial carbonate formation from supratidal groundwater springs; B: idealised facies associations within small embayments; C: post-depositional RSL for site.

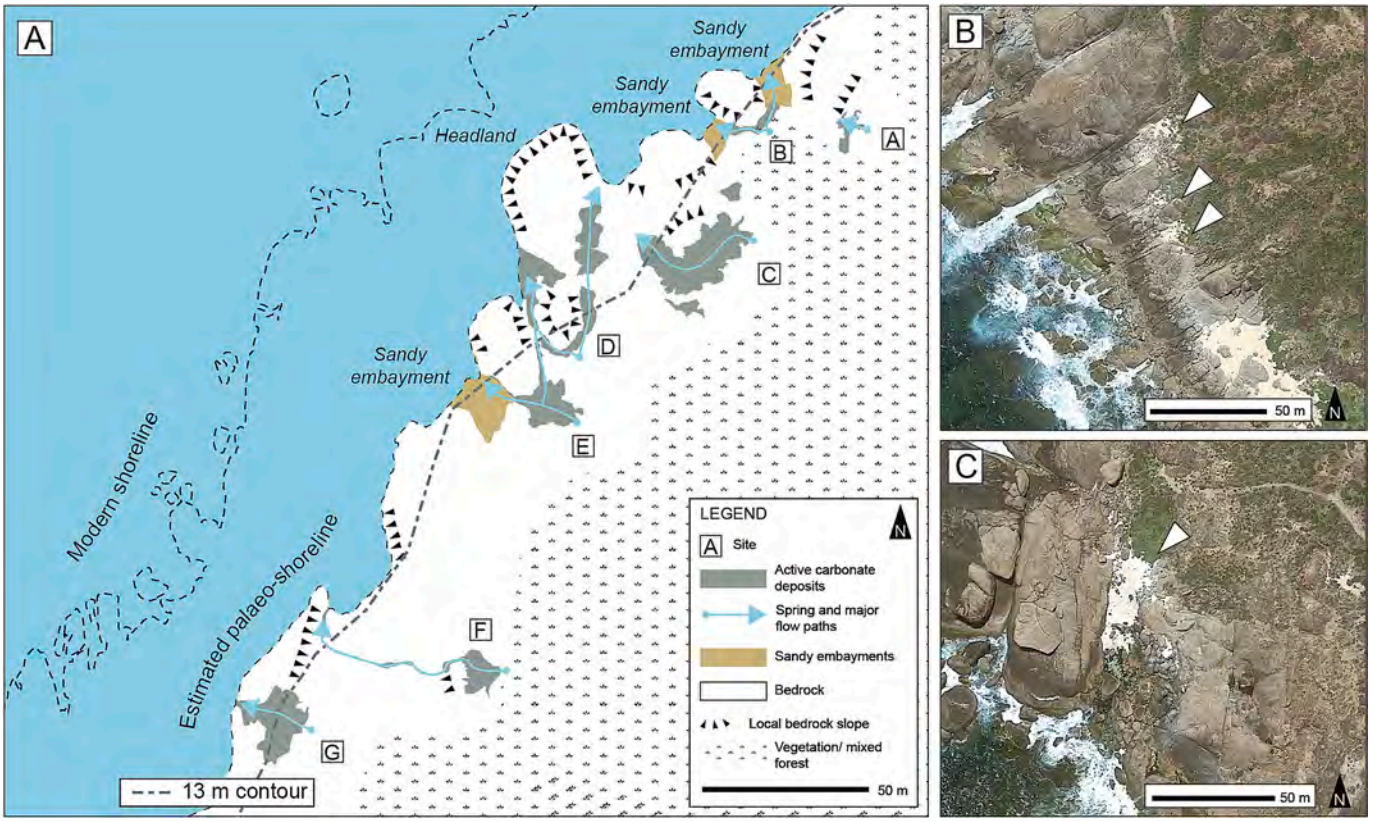

Fig. 20. A: Map of estimated palaeo-shoreline with groundwater springs, major flowpaths and carbonate deposits; estimated palaeo-shoreline, sandy embayments and headlands are inferred from facies distributions and 13 m DEM contour; B/C: modern aerial imagery of sandy embayments of comparable scale proximal to study area (south Cape Freycinet; aerial imagery: Google Earth Pro (2017)).

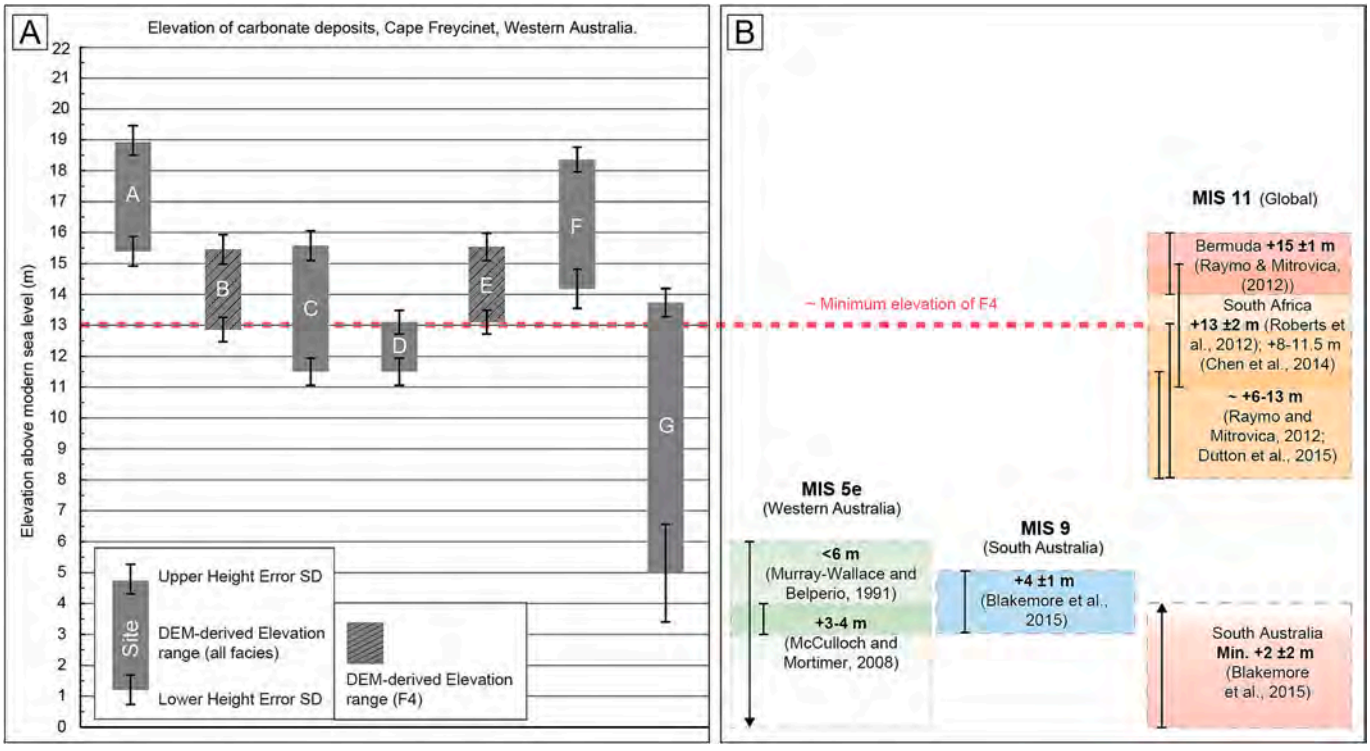

Fig. 21. Comparison of A: elevation of carbonate deposits, notably F4, microbially-cemented sand (see legend) at Cape Freycinet with B: palaeo-sea-level and shoreline data from MIS 5e, 9 and 11 from regional and global sites. Elevation range is derived from Copernicus DEM with Height Error Mask (HEM) quality corresponding to height error standard deviation.

coalescence, suggesting that they were coevally active. Discontinuous activity is suggested by inter-site variability in the degree of erosion and karstification. In particular, F2.4 rims deposited in a basin of F4 indicate alternating deposition and erosion (Fig. 4A). In modern tufa microbialites this is attributed to short-term discharge alternations or avulsion of flow paths (Forbes et al., 2010).

The absence of clear marine-deposited carbonates suggests that these deposits are marine-limited, with the lowest elevation deposits (microbially-cemented sand) representing an upper-intertidal limit to carbonate deposition. This allows a shoreline to be inferred on the basis of:

(i) Evidence of upper-intertidal to supratidal deposition, including: microbially-cemented sand facies, with seaward distributions, with coastal boulder intraclasts; marine gastropod shells and echinoid spines within tufa microbialite and tufa-lithoclast breccia facies.
(ii) Comparison with modern analogue supratidal groundwater spring carbonate facies and their respective relationships to sea-level.

5.4.2. Dating and correlation with palaeo-shorelines

Based on the elevation of deposits between 18.92 ± 0.48 m to 11.5 ± 0.44 m ASL; and a minimum elevation of the seaward microbially-cemented sand facies 12.86 ± 0.39 m ASL; a palaeo-shoreline can be reconstructed at ca. 13 m ASL (Fig. 21). The large elevation range (13.73 ± 0.46 m– 4.98 ± 1.58 m) at Site G is is attributed to continuing local tufa deposition during regression from the emergent shoreline.

The elevation of the shoreline units suggests deposition during a period of elevated sea level in a tectonically stable cratonic setting. Marine Isotope Stage (MIS) 5e, 9 and 11 are potential highstand sea-level correlatives. While Last Interglacial shorelines in Australia do exhibit some variability in elevation due to neotectonic deformation (Murray-Wallace and Belperio, 1991), the presence of a well-dated MIS 5e shoreline at ca. +3 m asl at Foul Bay, 17 km from the study area, supports the contention that the study area is tectonically stable. Without absolute dating, correlation with Quaternary sea-level states is tentative, however, the reconstructed palaeo-shoreline at Cape Freycinet suggests a highstand at ca. + 13 m, which correlates most closely with MIS 11 sea level (Fig. 21). Well-dated MIS 11 shorelines are scarce (Roberts et al., 2012), with many sites reliant on relative and semi-quantitative dating methods.

MIS 5e (~123–109 ka) sea level is recorded locally from Foul Bay suggest a local Last Interglacial shoreline at ca. +3 m (Chutcharavan and Dutton, 2021; McCulloch and Mortimer, 2008). This is consistent with other studies of shorelines during the first part of the Last Interglacial in Western Australia. Sea levels increased to ca. +3–4 m in the later part of the Last Interglacial (125–119 ka) (McCulloch and Mortimer, 2008). Sea level during MIS 9 (~337–300 ka) also exceeded present sea-level, however, it is poorly resolved (Barlow et al., 2017). Spratt and Lisiecki (2016) proposed a mean highstand of +9 ± 23 m; and regionally, Blakemore et al. (2015) suggested a + 4 ± 1 m sea-level for MIS 9 for the Mount Gambier region, South Australia.

Sea level during MIS 11 (~424–374 ka) is contentious (Candy et al., 2014; Olson and Hearty, 2009; Raymo and Mitrovica, 2012). Radiometrically-dated raised shorelines attributed to MIS 11 from Bermuda (Olson and Hearty, 2009) suggest high sea-levels at +21 m O.D. Comparable sea-levels have been reported elsewhere (Kaufman and Brigham-Grette, 1993; Lundberg and McFarlane, 2002; Bowen, 2003; Roberts, 2007; Van Hengstum et al., 2009; Bowen, 2010; Roberts et al., 2012), although some of these attributions have been strongly refuted (Bowen, 2010; McMurtry et al., 2007). Correcting for post-glacial crustal subsidence in the Bermuda and Bahamas Region Raymo and Mitrovica (2012) revised sea level in late MIS 11 as 6–13 m, aligned with MIS sea-level reconstructions from South Africa of +13 m ± 2 m (Roberts et al., 2012) and + 8–11.5 m (Chen et al., 2014).

The presence of a shoreline at ca. 13 m ASL, is thus tentatively assigned to MIS 11. If so, it represents one of a few MIS 11 shorelines recorded in Australia (Huntley et al., 1993; Murray-Wallace, 2018) and could, if dated, serve as a reliable global record of glacio-eustatic sea level at a far field site.

5.5. Preservation potential and application of rock coast microbialites as palaeo-shoreline indicators

5.5.1. Karren and karst features

Identification of palaeo-shorelines relies on the preservation of marginal marine facies. Following the cessation of palaeo-spring activity and active carbonate precipitation of tufa microbialites and associated marginal marine facies, their long-term preservation depends on post-depositional processes. The degree of calcification and early cementation at the study site was evidently sufficient to resist physical and chemical weathering (primarily solution) over long periods (~424–374 ka if their implied age is correct). The regional climate, especially precipitation, also provides a constraint on weathering rates of emergent carbonates (Cooper and Green, 2016).

Karren features in F2 and F5 are indicative of post-depositional weathering. Trittkarren features on F2 indicate corrosion by water sheets (Veress, 2009) that may focus on pre-existing steps or microscarps (Bögli, 1960; Ford and Williams, 1989), created by pre-existing micro-ripples and microterraces. Capillary action associated with surface water flow (Ford and Williams, 1989) over the surface of F2, led to the development of microrills. Between microbialite pustules to the distribution of trittkarren and microrills are thus influenced by the original tufa surface features.

Karren features on the surface of F5 are the result of the cemented soil/active soil interface and/or post-cementation weathering and erosion of the exposed deposits. Cavernous tafoni-like pitting is associated with salt weathering and/or wind and may be associated with case-hardening (Ford and Williams, 1989; Goudie, 2009) but tafoni may originate in the sub-soil environment and be enlarged subaerially following exhumation (Hunt, 1996) and seepage erosion (Smith, 1978). Pans and pit-like structures are interpreted as solution pits: round-bottomed to tapering pits varying in size from 1 cm to 1 m in diameter that formed in the subsoil environment by percolating water (Ford and Williams, 1989; Zseni, 2009).

These karren features are primarily the result of post-depositional solution following the cessation of palaeo-spring-related deposition. The post-depositional effects of karstification in terrestrial carbonates is an important control on their preservation potential (Jones and Renaut, 2010; Pentecost, 2005).

5.5.2. Marginal marine carbonates on rocky shorelines as palaeo-shoreline and sea-level indicators

Tufa and tufa microbialite deposits have been used to delineate, and establish the ages of, shorelines in lacustrine settings in the Tibetan Plateau (Hudson et al., 2015; Hudson and Quade, 2013; Lin et al., 2024), South America (Blard et al., 2011; Placzek et al., 2006) and eastern Africa (Casanova, 1994; Garcin et al., 2012; Gasse and Street, 1978; Hillaire-Marcel et al., 1986; Mologni et al., 2021). Lake Bonneville and Great Salt Lake palaeo-shoreline environments are recorded through the deposition of transitional carbonates including onshore groundwater spring carbonate deposits, beachrock (Felton et al., 2006), and lacustrine microbialite reefs (Felton et al., 2006; Godsey et al., 2011; Homewood et al., 2022; Vennin et al., 2019). Lake level variations and the evolution of the Lake Bonneville and Great Salt Lake system are recorded in the vertical distribution of microbialite deposits in a narrow shoreline 'belt' (Vennin et al., 2019). Geomorphological evidence including constructional flat benches, shoreline notches, stratigraphic sequences (Blard et al., 2011; Placzek et al., 2006) support the use of tufa and tufa microbialites as datable palaeo-shoreline indicators.

In contrast, terrestrial and marginal marine carbonates have scarcely been used to delineate former marine shorelines. Beachrock sensu stricto

has been advocated as a reliable sea-level indicator (Mauz et al., 2015) and other carbonate deposits such as aeolianites, tufa and speleothems in coastal environments (Faulkner and Crae, 2022; Faulkner and Crae, 2018; Howie and Ealey, 2010), all act as potential shoreline indicators. Microbialites occur in a range of coastal environments including hypersaline lagoons (Jahnert and Collins, 2012; Logan, 1961; Suosaari et al., 2022), open marine (Dill et al., 1986; Reid et al., 1995) and mixed environments within coastal ponds (Saint Martin and Saint Martin, 2015). Contemporary tufa microbialites at the intersection between groundwater springs and the upper-intertidal to supratidal zones, have been observed globally (Cooper et al., 2013; Forbes et al., 2010; Perissinotto et al., 2014; Rishworth et al., 2020b; Smith et al., 2018). Rishworth et al. (2020a) identified potential tufa microbialite barrage pools on submerged palaeo-shorelines attributed to discrete periods during MIS 6, 5d and 3 but emergent rock coast microbialites have not previously been reported.

In a regressive situation marginal marine microbialites, would experience declining marine influence, and the onset of chemical and physical weathering (evidenced by karren features). The effectiveness of these processes determines the long-term preservation potential. During transgression, preservation would be limited by wave-induced erosion and bioturbation and aided by rapid marine transgression and/or high sedimentation rates.

Rock coast shorelines are scarcely preserved and/or rarely noted in the geological record (Manikam et al., 2022) but they can provide reliable indications of former sea level (e.g., Dawson, 1984). As shoreline erosional features are uncommon in resistant and isotropic lithologies (Kennedy et al., 2014), marginal marine carbonate deposits like those reported here provide a potentially valuable tool for the identification of former rock coast shorelines and rock shoreline deposits (e.g., Allwood et al., 2006) and provide material for potential chronological control.

6. Conclusions

The tufa microbialite and associated deposits of Cape Freycinet, Western Australia form a distinctive assemblage of marginal marine facies from the upper-intertidal to supratidal zones of a former rock coast associated with groundwater springs. This study identifies the first emergent shoreline defined by marginal marine spring-associated carbonate deposits. Comparison with modern analogues allows five interlinked facies to define the former shoreline: oncoids (F1), tufa microbialite (F2), tufa-lithoclast breccia (F3), microbially-cemented sand (F4) and palaeosol (F5) from seven adjacent palaeo-spring deposits.

Depositional processes and environments are interpreted from multiscale description of facies and comparisons with modern analogues. A distinct marginal marine depositional model is presented from facies distributions and bedrock geomorphology. We describe carbonate deposition from a landward palaeosol facies (representing a hinterland vegetated soil), extending laterally into tufa microbialite on subhorizontal bedrock, associated with oncoids and finally tufa-lithoclast breccia. The most seaward facies is a microbially-cemented sand that represents upper-intertidal to supratidal beach deposition.

The interpretation of these facies (notably microbially-cemented sand and marine intraclasts) and resultant depositional model, indicates a palaeo-shoreline associated with groundwater springs, elevated ca. 13 m above modern sea-level. Through comparison with tectonically stable far-field locations elsewhere, this is tentatively attributed to MIS 11. This has potential implications for currently unresolved debates surrounding the MIS 11 sea-levels state. The study demonstrates, for the first time, the utility of marginal marine carbonate deposits in the upper-intertidal to supratidal zone to identify emergent rock coast shorelines (even in granitic lithologies) with potentially dateable material.

Funding

This work was supported by the Department for the Economy (DfE) sponsorship for postgraduate studentship and EPStromNet- Extant Peritidal Stromatolite Network (NERC grant award NE/V00834X/1).

CRediT authorship contribution statement

Thomas W. Garner: Writing – review & editing, Writing – original draft, Visualization, Methodology, Investigation, Formal analysis, Data curation, Conceptualization. **J. Andrew G. Cooper:** Writing – review & editing, Supervision, Investigation, Funding acquisition, Conceptualization. **Alan Smith:** Writing – review & editing, Supervision, Investigation, Funding acquisition, Conceptualization.

Declaration of competing interest

I have nothing to declare.

Acknowledgements

This work was made possible through the NERC-funded EPStromNet project and a Department for the Economy (DfE) sponsorship for postgraduate studentship. The authors would like to thank the EPStromNet team for in-field discussion and support; Mukesh Seyambu for production of thin sections; supervisor Joerg Arnscheidt, and Edward Anthony for helpful guidance during review.

Data availability

All data used in the publication are completely and directly provided in the manuscript; there are no ancillary datasets.

References

Allwood, A.C., Walter, M.R., Kamber, B.S., Marshall, C.P., Burch, I.W., 2006. Stromatolite reef from the early Archaean era of Australia. Nature 441, 714–718. https://doi.org/10.1038/nature04764.

Alonso-Zarza, A.M., Tanner, L.H., 2010. Carbonates in Continental Settings: Facies, Environments and Processes. Developments in Sedimentology, Elsevier, Amsterdam.

Angas, G.F., 1847. Savage Life and Scenes in Australia and New Zealand: Being an Artist's Impressions of Countries and People at the Antipodes, Cambridge Library Collection - History of Oceania. Cambridge University Press, Cambridge. https://doi.org/10.1017/CBO9781139107532.

Barlow, N.L.M., Long, A.J., Gehrels, W.R., Saher, M.H., Scaife, R.G., Davies, H.J., Penkman, K.E.H., Bridgland, D.R., Sparkes, A., Smart, C.W., Taylor, S., 2017. Relative Sea-level variability during the late Middle Pleistocene: new evidence from eastern England. Quat. Sci. Rev. 173, 20–39. https://doi.org/10.1016/j.quascirev.2017.08.017.

Beeler, S.R., Gomez, F.J., Bradley, A.S., 2020. Controls of extreme isotopic enrichment in modern microbialites and associated abiogenic carbonates. Geochim. Cosmochim. Acta 269, 136–149. https://doi.org/10.1016/j.gca.2019.10.022.

Benson, L., 1994. Carbonate deposition, Pyramid Lake subbasin, Nevada: 1. Sequence of formation and elevational distribution of carbonate deposits (Tufas). Palaeogeogr. Palaeoclimatol. Palaeoecol. 109, 55–87. https://doi.org/10.1016/0031-0182(94)90118-X.

Blakemore, A.G., Murray-Wallace, C.V., Westaway, K.E., Lachlan, T.J., 2015. Aminostratigraphy and sea-level history of the Pleistocene Bridgewater Formation, Mount Gambier region, southern Australia. Aust. J. Earth Sci. 62, 151–169. https://doi.org/10.1080/08120099.2015.1014523.

Blard, P.-H., Sylvestre, F., Tripati, A.K., Claude, C., Causse, C., Coudrain, A., Condom, T., Seidel, J.-L., Vimeux, F., Moreau, C., Dumoulin, J.-P., Lavé, J., 2011. Lake highstands on the Altiplano (Tropical Andes) contemporaneous with Heinrich 1 and the Younger Dryas: new insights from 14C, U–Th dating and δ18O of carbonates. Quat. Sci. Rev. 30, 3973–3989. https://doi.org/10.1016/j.quascirev.2011.11.001.

Bögli, A., 1960. Kalklosung und Karrenbildung. Z. Für Geomorphol. Suppl.-Band 2, 4–21.

Bowen, D., 2003. Uncertainty in Oxygen Isotope Stage 11 Sea-Level: an Estimate of ~13~2 M from Great Britain. Wash. DC Am. Geophys. Union Geophys. Monogr. Ser, 131–144. https://doi.org/10.1029/137GM10.

Bowen, D., 2010. Sea level ~400 000 years ago (MIS 11): Analogue for present and future sea-level? Clim. Past 6. https://doi.org/10.5194/cp-6-19-2010.

Bullock, P., Fedoroff, N., Jongerius, A., 1985. Handbook for Soil Thin Section Description. Waine.

Bureau of Meteorology, 2024. Monthly Climate Statistics for Australian Locations: Witchcliffe.

Burne, R., Moore, L., 1987. Microbialites: organosedimentary deposits of benthic microbial communities. Palaios 2, 241–254. https://doi.org/10.2307/3514674.
Burr, Thos, Grey, G., 1845. Account of Governor G. Grey's exploratory journey along the South-Eastern Sea-Board of South Australia. J. R. Geogr. Soc. Lond. 15, 160–184. https://doi.org/10.2307/1797905.
Candy, I., Schreve, D.C., Sherriff, J., Tye, G.J., 2014. Marine Isotope Stage 11: Palaeoclimates, palaeoenvironments and its role as an analogue for the current interglacial. Earth Sci. Rev. 128, 18–51. https://doi.org/10.1016/j.earscirev.2013.09.006.
Casanova, J., 1994. Stromatolites from the East African Rift: A Synopsis. In: Bertrand-Sarfati, J., Monty, C. (Eds.), Phanerozoic Stromatolites II. Springer, Netherlands, Dordrecht, pp. 193–226. https://doi.org/10.1007/978-94-011-1124-9_8.
Chen, F., Friedman, S., Gertler, C.G., Looney, J., O'Connell, N., Sierks, K., Mitrovica, J.X., 2014. Refining estimates of Polar Ice Volumes during the MIS11 Interglacial using Sea Level Records from South Africa. J. Clim. 27, 8740–8746. https://doi.org/10.1175/JCLI-D-14-00282.1.
Chutcharavan, P.M., Dutton, A., 2021. A global compilation of U-series-dated fossil coral sea-level indicators for the last Interglacial period (Marine Isotope Stage 5e). Earth Syst. Sci. Data 13, 3155–3178. https://doi.org/10.5194/essd-13-3155-2021.
Collins, A.S., 2003. Structure and age of the northern Leeuwin Complex, Western Australia: constraints from field mapping and U–Pb isotopic analysis. Aust. J. Earth Sci. 50, 585–599. https://doi.org/10.1046/j.1440-0952.2003.01014.x.
Cooper, J.A.G., Green, A.N., 2016. Geomorphology and preservation potential of coastal and submerged aeolianite: examples from KwaZulu-Natal, South Africa. Geomorphology 271, 1–12. https://doi.org/10.1016/j.geomorph.2016.07.028.
Cooper, A., Smith, A., Arnscheidt, J., 2013. Contemporary stromatolite formation in high intertidal rock pools, Giant's Causeway, Northern Ireland: preliminary observations. J. Coast. Res. 1675–1680. https://doi.org/10.2112/SI65-283.1.
Cooper, A., Smith, A., Rishworth, G., Dodd, C., Forbes, M., Cawthra, H., Anderson, C., 2022. Microbialites of modern siliciclastic rock coasts. J. Sediment. Res. 92, 619–634. https://doi.org/10.2110/jsr.2021.071.
COP-DEM, 2024. Copernicus DEM - Global and European Digital Elevation Model. https://doi.org/10.5270/ESA-c5d3d65.
Courtney Mustaphi, C., Pisaric, M., 2014. A classification for macroscopic charcoal morphologies found in Holocene lacustrine sediments. Prog. Phys. Geogr. 38. https://doi.org/10.1177/0309133314548886.
Cresswell, G.R., Golding, T.J., 1980. Observations of a south-flowing current in the southeastern Indian Ocean. Deep Sea Res. Part Oceanogr. Res. Pap. 27, 449–466. https://doi.org/10.1016/0198-0149(80)90055-2.
Dahanayake, K., 1978. Sequential position and environmental significance of different types of oncoids. Sediment. Geol. 20, 301–316. https://doi.org/10.1016/0037-0738(78)90060-X.
Dawson, A.G., 1984. Quaternary sea-level changes in Western Scotland. Quat. Sci. Rev. 3, 345–368. https://doi.org/10.1016/0277-3791(84)90012-X.
Della Porta, G., 2015. Carbonate build-ups in lacustrine, hydrothermal and fluvial settings: Comparing depositional geometry, fabric types and geochemical signature. In: Bosence, D.W.J., Gibbons, K.A., Heron, D.P.L., Morgan, W.A., Pritchard, T., Vining, B.A. (Eds.), Microbial Carbonates in Space and Time: Implications for Global Exploration and Production. Geological Society of London. https://doi.org/10.1144/SP418.4.
Dill, R.F., Shinn, E.A., Jones, A.T., Kelly, K., Steinen, R.P., 1986. Giant subtidal stromatolites forming in normal salinity waters. Nature 324, 55–58. https://doi.org/10.1038/324055a0.
Dodd, C., Anderson, C.R., Perissinotto, R., du Plooy, S.J., Rishworth, G.M., 2018. Hydrochemistry of peritidal stromatolite pools and associated freshwater inlets along the Eastern Cape coast, South Africa. Sediment. Geol. 373, 163–179. https://doi.org/10.1016/j.sedgeo.2018.06.002.
Dupraz, C., Reid, R.P., Braissant, O., Decho, A.W., Norman, R.S., Visscher, P.T., 2009. Processes of carbonate precipitation in modern microbial mats. In: Earth-Sci. Rev., Microbial Mats in Earth's Fossil Record of Life: Geobiology, 96, pp. 141–162. https://doi.org/10.1016/j.earscirev.2008.10.005.
Eberhard, S., 2004. Ecology and Hydrology of a Threatened Groundwater-Dependent Ecosystem: The Jewel Cave Karst System in Western Australia - Murdoch University (PhD). Murdoch University, Perth.
Edwards, M.J.K., Anderson, C.R., Perissinotto, R., Rishworth, G.M., 2017. Macro- and meso-fabric structures of peritidal tufa stromatolites along the Eastern Cape coast of South Africa. Sediment. Geol. 359, 62–75. https://doi.org/10.1016/j.sedgeo.2017.08.006.
Eriksson, P.G., Porada, H., Banerjee, S., Bouougri, E., Sarkar, S., Bumby, A.J., 2007. 4(c). Mat-destruction features. In: Atlas of Microbial Mat Features Preserved within the Siliciclastic Rock Record. Atlases in Geoscience, Elsevier, Amsterdam, p. 47.
Fahner, C., Pattiaratchi, C., 1994. The Physical oceanography of Geographe Bay. Western Australia. https://doi.org/10.13140/2.1.2528.0965.
Faulkner, T., Crae, J., 2018. Distribution of tufa and speleothem deposits on the island of Lismore, Argyll, Scotland. Cave Karst Sci. 45, 101–110.
Faulkner, T., Crae, J., 2022. Exotic tufa and speleothem deposits on the calcareous island of Lismore, Argyll, Scotland. In: Published in the Proceedings of the 18th International Congress of Speleology, France, 2022, 5, pp. 55–58.
Felton, A., Jewell, P.W., Chan, M., Currey, D., 2006. Controls of Tufa Development in Pleistocene Lake Bonneville, Utah. J. Geol. 114, 377–389. https://doi.org/10.1086/501218.
Feng, M., Li, Y., Meyers, G., 2004. Multidecadal variations of Fremantle Sea level: Footprint of climate variability in the tropical Pacific. Geophys. Res. Lett. 31. https://doi.org/10.1029/2004GL019947.
Feng, M., Weller, E., Hill, K., 2009. In: Poloczanska, E.S., Hobday, A.J., Richardson, A.J. (Eds.), The Leeuwin current. NCCARF Publication.
Flügel, E., 2010. Microfacies of Carbonate Rocks: Analysis, Interpretation and Application. Springer, Berlin, Heidelberg. https://doi.org/10.1007/978-3-642-03796-2.
Forbes, M., Vogwill, R., Onton, K., 2010. A characterisation of the coastal tufa deposits of south–West Western Australia. Sediment. Geol. 232, 52–65. https://doi.org/10.1016/j.sedgeo.2010.09.009.
Ford, T.D., Pedley, H.M., 1996. A review of tufa and travertine deposits of the world. Earth Sci. Rev. 41, 117–175. https://doi.org/10.1016/S0012-8252(96)00030-X.
Ford, D., Williams, P., 1989. Karst Geomorphology and Hydrology. Springer, Dordrecht.
Freytet, P., Verrecchia, E.P., 1998. Freshwater organisms that build stromatolites: a synopsis of biocrystallization by prokaryotic and eukaryotic algae. Sedimentology 45, 535–563. https://doi.org/10.1046/j.1365-3091.1998.00155.x.
Garcin, Y., Melnick, D., Strecker, M.R., Olago, D., Tiercelin, J.-J., 2012. East African mid-Holocene wet–dry transition recorded in palaeo-shorelines of Lake Turkana, northern Kenya Rift. Earth Planet. Sci. Lett. 331–332, 322–334. https://doi.org/10.1016/j.epsl.2012.03.016.
Garner, T., Smith, A.M., Rishworth, G., Forbes, M., 2024. Reviews and syntheses: Tufa microbialites on rocky coasts – towards an integrated terminology. Biogeosciences 21, 4785–4807. https://doi.org/10.5194/bg-21-4785-2024.
Gasse, E., Street, F.A., 1978. Late Quaternary Lake-level fluctuations and environments of the northern Rift valley and Afar region (Ethiopia and Djibouti). Palaeogeogr. Palaeoclimatol. Palaeoecol. 24, 279–325. https://doi.org/10.1016/0031-0182(78)90011-1.
Geoscience Australia and Australian Stratigraphy Commission, 2017. Australian Stratigraphic Units Database [WWW Document]. URL. https://asud.ga.gov.au/ (accessed 11.20.23).
Ginsburg, R.N., Planavsky, N.J., 2008. Diversity of Bahamian Microbialite Substrates. In: Dilek, Y., Furnes, H., Muehlenbachs, K. (Eds.), Links between Geological Processes, Microbial Activities&Evolution of Life: Microbes and Geology, Modern Approaches in Solid Earth Sciences. Springer, Netherlands, Dordrecht, pp. 177–195. https://doi.org/10.1007/978-1-4020-8306-8_6.
Godsey, H., Oviatt, C., Miller, D., Chan, M., 2011. Stratigraphy and chronology of offshore to nearshore deposits associated with the Provo shoreline, Pleistocene Lake Bonneville, Utah. Palaeogeogr. Palaeoclimatol. Palaeoecol. 310, 442–450. https://doi.org/10.1016/j.palaeo.2011.08.005.
Gomez, F., Kah, L., Bartley, J., Astini, R., 2014. Microbialites in a high-altitude Andean Lake: multiple controls on carbonate precipitation and lamina accretion. PALAIOS 29, 233–249. https://doi.org/10.2110/palo.2013.049.
Goudie, A., 2009. Cavernous weathering. In: Karst Rock Features. Karren Sculpturing. ZRC Publishing, Ljubljana, pp. 85–87.
Grey, K., Awramik, S., 2020. Handbook for the study and description of microbialites. In: Geological Survey of Western Australia: Bulletin, 147.
Hägele, D., Leinfelder, R., Grau, J., Burmeister, E.-G., Struck, U., 2006. Oncoids from the river Alz (southern Germany): Tiny ecosystems in a phosphorus-limited environment. Palaeogeogr. Palaeoclimatol. Palaeoecol. 237, 378–395. https://doi.org/10.1016/j.palaeo.2005.12.016.
Hammer, Ø., Dysthe, D.K., Jamtveit, B., 2007. The dynamics of travertine dams. Earth Planet. Sci. Lett. 256, 258–263. https://doi.org/10.1016/j.epsl.2007.01.033.
Harwood Theisen, C., Sumner, D.Y., 2016. Thrombolite fabrics and origins: Influences of diverse microbial and metazoan processes on Cambrian thrombolite variability in the Great Basin, California and Nevada. Sedimentology 63, 2217–2252. https://doi.org/10.1111/sed.12304.
Hemer, M.A., Simmonds, I., Keay, K., 2008. A classification of wave generation characteristics during large wave events on the Southern Australian margin. Cont. Shelf Res. 28, 634–652. https://doi.org/10.1016/j.csr.2007.12.004.
Hillaire-Marcel, C., Carro, O., Casanova, J., 1986. 14C and Th/U dating of pleistocene and holocene stromatolites from East African Paleolakes. Quat. Res. 25, 239–312. https://doi.org/10.1016/0033-5894(86)90004-9.
Homewood, P., Mettraux, M., Vanden Berg, M., Foubert, A., Neumann, R., Newell, D., Atwood, G., 2022. Onshore groundwater spring carbonate mounds to lacustrine microbialites, the perplexing record of a transitional Great Salt Lake carbonate shoreline at Lakeside, Utah. Depositional Rec. 8, 9–38. https://doi.org/10.1002/dep2.148.
Howie, F., 2009. Beachrock development along the north coast of cornwall. Geosci. South-West Engl. 12.
Howie, F., Ealey, P., 2010. An appraisal of Quaternary calcium carbonate deposits in Cornwall. Geosci. South-West Engl. 12, 233–240.
Hudson, A.M., Quade, J., 2013. Long-term east-west asymmetry in monsoon rainfall on the Tibetan Plateau. Geology 41, 351–354. https://doi.org/10.1130/G33837.1.
Hudson, A.M., Quade, J., Huth, T.E., Lei, G., Cheng, H., Edwards, L.R., Olsen, J.W., Zhang, H., 2015. Lake level reconstruction for 12.8–2.3 ka of the Ngangla Ring Tso closed-basin lake system, southwest Tibetan Plateau. Quat. Res. 83, 66–79. https://doi.org/10.1016/j.yqres.2014.07.012.
Hunt, C., 1996. Tafoni (pseudokarst) features in the Maltese Islands. Cave Karst Sci. 23, 57–62.
Huntley, D.J., Hutton, J.T., Prescott, J.R., 1993. The stranded beach-dune sequence of south-East South Australia: A test of thermoluminescence dating, 0–800 ka. Quat. Sci. Rev. 12, 1–20. https://doi.org/10.1016/0277-3791(93)90045-N.
Jahnert, R.J., Collins, L.B., 2012. Characteristics, distribution and morphogenesis of subtidal microbial systems in Shark Bay, Australia. Mar. Geol. 303–306, 115–136. https://doi.org/10.1016/j.margeo.2012.02.009.
Janssen, D., Collins, A., Fitzsimons, I., 2003. Structure and Tectonics of the Leeuwin Complex and Darling Fault Zone, Southern Pinjarra Orogen, Western Australia—A Field Guide.
Johnson, M.E., 1988. Why are ancient rocky shores so uncommon? J. Geol. 96, 469–480.

Johnson, M.E., 1992. Studies on Ancient Rocky Shores: a brief history and annotated bibliography. J. Coast. Res. 8, 797–812.
Jones, B., 2011. Biogenicity of terrestrial oncoids formed in soil pockets, Cayman Brac, British West Indies. Sediment. Geol. 236, 95–108. https://doi.org/10.1016/j.sedgeo.2010.12.009.
Jones, B., Renaut, R.W., 2010. Calcareous spring deposits in continental settings. In: Alonso-Zarza, A.M., Tanner, L.H. (Eds.), Developments in Sedimentology, Carbonates in Continental Settings: Facies, Environments, and Processes. Elsevier, pp. 177–224. https://doi.org/10.1016/S0070-4571(09)06104-4.
Jukes, J.B., 1850. A Sketch of the Physical Structure of Australia: So Far as it Is at Present Known, Cambridge Library Collection - Earth Science. Cambridge University Press, Cambridge. https://doi.org/10.1017/CBO9781139014007.
Kano, A., Matsuoka, J., Kojo, T., Fujii, H., 2003. Origin of annual laminations in tufa deposits, Southwest Japan. Palaeogeogr. Palaeoclimatol. Palaeoecol. 191, 243–262. https://doi.org/10.1016/0031-0182(02)00717-4.
Kaufman, D.S., Brigham-Grette, J., 1993. Aminostratigraphic correlations and paleotemperature implications, Pliocene-Pleistocene high-sea-level deposits, northwestern Alaska. Quat. Sci. Rev. 12, 21–33. https://doi.org/10.1016/0277-3791(93)90046-O.
Kemp, R.A., 1985. Soil Micromorphology and the Quaternary.
Kennedy, D.M., Ierodiaconou, D., Schimel, A., 2014. Granitic coastal geomorphology: applying integrated terrestrial and bathymetric LiDAR with multibeam sonar to examine coastal landscape evolution. Earth Surf. Process. Landf. 39, 1663–1674. https://doi.org/10.1002/esp.3615.
Kneale, D., Viles, H.A., 2000. Beach cement: incipient CaCO3-cemented beachrock development in the upper intertidal zone, North Uist, Scotland. Sediment. Geol. 132, 165–170. https://doi.org/10.1016/S0037-0738(00)00029-4.
Leinfelder, R.R., Hartkopf-Fröder, C., 1990. In situ accretion mechanism of concavo-convex lacustrine oncoids ('swallow nests') from the Oligocene of the Mainz Basin, Rhineland, FRG. Sedimentology 37, 287–301. https://doi.org/10.1111/j.1365-3091.1990.tb00960.x.
Lencina, A.I., Soria, M.N., Colla, M.F., Cury, L.F., Farías, M.E., Gomez, F.J., 2023. In situ growth of modern oncoids from Salado river, Salar de la Laguna Verde complex, Argentina. Sediment. Geol. 451, 106396. https://doi.org/10.1016/j.sedgeo.2023.106396.
Lin, X., Lan, J., Sun, Y., Sinha, A., Cheng, X., Lin, F., Zhang, J., Li, Y., Cheng, P., Chang, H., Hussain, S.A., Wang, L., Tan, L., 2024. Middle to late Holocene lake level variations recorded by shoreline tufa of Longmu Co Lake, northwestern Tibet Plateau. The Holocene. https://doi.org/10.1177/09596836241254474, 09596836241254474.
Lipar, M., Webb, J., 2015. The Middle–Late Pleistocene Bridgewater formation on Cape Bridgewater, south-western Victoria: chronostratigraphy and palaeoclimatic significance. Proc. R. Soc. Vic. 127, 81. https://doi.org/10.1071/RS15020.
Logan, B.W., 1961. Cryptozoon and Associate Stromatolites from the recent, Shark Bay, Western Australia. J. Geol. 69, 517–533. https://doi.org/10.1086/626769.
Logan, B.W., Rezak, R., Ginsburg, R.N., 1964. Classification and Environmental significance of Algal Stromatolites. J. Geol. 72, 68–83.
Logan, B.W., Davies, G.R., Read, J.F., Cebulski, D.E., 1970. Carbonate Sedimentation and Environments, Shark Bay, Western Australia. American Association of Petroleum Geologists. https://doi.org/10.1306/M13369.
Logan, B.W., Read, J.F., Hagan, G.M., Hoffman, P., Brown, R.G., Woods, P.J., Gebelein, C.D., 1974. Evolution and Diagenesis of Quaternary Carbonate Sequences, Shark Bay, Western Australia. American Association of Petroleum Geologists. https://doi.org/10.1306/M22379.
Luke, G.J., Burke, K.L., O'Brien, T.M., 1987. Evaporation Data for Western Australia (Resource Management Technical Reports), vol. 65. Department of Primary Industries and Regional Development, Perth.
Lundberg, J., McFarlane, D., 2002. Isotope stage 11 sea level in the Netherlands Antilles. Geol. Soc. Am. Annu. Meet. 2002 Denver Annual Meeting (October 27-30, 2002), Session 9, Paper 9-8. https://www.researchgate.net/publication/256843309_Isotope_stage_11_sea_level_in_the_Netherlands_Antilles (accessed 04 February 2025).
Mack, G.H., James, W.C., Monger, H.C., 1993. Classification of paleosols. Geol. Soc. Am. Bull. 105, 129–136. https://doi.org/10.1130/0016-7606(1993)105<0129:COP>2.3.CO;2.
Manikam, S.L., Green, A.N., Cooper, A., Deacon, G., Flemming, B., 2022. Development and preservation of transgressive sandy versus rocky shorelines: observations from the SE African shelf. Geomorphology 419, 108485. https://doi.org/10.1016/j.geomorph.2022.108485.
Mauz, B., Vacchi, M., Green, A., Hoffmann, G., Cooper, A., 2015. Beachrock: A tool for reconstructing relative sea level in the far-field. Mar. Geol. 362, 1–16. https://doi.org/10.1016/j.margeo.2015.01.009.
Mawson, D., 1929. Some South Australian Algal limestones in process of formation. Q. J. Geol. Soc. 85, 613–620. https://doi.org/10.1144/GSL.JGS.1929.085.01-04.18.
McCulloch, M.T., Mortimer, G.E., 2008. Applications of the 238U–230Th decay series to dating of fossil and modern corals using MC-ICPMS. Aust. J. Earth Sci. 55, 955–965. https://doi.org/10.1080/08120090802097435.
McMurtry, G.M., Tappin, D.R., Sedwick, P.N., Wilkinson, I., Fietzke, J., Sellwood, B., 2007. Elevated marine deposits in Bermuda record a late Quaternary megatsunami. In: Sediment. Geol., Sedimentary Features of Tsunami Deposits - Their Origin, Recognition and Discrimination: An Introduction, 200, pp. 155–165. https://doi.org/10.1016/j.sedgeo.2006.10.009.
Mologni, C., Bruxelles, L., Schuster, M., Davtian, G., Ménard, C., Orange, F., Doubre, C., Cauliez, J., Taezaz, H.B., Revel, M., Khalidi, L., 2021. Holocene East African monsoonal variations recorded in wave-dominated clastic paleo-shorelines of Lake Abhe, Central Afar region (Ethiopia & Djibouti). Geomorphology 391, 107896. https://doi.org/10.1016/j.geomorph.2021.107896.
Murray-Wallace, C.V., 2018. Quaternary History of the Coorong Coastal Plain. An Archive of Environmental and Global Sea-Level Changes. Springer International Publishing, Cham, Southern Australia. https://doi.org/10.1007/978-3-319-89342-6.
Murray-Wallace, C.V., Belperio, A.P., 1991. The last interglacial shoreline in Australia — a review. Quat. Sci. Rev. 10, 441–461. https://doi.org/10.1016/0277-3791(91)90006-G.
Olson, S., Hearty, P., 2009. A sustained +21 m sea-level highstand during MIS 11 (400 Ka): direct fossil and sedimentary evidence from Bermuda. Quat. Sci. Rev. 28, 271–285. https://doi.org/10.1016/j.quascirev.2008.11.001.
Pattiaratchi, C., Eliot, M., 2009. Sea level variability in South-West Australia: from hours to decades. In: Proceedings of the International Coastal Engineering Conference. https://doi.org/10.1142/9789814277426_0099.
Pattiaratchi, C., Hegge, B., Gould, J., Eliot, I., 1997. Impact of sea-breeze activity on nearshore and foreshore processes in southwestern Australia. Cont. Shelf Res. 17, 1539–1560. https://doi.org/10.1016/S0278-4343(97)00016-2.
Pedley, H.M., 1990. Classification and environmental models of cool freshwater tufas. Sediment. Geol. 68, 143–154. https://doi.org/10.1016/0037-0738(90)90124-C.
Pentecost, A., 2005. Travertine. Springer.
Perissinotto, R., Bornman, T.G., Steyn, P.-P., Miranda, N.A.F., Dorrington, R.A., Matcher, G.F., Strydom, N., Peer, N., 2014. Tufa stromatolite ecosystems on the South African south coast. South Afr. J. Sci. 110, 01–08. https://doi.org/10.1590/sajs.2014/20140011.
Placzek, C., Quade, J., Patchett, P.J., 2006. Geochronology and stratigraphy of late Pleistocene lake cycles on the southern Bolivian Altiplano: implications for causes of tropical climate change. GSA Bull. 118, 515–532. https://doi.org/10.1130/B25770.1.
Playford, P.E., Low, G.H., Cockbain, A.E., 1976. Geology of the Perth Basin, Western Australia, Bulletin. Geological Survey of Western Australia, Perth, W.A.
Raymo, M.E., Mitrovica, J.X., 2012. Collapse of polar ice sheets during the stage 11 interglacial. Nature 483, 453–456. https://doi.org/10.1038/nature10891.
Reid, R.P., Macintyre, I.G., Browne, K.M., Steneck, R.S., Miller, T., 1995. Modern marine stromatolites in the Exuma Cays, Bahamas: uncommonly common. Facies 33, 1–17. https://doi.org/10.1007/BF02537442.
Riding, R., 1983. Cyanoliths (Cyanoids): oncoids formed by calcified cyanophytes. In: Peryt, T.M. (Ed.), Coated Grains. Springer, Berlin, Heidelberg, pp. 276–283. https://doi.org/10.1007/978-3-642-68869-0_24.
Riding, R., 1991. Calcareous Algae and Stromatolites, pp. 21–51. https://doi.org/10.1007/978-3-642-52335-9_2.
Rishworth, G.M., Perissinotto, R., Bird, M.S., 2016a. Coexisting living stromatolites and infaunal metazoans. Oecologia 182, 539–545. https://doi.org/10.1007/s00442-016-3683-5.
Rishworth, G.M., van Elden, S., Perissinotto, R., Miranda, N.A.F., Steyn, P.-P., Bornman, T.G., 2016b. Environmental influences on living marine stromatolites: insights from benthic microalgal communities. Environ. Microbiol. 18, 503–513. https://doi.org/10.1111/1462-2920.13116.
Rishworth, G.M., Perissinotto, R., Bird, M.S., Pelletier, N., 2017a. Grazer responses to variable macroalgal resource conditions facilitate habitat structuring. R. Soc. Open Sci. 5, 171428. https://doi.org/10.1098/rsos.171428.
Rishworth, G.M., Perissinotto, R., Bornman, T.G., Lemley, D.A., 2017b. Peritidal stromatolites at the convergence of groundwater seepage and marine incursion: patterns of salinity, temperature and nutrient variability. J. Mar. Syst. 167, 68–77. https://doi.org/10.1016/j.jmarsys.2016.11.010.
Rishworth, G.M., Edwards, M.J.K., Cónsole-Gonella, C., Perissinotto, R., 2019. Modern active microbialite-metazoan relationships in peritidal systems on the Eastern Cape coast of South Africa: Ecological significance and implication for the palaeontological record. J. Afr. Earth Sci. 153, 1–8. https://doi.org/10.1016/j.jafrearsci.2019.02.013.
Rishworth, G.M., Cawthra, H.C., Dodd, C., Perissinotto, R., 2020a. Peritidal stromatolites as indicators of stepping-stone freshwater resources on the Palaeo-Agulhas Plain landscape. Quat. Sci. Rev. Palaeo-Agulhas Plain 235, 105704. https://doi.org/10.1016/j.quascirev.2019.03.026.
Rishworth, G.M., Dodd, C., Perissinotto, R., Bornman, T.G., Adams, J.B., Anderson, C.R., Cawthra, H.C., Dorrington, R.A., du Toit, H., Edworthy, C., Gibb, R.-L.A., Human, L. R.D., Isemonger, E.W., Lemley, D.A., Miranda, N.A.F., Peer, N., Raw, J.L., Smith, A. M., Steyn, P.-P., Strydom, N.A., Teske, P.R., Welman, S., 2020b. Modern supratidal microbialites fed by groundwater: functional drivers, value and trajectories. Earth Sci. Rev. 210, 103364. https://doi.org/10.1016/j.earscirev.2020.103364.
Roberts, D.L., 2007. Onshore expression of multiple orbitally driven late Quaternary marine incursions on the ultra-stable southern south African coast. Quat. Int. 167, 3–486.
Roberts, D.L., Karkanas, P., Jacobs, Z., Marean, C.W., Roberts, R.G., 2012. Melting ice sheets 400,000 yr ago raised sea level by 13m: past analogue for future trends. Earth Planet. Sci. Lett. 357–358, 226–237. https://doi.org/10.1016/j.epsl.2012.09.006.
Roche, A., Vennin, E., Bundeleva, I., Bouton, A., Payandi-Rolland, D., Suchet, P., Gaucher, E., Courvoisier, H., Visscher, P., 2019. The role of the substrate on the mineralization potential of Microbial Mats in A Modern Freshwater River (Paris Basin, France). Minerals 9, 359. https://doi.org/10.3390/min9060359.
Rodrigues, A.C., da Santos, L.R., Cury, L.F., Rumbelsperger, A.B., 2022. Continental freshwater carbonate coated grains: oncoids in Quaternary deposits of the Serra da Bodoquena region, Central-West Brazil. Braz. J. Geol. 52. https://doi.org/10.1590/2317-4889202220210042.
Saint Martin, J.-P., Saint Martin, S., 2015. Discovery of calcareous microbialites in coastal ponds of western Sardinia (Italy), 2015, pp. 35–53.
Scheffers, S.R., Scheffers, A., Kelletat, D., Bryant, E.A., 2008. The Holocene paleo-tsunami history of West Australia. Earth Planet. Sci. Lett. 270, 137–146. https://doi.org/10.1016/j.epsl.2008.03.027.

Shapiro, R.S., 2000. A comment on the systematic confusion of thrombolites. PALAIOS 15, 166–169. https://doi.org/10.2307/3515503.
Sheppard, T.H., 2006. Sequence architecture of ancient rocky shorelines and their response to sea-level change: an early Jurassic example from South Wales, UK. J. Geol. Soc. 163, 595–606. https://doi.org/10.1144/0016-764920-015.
Smith, B.J., 1978. The origin and geomorphic implications of cliff-foot recesses and tafoni on limestone hamadas in the Northwest Sahara. Z. Für Geomorphol. 22, 21–43.
Smith, A., Uken, R., 2003. Living marine stromatolites at Kei River mouth. South Afr. J. Sci. 99.
Smith, A.M., Andrews, J.E., Uken, R., Thackeray, Z., Perissinotto, R., Leuci, R., Marca-Bell, A., 2011. Rock pool tufa stromatolites on a modern South African wave-cut platform: partial analogues for Archaean stromatolites? Terra Nova 23, 375–381. https://doi.org/10.1111/j.1365-3121.2011.01022.x.
Smith, A., Cooper, A., Misra, S., Bharuth, V., Guastella, L., Botes, R., 2018. The extant shore platform stromatolite (SPS) facies association: a glimpse into the Archean? Biogeosciences 15, 2189–2203. https://doi.org/10.5194/bg-15-2189-2018.
Smith, A., Cooper, A., Guastella, L., Bharath, V., 2020. Wave influences in contemporary and Mesoarchaean stromatolites. Sediment. Geol. 396, 105558. https://doi.org/10.1016/j.sedgeo.2019.105558.
Spratt, R.M., Lisiecki, L.E., 2016. A Late Pleistocene sea level stack. Clim. Past 12, 1079–1092. https://doi.org/10.5194/cp-12-1079-2016.
Suosaari, E.P., Reid, R.P., Mercadier, C., Vitek, B.E., Oehlert, A.M., Stolz, J.F., Giusfredi, P.E., Eberli, G.P., 2022. The microbial carbonate factory of Hamelin Pool, Shark Bay, Western Australia. Sci. Rep. 12, 12902. https://doi.org/10.1038/s41598-022-16651-z.
Van Hengstum, P.J., Scott, D., Javaux, E., 2009. Foraminifera in elevated Bermudian caves provide further evidence for +21 m eustatic sea level during Marine Isotope Stage 11. Quat. Sci. Rev. 28. https://doi.org/10.1016/j.quascirev.2009.05.017.
Vennin, E., Bouton, A., Bourillot, R., Pace, A., Roche, A., Brayard, A., Thomazo, C., Virgone, A., Gaucher, E.C., Desaubliaux, G., Visscher, P.T., 2019. The lacustrine microbial carbonate factory of the successive Lake Bonneville and Great Salt Lake, Utah, USA. Sedimentology 66, 165–204. https://doi.org/10.1111/sed.12499.
Veress, M., 2009. Trittkarren, in: Karst Rock Features. In: Karren Sculpturing. ZRC Publishing, Ljubljana, pp. 151–159.
Vousdoukas, M.I., Velegrakis, A.F., Plomaritis, T.A., 2007. Beachrock occurrence, characteristics, formation mechanisms and impacts. Earth Sci. Rev. 85, 23–46. https://doi.org/10.1016/j.earscirev.2007.07.002.
Walter, M.R., Heys, G.R., 1985. Links between the rise of the metazoa and the decline of stromatolites. In: Precambrian Res., Proceedings of International Symposium Late Precambrian Geology, 29, pp. 149–174. https://doi.org/10.1016/0301-9268(85)90066-X.
Walter, M.R., Golubic, S., Preiss, W.V., 1973. Recent stromatolites from hydromagnesite and aragonite depositing lakes near the Coorong Lagoon, South Australia. J. Sediment. Res. 43, 1021–1030. https://doi.org/10.1306/74D728DD-2B21-11D7-8648000102C1865D.
Webb, G.E., Jell, J.S., Baker, J.C., 1999. Cryptic intertidal microbialites in beachrock, Heron Island, Great Barrier Reef: implications for the origin of microcrystalline beachrock cement. Sediment. Geol. 126, 317–334. https://doi.org/10.1016/S0037-0738(99)00047-0.
Weston, R.-L.A., Perissinotto, R., Rishworth, G.M., Steyn, P.-P., 2018. Macroinvertebrate variability between microhabitats of peritidal stromatolites along the south African coast. Mar. Ecol. Prog. Ser. 605, 37–47. https://doi.org/10.3354/meps12741.
Winsborough, B.M., Seeler, J.-S., Golubic, S., Folk, R.L., Maguire, B., 1994. Recent Fresh-Water Lacustrine Stromatolites, Stromatolitic Mats and Oncoids from Northeastern Mexico. In: Bertrand-Sarfati, J., Monty, C. (Eds.), Phanerozoic Stromatolites II. Springer, Netherlands, Dordrecht, pp. 71–100. https://doi.org/10.1007/978-94-011-1124-9_4.
Zamanian, K., Pustovoytov, K., Kuzyakov, Y., 2016. Pedogenic carbonates: forms and formation processes. Earth Sci. Rev. 157, 1–17. https://doi.org/10.1016/j.earscirev.2016.03.003.
Zatoń, M., Kremer, B., Marynowski, L., Wilson, M.A., Krawczyński, W., 2012. Middle Jurassic (Bathonian) encrusted oncoids from the Polish Jura, southern Poland. Facies 58, 57–77. https://doi.org/10.1007/s10347-011-0273-1.
Zhang, W., Shi, X., Jiang, G., Tang, D., Wang, X., 2015. Mass-occurrence of oncoids at the Cambrian Series 2–Series 3 transition: Implications for microbial resurgence following an early Cambrian extinction. Gondwana Res. 28, 432–450. https://doi.org/10.1016/j.gr.2014.03.015.
Zseni, A., 2009. Subsoil Shaping, in: Karst Rock Features. In: Karren Sculpturing. ZRC Publishing, Ljubljana, pp. 103–121.